

---

**This manuscript is a preprint** and it has been submitted for publication in **Earth-Science Reviews**. The manuscript underwent peer-review, and it was formally accepted for publication on 25 May 2022.

The final version of this manuscript will be available via the '*Peer-reviewed Publication DOI*' link on the right-hand side of this webpage.

Please feel free to contact any of the authors; we welcome feedback.

---

1 **Tectono-sedimentary evolution of Southern Mexico. Implications for Cretaceous and younger**  
2 **source-to-sink systems in the Mexican foreland basins and the Gulf of Mexico**

3  
4 **Villagómez, D. <sup>1,\*</sup>, Steffensen, C. <sup>2</sup>, Pindell, J. <sup>1</sup>, Molina-Garza, R.S. <sup>3</sup>, Gray, G. <sup>4</sup>, Graham, R. <sup>5</sup>,**  
5 **O'Sullivan, P. <sup>6</sup>, Stockli, D. <sup>7</sup>, Spikings, R. <sup>8</sup>**

6  
7 <sup>1</sup> Tectonic Analysis Ltd, Duncton, West Sussex GU28 0LH, UK

8 <sup>2</sup> Viking GeoSolutions LLC, Houston TX 77224 USA

9 <sup>3</sup> Centro de Geociencias, Universidad Nacional Autónoma de México, Juriquilla 76230, México

10 <sup>4</sup> Department of Earth, Environmental and Planetary Sciences, Rice University, Houston, TX 77055,  
11 USA

12 <sup>5</sup> Department of Geology, Imperial College, London SW7 2BP, UK

13 <sup>6</sup> GeoSep Services, Moscow, ID 83843, USA

14 <sup>7</sup> Department of Geological Sciences, University of Texas at Austin, TX 78712-1722, USA

15 <sup>8</sup> Department of Mineralogy, Faculty of Sciences, University of Geneva, 1205 Geneva, Switzerland

16  
17 \* Corresponding author (email: [Diego.Villagomez@gmail.com](mailto:Diego.Villagomez@gmail.com))

18 **Abstract**

19  
20 An extensive dataset of existing and new geo/thermochronological data from several areas in  
21 Southern Mexico constrains the tectonic history of the region, as well as various source-to-sink  
22 relationships and local burial histories. Our interpretation acknowledges that not all cooling/heating  
23 observed in the source areas is due to erosional exhumation/burial but, in some cases, due to  
24 advective heat transfer from magmatic sources, which potentially overprinted earlier events. In this  
25 work, we identified several areas that have been exhumed since the Early Cretaceous and potentially  
26 provided clastic material to the southern Gulf of Mexico area.

27  
28 We help to document how the Mexican (Laramide) Orogeny propagated eastwards and southwards  
29 from the Late Cretaceous through the early Oligocene. The first sediments reaching the Tampico–  
30 Misantra and Veracruz basins derived mostly from eroded Cretaceous carbonate material that  
31 covered the Sierra Madre Oriental, the Sierra de Juárez Complex and the Cuicateco belts, as well as  
32 foredeep/intra-orogenic basin deposits formerly covering them. Possibly by the end of the Mexican  
33 Orogeny, the clastic Jurassic and older crystalline basement rocks became exposed and became the  
34 main sources of quartz-rich clastic material to the most easterly foreland basins and Gulf of Mexico.  
35 Exposure was probably assisted by higher angle basement thrusts such as the Vista Hermosa/Valle  
36 Nacional faults. The Mixtequita and Guichicovi blocks have also provided an important source of  
37 quartz-rich and metamorphic lithic-rich material to the southern Veracruz Basin possibly since the  
38 Eocene.

39  
40 For most of the Cenozoic, the Chiapas and the Sureste basins were sourced from areas south of the  
41 Chiapas Massif, i.e., the North America–Caribbean plate boundary zone along today's Chiapas  
42 coastal plain. This plate boundary zone accommodated relative displacement between Mexico and  
43 the Chortis Block of the Caribbean Plate. Paleocene–middle Miocene sediments within the Chiapas  
44 Basin were at least partially sourced from i) metamorphic complexes in the northern Chortis Block; ii)  
45 the parautochthonous Chontal Complex, an oceanic-like basin sandwiched between Chortis and  
46 southern Mexico; iii) the elongating volcanic arc along southern Mexico and western Chortis; and iv)  
47 the Cretaceous and Jurassic sedimentary cover of the southern flank of the Chiapas Massif,

48  
49 The westward telescoping of southern Mexico onto the Cocos Plate in the wake of Chortis has  
50 produced flat slab subduction geometry and eastwardly-younging uplift of the Xolapa Belt (Oligo–  
51 Miocene) and the Chiapas Massif (late Miocene). It also caused reorganization of the drainage  
52 systems providing material to the Chiapas and Sureste basins.

53  
54 Our results highlight the importance of understanding relative block and plate boundary  
55 displacements in a dynamic hinterland and consider the role of major faults when interpreting source-  
56 to-sink relationships in the area. We describe the latter relationships for several geologic time  
57 intervals in which reservoir-prone sediments were delivered to the southern Gulf of Mexico. Finally,  
58 we integrate the source-to-sink history to provide an assessment of reservoir quality and hydrocarbon  
59 prospectivity in the region.  
60

61

## 1 Introduction

Source-to-sink analyses aim to integrate the collective sedimentary systems that extend from eroding mountainous areas, through transfer zones and finally to depositional sink areas, usually deep-sea basins (Allen, 2017). Although these types of analyses are not a new concept (see Walsh et al., 2016; Helland-Hansen et al., 2016), their utility for the determination of the dispersal of sediments and potential resources contained in those sediments is unparalleled (Allen and Allen, 2013). Variations in the distribution and amount of sediments reaching the depositional areas reflect ultimately changes in tectonic activity and/or climate, particularly in active and highly dynamic areas such as the North American continental interior (Galloway et al., 2011).

The tectonic and/or erosional exhumation of continental and oceanic litho-tectonic units exposed in southern Mexico has significantly contributed to the sediment flux into the Gulf of Mexico and adjacent basins, beginning in the late Mesozoic (Winker and Buffler, 1988; Gray et al., 2021; Graham et al., 2020; Sierra-Rojas et al., 2020; Beltrán-Triviño et al., 2021). Although a number of individual studies have assessed the post-Jurassic uplift and exhumation history of certain areas in northern (Fitz-Díaz et al., 2014; 2018, Gray et al., 2001; 2021) and southern Mexico (Ducea et al., 2004; Witt et al., 2012; Abdullin et al., 2016; Gray et al., 2021; Villagómez and Pindell, 2020a, 2020b; Hernández-Vergara et al., 2021), we still lack a synthesis explaining when and how the continental margin was exhumed and where the potential sink areas were located.

We have determined the Cretaceous and younger exhumation history for southern Mexico by using a number of geochronological and thermochronological techniques on litho-tectonic units from the southern Sierra Madre Oriental to western Guatemala. We have linked these “source” areas to potential depositional areas based on published studies and industrial data. Our work also addresses some depositional aspects of clastic sediments reaching the Gulf of Mexico basins.

Our results show that the Cretaceous and younger exhumation history of the region directly relates to the progressive evolution of the Farallon/Cocos–North America–Caribbean plate boundaries, including the relative displacement of the Chortis Block along Mexico as part of the NW Caribbean Plate. This paper presents a series of paleogeographic and depositional reconstructions that account for i) regional tectonics, ii) exhumation-related information, iii) detrital provenance analysis, and iv) depositional studies in the different foreland basins of southern Mexico.

This work highlights the importance of sedimentary reworking as a fundamental aspect when determining provenance and reservoir quality in Southern Mexico. These “second cycle” sediments are more texturally and compositionally mature when re-deposited farther out into the basin, therefore with improved reservoir characteristics.

## 2 Geological setting

The following summary and **Appendix 1** synthesize the geology of the main litho-tectonic units in Southern Mexico, which are shown in **Figure 1**. Most of the litho-tectonic units described here are primarily identified based on their stratigraphy and deformation history, and do not necessarily carry any genetic implication even if some of them were allochthonous prior to a given time. Nonetheless, they are usually bounded by major faults (currently exposed at surface or not) with a clear geological relevance and displacement history based on geological mapping and/or exhumation-related information. For the purposes of this contribution, we have subdivided the Cuicateco Belt into several workable sub-units or sub-belts based on mapped faults and differential lithologies. The different regional-scale litho-tectonic units discussed below are characterized by internal geological homogeneity, tectonic style, exhumation, and deformation history and are bordered by the structures shown in **Figure 1**. Some of the most important litho-tectonic units and major structures are shown in cross sections (**Figures 2a and 2b**)

### 2.1 Geologic and tectonic aspects of the different litho-tectonic units

#### 2.1.1 Xolapa

120 The Xolapa Complex records Jurassic–Cretaceous magmatism with concurrent Upper Jurassic–  
1 121 Lower Cretaceous sedimentation followed by an intense and eastwardly diachronous Cenozoic  
2 122 magmatism. This history suggests that Xolapa corresponds to a Jurassic–Cretaceous arc and  
3 123 associated peri-arc basin (Talavera-Mendoza et al., 2013; Peña-Alonso et al., 2018). The rocks also  
4 124 record several tectono-thermal events including: i) Late Jurassic tectonic foliation development, ii) a  
5 125 pre-129 migmatization (Herrmann et al., 1994; Solari et al., 2007), iii) Paleocene–early Eocene  
6 126 migmatization and ductile to brittle deformation (Peña-Alonso et al., 2017), and iv) conspicuous  
7 127 Eocene–Oligocene sinistral shearing (Peña-Alonso et al., 2017, 2021; Kazachkina et al., 2020).  
8 128

9 129 The northern limit of the Xolapa Unit is a series of faults with ductile and brittle kinematic indicators  
10 130 such as (Las Ventas)–Tierra Colorada (Riller et al., 1992), and the Chacalapa mylonitic (Tolson,  
11 131 2005) faults (**Figures 1 and 2a**). All of these faults may represent a strand of the long-lived North  
12 132 America–Chortis plate boundary (Graham et al., 2020), and seem to be offset by the offshore  
13 133 Chipehua Fault (Sánchez-Barreda, 1981).  
14 134

#### 15 135 2.1.2 Mixteca and Oaxaca blocks

16 136  
17 137 The basement of these blocks comprises Late Mesoproterozoic gneisses and Paleozoic granitoids,  
18 138 amphibolite and metasediments (Keppie et al., 2003; Weber et al., 2010) intruded by Permian–Early  
19 139 Triassic anatectic granites. The Mixteca and Oaxaca blocks (which are separated by lithospheric  
20 140 Caltepec Fault; Elías-Herrera and Ortega-Gutiérrez, 2002) have likely behaved as a coherent crustal  
21 141 block at least since Middle Jurassic (Nieto-Samaniego et al., 2006; Peña-Alonso et al., 2017). The  
22 142 two blocks have a thick Mesozoic sedimentary cover with only limited evidence of Jurassic syn-rift  
23 143 extension (Martini and Ortega-Gutiérrez, 2018; Campos-Madrigal et al., 2013; Zepeda-Martínez et al.,  
24 144 2021), widespread Upper Jurassic shallow water deposition and a record of Early Cretaceous back-  
25 145 arc extension (Sierra-Rojas et al., 2016). On the east, the Oaxaca basement is covered by the deep-  
26 146 water Lower Cretaceous Jaltepetongo Fm. (Sierra-Rojas et al., 2020). Both blocks are covered by  
27 147 extensive Albian–Cenomanian platform deposits, as well as by a series of Coniacian to Paleogene  
28 148 clastic continental deposits. Late Cretaceous–Eocene compressional deformation is observed in both  
29 149 the Mixteca and Oaxaca blocks (Nieto-Samaniego et al., 2006; Fitz-Díaz et al., 2018; Ruiz-Arriaga,  
30 150 2018). The latter deformation is related to the so-called Mexican Orogeny, traditionally referred to as  
31 151 the Laramide Orogeny (see discussion in Fitz-Díaz et al., 2018). The Oaxaca Block is widely intruded  
32 152 by Oligocene–Miocene arc-related intrusive bodies (e.g., Ejutla Batholith) and covered by Oligo-  
33 153 Miocene volcanic rocks which locally host magmatic-hydrothermal deposits mostly of Miocene age  
34 154 (Camprubí et al., 2019). The Oaxaca Block is bounded to the East by the brittle, west-dipping normal  
35 155 Oaxaca Fault (**Figures 1 and 2a**), which is possibly a late reactivation of a structure that may have  
36 156 been associated with the Jurassic strike-slip assembly of Southern Mexico (Pindell et al., 2020a) and  
37 157 the opening of the Gulf of Mexico (Fitz-Díaz et al., 2022).  
38 158

#### 39 159 2.1.3 Sierra de Juárez Complex

40 160  
41 161 We consider the Sierra de Juárez Complex to include the crystalline rocks located along and between  
42 162 the Oaxaca Fault and the Siempre Viva Fault to the east. The Siempre Viva Fault is a major thrust  
43 163 that puts the Sierra de Juárez Complex above the Cuicateco Belt (**Figure 1**). The Sierra de Juárez  
44 164 Complex forms a ~170 km long and ~10–15 km wide migmatitic-mylonitic belt previously interpreted  
45 165 as a thrust zone reactivated by possibly dextral shearing during the opening of the Gulf of Mexico  
46 166 (Delgado-Argote, 1988; Alaniz-Alvarez et al., 1996). This complex includes a series of ortho- and  
47 167 para-gneisses that show evidence of partial migmatization and mylonitization. The metamorphic rocks  
48 168 have been separately named Sierra de Juárez Mylonitic Belt in the south (Alaniz-Alvarez et al., 1994)  
49 169 or Teotitlán Migmatitic Complex in the north (Ángeles-Moreno, 2006; Ángeles-Moreno et al. 2012).  
50 170 Most recently, they have been interpreted to share a common deformational history related to hyper-  
51 171 extension (Villagómez, 2014; Pindell et al., 2020a; Graham et al., 2020). The protoliths of the  
52 172 metamorphic rocks have Paleozoic, Neoproterozoic and Mesoproterozoic (Espejo-Bautista et al.,  
53 173 2021) ages and the rocks are intruded by Late Jurassic–earliest Cretaceous plutons (Pindell et al.,  
54 174 2020a; this work). Migmatization related to decompression has been dated at ~147–133 Ma  
55 175 (Ángeles-Moreno, 2006; Coombs, 2016; Pindell et al., 2020a) and was likely synchronous with  
56 176 mylonitization in the latest Jurassic–earliest Cretaceous (Graham et al., 2020; Pindell et al., 2020a).  
57 177

#### 58 178 2.1.4 Cuicateco Belt

59 179  
60  
61  
62  
63  
64  
65

180 The Cuicateco Belt, also known as the Juárez Terrane (Campa and Coney, 1983), includes a series  
1 181 of sub-belts located between the Siempre Viva Fault and the Valle Nacional/Soyaltepec thrusts  
2 182 (**Figure 1**). The southern region is dissected by a series of faults (e.g., Villa Alta, Vista Hermosa,  
3 183 Aloapán faults; **Figure 1**) that have brought the crystalline basement to surface levels. This deeper  
4 184 level of exposure in the southern region has removed much of the conspicuous Cretaceous–lower  
5 185 Cenozoic sedimentary cover observed in other regions of Southern Mexico. The northern region of  
6 186 the Cuicateco Belt is clearly less exhumed and preserves the so-called Cretaceous Córdoba Platform  
7 187 (Ortuño-Arzate et al., 2003).

8 188  
9 189 *Southern region:* Although poor exposure prevents a better lithological discrimination, three main sub-  
10 190 belts (Units 4a–c; **Figure 1**) can be distinguished in the southern portion of the Cuicateco Belt, which  
11 191 from west to east are (see also **Appendix 1**):

12 192 a) Paleozoic metasedimentary rocks covered by variably deformed sediments of the Todos Santos  
13 193 (Jurassic), Jaltepetongo, Chivillas (Lower Cretaceous) and Tamaulipas and Tecamalucán (mid–Upper  
14 194 Cretaceous). This sub-belt is pervasively intruded by Neogene plutons.

15 195 b) A massive sub-belt of Paleozoic schists named Mazateco Complex in the North (Ángeles-Moreno,  
16 196 2006; Ángeles-Moreno et al., 2012) and Mazatlán Complex in the South, floored by Paleozoic  
17 197 metasediments and metaigneous rocks of the Tuxtepec Complex (Ordovician maximum depositional  
18 198 age; Molina-Garza et al., 2020a).

19 199 c) A plutonic metamorphic complex that includes serpentized gabbros of the Tuxtepec Complex;  
20 200 thrust over and overlain by Jurassic Todos Santos Formation and partially covered by Lower  
21 201 Cretaceous back-arc volcanic rocks of the Xonamanca Fm.

22 202  
23 203 *Northern region* (Unit 4d; **Figure 1**): The Córdoba Platform and Zongolica fold-and-thrust belt includes  
24 204 Upper Jurassic marine strata and Lower Cretaceous back-arc volcanic and sedimentary rocks of the  
25 205 Xonamanca and Chivillas formations followed by middle Cretaceous platform deposits and Upper  
26 206 Cretaceous siliciclastic deposits (Lawton et al., 2020). All of these Mesozoic sedimentary successions  
27 207 are deformed, forming a NNW–SSE oriented fold-and-thrust belt with eastward vergence. The origin  
28 208 of this belt, also known as the Zongolica fold-and-thrust belt, is related to the Mexican Orogeny and  
29 209 occurred during Late Cretaceous and early Cenozoic time (Fitz-Díaz et al., 2018; Carfantán, 1985).  
30 210 There are a few remnants of piggy-back basins with Paleocene and Eocene clastics deposited  
31 211 between thrust carbonate rocks (Ortuño-Arzate et al., 2003).

#### 32 212 33 213 2.1.5 Veracruz Basin

34 214  
35 215 The western flank of this basin contains Cretaceous lithologies similar to those observed in the  
36 216 Córdoba platform, but the main depocenter is filled with Cenozoic foreland deposits above an  
37 217 uncertain Mesozoic stratigraphy. This is because drilling has rarely reached the Mesozoic, and some  
38 218 evolutionary models (e.g., Pindell and Kennan, 2001; 2009; Pindell et al., 2016; 2021) consider the  
39 219 eastern half of the basin as part of the Jurassic oceanic Gulf of Mexico. The Cenozoic deposits were  
40 220 dominated by deep-water submarine fans, at least until the latest Pliocene. Miocene re-activation of  
41 221 older structures is recognizable even beyond the deformation front into the western Veracruz Basin  
42 222 (**Figure 1**) and was responsible for the observed folding and thrusting beneath the coastal plain (Prost  
43 223 and Aranda, 2001; Graham et al., 2020).

#### 44 224 45 225 2.1.6 Sierra Madre Oriental

46 226  
47 227 The Sierra Madre Oriental remains one of the most prominent topographical expressions of the  
48 228 Mexican Orogeny (**Figure 1**). Folded and thrust rocks currently exposed in the Sierra Madre  
49 229 Oriental Belt include Upper Triassic through middle Eocene strata. The Sierra Madre Oriental Belt  
50 230 grew during the Mexican Orogeny as a forward propagating system from ~90 Ma to ~43 Ma (Fitz-Díaz  
51 231 et al., 2014; Gray et al., 2021). This progressive but episodic deformation started in the western  
52 232 hinterland and propagated eastwards (Fitz-Díaz et al., 2014, 2018; Gray et al., 2001, 2021) forming  
53 233 various generations of km-scale folds. The frontal region of the southern Sierra Madre Oriental  
54 234 accommodated sedimentary and tectonic overburden throughout most of Mexican Orogeny times  
55 235 (Fitz-Díaz et al., 2018).

#### 56 236 57 237 2.1.7 Tampico–Misantla Basin

58 238  
59 239  
60  
61  
62  
63  
64  
65

239 This basin corresponds to the foreland basin related to the Mexican Orogeny, although Jurassic rifts  
1 240 form its deeper parts. Maastrichtian–Eocene synorogenic turbidites were deposited in foredeep  
2 241 depocenters and onlapped topographical highs (e.g., Tuxpan Platform; Carrillo, 1980; Horbury et al.,  
3 242 2003). The turbidites, composed of siliciclastic and calcareous detritus, were overlain by post-  
4 243 orogenic Oligocene–Miocene eastward propagating sedimentary wedges. It has been a depositional  
5 244 area throughout the Cenozoic with possibly a few episodes of erosion between 30 and 10 Ma (Gray et  
6 245 al., 2021; Villagómez et al., 2019).

#### 2.1.8 Mixtequita Massif

249 Several authors (Pindell and Kennan, 2001, 2009; Nguyen and Mann, 2016) trace the landward  
11 250 expression of the East Mexico Transform (previously named Tamaulipas–Golden Lane–Chiapas fault  
12 251 by Pindell, 1985; or Western Main Transform fault by Martön and Buffler, 1994) through the Veracruz  
13 252 Basin and Tehuantepec as lying along the western side of the Mixtequita Massif (**Figure 1**). The  
14 253 metamorphic and granitic rocks located east of this fault zone (locally named the Petapa Fault;  
15 254 Molina-Garza et al., 2020a) include the Mixtequita Unit in the north (Permian and Jurassic granitoids)  
16 255 and the Guichicovi Unit in the south (Precambrian granulitic gneisses). The Mixtequita was probably  
17 256 derived from partial melting of the Guichicovi (Weber and Hecht, 2003). Both units are surrounded by  
18 257 Jurassic Todos Santos with some possible Todos Santos outliers upon them, suggesting strong  
19 258 extensional unroofing during rifting and after the partial melting (Pindell et al., 2021).

260 The northern border of the Mixtequita Block is buried beneath the southern Veracruz Basin (Pindell et  
22 261 al., 2016, 2020a) whereas the eastern border seems to be continuous with the greater Chiapas  
23 262 Massif, although beneath Cenozoic sediments (Molina-Garza et al., 2020a). The southern flank of the  
24 263 Guichicovi Block is overthrust by folded and cleaved Todos Santos, as well as by Cretaceous  
25 264 metasediments from the Chontal Complex (see below). The Mixtequita and Guichicovi units  
26 265 experienced a long history of sedimentary and tectonic burial during the Cretaceous and were  
27 266 arguably cooled and exhumed in the late Eocene (Molina-Garza et al., 2020a).

#### 2.1.9 Chontal Complex

270 Upper Cretaceous metamorphosed volcanic and basinal sedimentary rocks, possibly extruded and  
32 271 deposited in an oceanic back-arc setting (Carfantán, 1981; Pindell et al., 2011; Molina-Garza et al.,  
33 272 2020a). These rocks are interpreted as being accreted to the paleo-Pacific continental margin of  
34 273 southern Mexico, forming the so-called Chivela Nappes (**Figure 1**; Molina-Garza et al., 2020a). As  
35 274 revealed by magnetic anomalies and field mapping, the Chontal Complex is thrust tens of  
36 275 kilometres over the Mixtequita Block (Molina-Garza et al., 2020a).

277 Detrital zircon U–Pb ages from the Chontal metasediments have maximum depositional ages of 77  
39 278 Ma (Pérez-Gutiérrez et al., 2009). The rocks experienced low-grade metamorphism (Molina-Garza et  
40 279 al., 2020a) and deformation after Maastrichtian times (protolith U–Pb age of 66 Ma age; Pérez-  
41 280 Gutiérrez et al., 2009). These metamorphic rocks are partially and unconformably overlain by  
42 281 continental Oligocene–late Eocene sediments (Carfantán, 1981) of the Huamelula Fm. The  
43 282 Huamelula sediments contain Chontal-like lithologies, as well as older granite boulders (Molina-Garza  
44 283 et al., 2020a), providing a minimum age constraint for the metamorphism and accretion of the Chontal  
45 284 Complex to the Mexican margin. These relationships indicate that the Chontal rocks were  
46 285 metamorphosed to low-grade conditions and then were exhumed to surface levels by the late  
47 286 Eocene, possibly during final accretion. All the units were subsequently intruded by Miocene  
48 287 granitoids.

#### 2.1.10 Chiapas Massif and Basin

291 The Chiapas Massif is mainly composed of Permian granitoids, which intrude Upper Paleozoic  
53 292 metasedimentary rocks (Weber et al., 2006; 2007). The massif was likely detached from the  
54 293 basement of the Tampico–Misantla Basin (Tamaulipas Arch and other basement highs) in Bathonian  
55 294 times (Villagómez et al., 2019; Pindell et al., 2020a), when it began to rotate clockwise along with the  
56 295 Yucatán Block along the East Mexico Transform (**Figure 1**; Molina-Garza et al., 1992; Pindell et al.,  
57 296 2016). The Chiapas Massif has been roughly at North American paleo-latitudes since the Hauterivian.  
58 297 However, a small clockwise rotation (15–20°) has been recorded by paleomagnetic studies on

298 overlying middle Eocene strata prior to late Miocene, probably in the middle Miocene (Molina-Garza  
299 et al., 2020b).

300  
301 The Chiapas Basin developed above the southwest Yucatán Block since the Early Jurassic. Bed-  
302 plane shearing due to shortening and/or salt deformation in the Chiapas fold-and-thrust belt arguably  
303 started in the Eocene (Witt et al., 2012; Villagómez and Pindell, 2020a; Hernández-Vergara et al.,  
304 2021), although most deformation is middle Miocene to Recent (Chávez-Valois et al., 2009).  
305 Shortening in the Chiapas fold-and-thrust belt was most probably driven by the clockwise rotational  
306 translation of the Chiapas Massif, which in turn was likely caused by the onset of Cocos subduction  
307 beneath Chiapas in the wake of Chortis during middle to late Miocene times (Pindell and Miranda,  
308 2011; Pindell et al., 2020b; Graham et al., 2020; Molina-Garza et al., 2021).

309  
310 The Chiapas Massif is presently bounded to the South by the Tonalá Fault (**Figures 1 and 2b**), a sub-  
311 vertical ductile transcurrent shear zone (Molina-Garza et al., 2015, 2021), which, along with the  
312 Motagua and Baja Verapaz faults, is likely to represent major strands of the North America–  
313 Caribbean plate boundary zone (Graham et al., 2020).

#### 314 315 2.1.11 Eastern Chiapas, Chortis (mobile) and the Tehuantepec Shelf

316  
317 The geology of the southeasternmost tip of the morphological Chiapas Massif (south of the Polochic  
318 Fault) is composed of Lower Paleozoic metasedimentary rocks (Weber et al., 2008), which arguably  
319 resemble the lithologies of Chortis (**Appendix 1**). In Mexico, this tip of the Massif has been named the  
320 Huixtla Block and interpreted by Villagómez and Pindell (2020a) as more highly exhumed,  
321 allochthonous with respect to Chiapas Massif, and with a slightly older exhumation history than the  
322 rest of the massif.

323  
324 In addition, two volcanoclastic rocks obtained from the Salina Cruz-1 well offshore Tehuantepec  
325 contained consistently unimodal U–Pb ages of 88 Ma and 69 Ma (Tectonic Analysis Ltd., pers.  
326 comm., 2022, unpublished data). This shows that the dated units correspond to Upper Cretaceous  
327 volcanoclastic rocks, which are not known in autochthonous onshore areas. However, these rocks are  
328 relatively close in age with plutons observed onshore in the Huixtla Block, south of the Polochic Fault  
329 ( $64.8 \pm 1.3$  Ma; Villagómez and Pindell, 2020a), suggesting that offshore Tehuantepec Shelf and the  
330 Huixtla Block might be the western continuation or tail of the mobile Chortis Block.

### 331 332 **3 Published thermochronology in Southern Mexico**

#### 333 334 **3.1 Thermochronology basics and applications**

335  
336 Thermochronology provides information on the timing, duration and magnitude of heating and cooling  
337 events recorded by rocks (Braun et al., 2006). This information can be further used to evaluate the  
338 influence of tectonic and magmatic events, crustal or stratal exhumation of mountainous areas, basin-  
339 forming mechanisms, delivery of clastic material to sedimentary basins, as well as burial and erosion  
340 history of sedimentary basins (Armstrong, 2005). This information is therefore critical when  
341 determining the timing and possible pathways of sediments delivered to a depositional site, for  
342 instance the Gulf of Mexico.

343  
344 All isotopic systems in minerals behave as open systems if the ambient temperature is sufficiently  
345 high. In such cases, isotopes are able to rapidly partition into fluid rich phases and solid phases with  
346 lower concentrations of the solute (i.e., daughter isotope). It is reasonable to assume that daughter  
347 isotope loss is dominated by thermally activated diffusion, hence we can define a temperature range  
348 where daughter isotopes are partially retained within their lattice of origin. It is also possible to define  
349 a closure temperature (Dodson, 1973), which lies within the temperature range of daughter isotope  
350 retention and is approximately equivalent to the temperature at which more than half of the daughter  
351 isotopes are retained.

352  
353 Various geo- and thermo-chronometers with a wide range of retention temperatures are customarily  
354 employed in thermochronology in order to elucidate the thermal path of a rock within the middle and  
355 upper crust. Common methods currently used are U–Pb in zircon (closure temperatures  $>900^\circ\text{C}$ ,  
356 considered a geochronometer, and usually a proxy for zircon crystallization),  $^{40}\text{Ar}/^{39}\text{Ar}$  in a variety of  
357 mineral phases, and fission track and (U–Th)/He in zircon and apatite.

358

1 359 The closure temperature of the  $^{40}\text{Ar}/^{39}\text{Ar}$  system depends on the dated mineral phase. For instance,  
2 360 temperatures for hydrous phases such as hornblende and muscovite range between  $\sim 545\text{--}511^\circ\text{C}$  and  
3 361  $\sim 440\pm 40^\circ\text{C}$  respectively (McDougall and Harrison, 1999; Harrison et al., 2009). The retention  
4 362 temperatures of radiogenic  $^{40}\text{Ar}$  are lower in K-feldspar, ranging from  $\sim 350^\circ\text{C}$  to  $\sim 150^\circ\text{C}$  (Lovera et al.,  
5 363 1991).

6 364  
7 365 Other methods that are relevant to this study include the following: zircon fission track (ZFT), zircon  
8 366 (U–Th)/He, apatite fission track (AFT) and apatite (U–Th)/He, which provide thermal information on  
9 367 temperatures between  $\sim 290\text{--}210^\circ\text{C}$ ,  $\sim 200\text{--}130^\circ\text{C}$ ,  $\sim 120\text{--}60^\circ\text{C}$  and  $\sim 90\text{--}40^\circ\text{C}$ , respectively (Bernet  
10 368 and Garver, 2005; Wolfe and Stockli, 2010; Ketcham et al., 2007; Farley, 2002).

### 11 369 **3.2 Published high- and medium-temperature thermochronological data in southern Mexico**

12 370  
13 371 Except for a few thermochronological studies focusing on Oaxaca/Mixteca (e.g., Vega-Granillo et al.,  
14 372 2007; Kirsch et al., 2014), Xolapa (Morán-Zenteno et al., 1996), the Sierra Madre Oriental (e.g., Fitz-  
15 373 Díaz et al., 2014, 2018) the Sierra Juárez Complex (Delgado-Argote et al., 1992; Ángeles-Moreno,  
16 374 2006), and the Chiapas Massif and Basin (Villagomez and Pindell, 2020a; Hernández-Vergara et al.,  
17 375 2021; Fitz-Díaz et al., 2022), many uncertainties remain on the significance of the high- and medium-  
18 376 temperature thermochronological information (e.g., multi-phase  $^{40}\text{Ar}/^{39}\text{Ar}$ ).  
19 377

20 378  
21 379 The most reliable and robust thermochronological data obtained in Sierra Juárez Complex were  
22 380 presented by Ángeles-Moreno (2006) and they correspond to undisturbed plateau  $^{40}\text{Ar}/^{39}\text{Ar}$  ages in  
23 381 muscovite (closure temperature of  $\sim 440\pm 40^\circ\text{C}$ ; Harrison et al., 2009) from three metamorphic rocks  
24 382 collected south of Tehuacán (one granitic gneiss, one granitic dike and one white mica schist). The  
25 383 muscovite  $^{40}\text{Ar}/^{39}\text{Ar}$  ages are indistinguishable within error and range from 130 Ma to 133 Ma. A fourth  
26 384 hornblende  $^{40}\text{Ar}/^{39}\text{Ar}$  age from a migmatitic gneiss from the same Sierra de Juárez Complex yielded  
27 385 an age ( $\sim 144$  Ma) which is older than its zircon U–Pb age (140 Ma; Ángeles-Moreno, 2006),  
28 386 suggesting that excess argon was present in the hornblendes (making the  $^{40}\text{Ar}/^{39}\text{Ar}$  age suspect).  
29 387

30 388 Hornblende  $^{40}\text{Ar}/^{39}\text{Ar}$  ages obtained by Delgado-Argote et al. (1992) from three granitoid rocks  
31 389 collected from the road between Teotitlán and Vigastepec yielded slightly disturbed spectra (showing  
32 390 excess  $^{40}\text{Ar}$  in the initial steps). Ages from the two less disturbed samples suggest that the rocks were  
33 391 cooled at the closure temperature of hornblende between 132 Ma and 134 Ma. All white mica and  
34 392 hornblende ages range from  $\sim 134$  Ma and  $\sim 130$  Ma, which undoubtedly indicates a regional period of  
35 393 rapid cooling during Hauterivian time in the western Cuiccateco Belt.  
36 394

### 37 395 **3.3 Published low-temperature thermochronological data in Mixteca/Oaxaca, Xolapa, Chiapas** 38 396 **and Chortis**

39 397  
40 398 There are a few reliable AFT and apatite U–Th/He data from the Mixteca and Oaxaca blocks. The  
41 399 Xolapa Block, on the contrary, has been extensively studied by a number of authors (e.g., Ducea et  
42 400 al., 2004; Shoemaker et al., 2004; Villagómez and Pindell, 2020b) and summarized in Villagómez and  
43 401 Pindell (2020b). The latter authors sampled for AFT and apatite and zircon (U–Th)/He a number of  
44 402 Eocene and older rocks along the whole extension of the Xolapa Block across three main traverses  
45 403 between Acapulco and Puerto Angel (**Figure 3**). Their thermochronological results yielded a clear  
46 404 eastward-younging trend with thermal models constraining cooling between  $\sim 32\text{--}20$  Ma in the west  
47 405 (Acapulco location) and  $\sim 19\text{--}11$  Ma in the east (Puerto Angel location). Villagómez and Pindell  
48 406 (2020b) demonstrated that cooling along the present-day Pacific margin was eastwardly diachronous.  
49 407 These authors explained cooling as a consequence of erosional exhumation with moderate  
50 408 exhumation rates of around 0.3 to 0.6 km/My during the previously mentioned periods of time.  
51 409

52 410 Apatite Fission Track and U–Th/He cooling ages from the Chiapas Massif are mostly middle and late  
53 411 Miocene (Witt et al., 2012; Villagómez and Pindell, 2020a). The last and main period of cooling and  
54 412 exhumation observed in the northwestern and central portions of the Chiapas Massif probably started  
55 413 at around 10–8 Ma (Villagómez and Pindell, 2020a). Exhumation rates in these regions range from  
56 414 0.7 to 0.4 km/My. The easternmost tip of the morphological Chiapas Massif (South of the Polochic  
57 415 Fault; an area that shows a geology which greatly resembles part of the Chortis Block) started to cool  
58 416 earlier (at 15–14 Ma) than the rest of the Chiapas Massif ( $<10$  Ma; Villagómez and Pindell, 2020a).  
59 417 This middle Miocene cooling is relevant because it was obtained from rocks that are located away  
60 418



418 from thermal influences of Miocene magmatism emplaced along the Tonalá Shear Zone. Villagómez  
1 419 and Pindell (2020a) considered this block (so-called the Huixtla Block, south the Polochic Fault) to be  
2 420 part of the tail of the Chortis block rather than part of the Chiapas Massif.

3 421  
4 422 Although it has not been thoroughly studied, there are a few publications that have dealt with  
5 423 thermochronological aspects of the Chortis Block in Central Guatemala, in particular from the  
6 424 Chuacús and Las Ovejas complexes (e.g., Ratschbacher et al., 2009; Simon-Labric et al., 2013).  
7 425 These regions are allochthonous with respect to present-day Guatemala (Solari et al., 2013).  
8 426 Published zircon U–Th/He and Ar–Ar data from the Chuacús Complex (north of the Motagua Fault  
9 427 and south of the Polochic Fault; **Figure 7a**) record early Paleocene–early Miocene cooling ages  
10 428 (Ratschbacher et al., 2009; Simon-Labric et al., 2013). In addition, zircon U–Th/He and AFT cooling  
11 429 ages from Las Ovejas Complex (south of the Motagua Fault; **Figure 7a**) suggest the region  
12 430 experienced cooling from 40 Ma to 10 Ma (Ratschbacher et al., 2009; Simon-Labric et al., 2013).  
13 431 Overall, these data suggest that the northern complexes of Chortis (Chuacús and Las Ovejas) cooled  
14 432 and were exhumed from early Paleocene to late Miocene, and possibly are still being exhumed today  
15 433 (Brocard et al., 2020).

### 16 434 17 435 **3.4 Published thermochronological data in the southernmost Sierra Madre Oriental Belt and** 18 436 **the northern Cuicateco Belt (eastern Córdoba platform)**

19 437  
20 438 The Sierra Madre Oriental has been considerably studied for thermochronology and the data show  
21 439 that the Mexican Orogeny deformation possibly started at ~90 Ma in the hinterland (western foothills)  
22 440 and at ~50 Ma along the eastern edge of the belt (Fitz-Díaz et al., 2014, 2018; Gray et al., 2001;  
23 441 2021). This generally forward propagating system during the Mexican Orogeny saw the development  
24 442 of a syn-tectonic basin above the eastern toe of the active belt. This basin in the northern Sierra  
25 443 Madre Oriental (called Mayrán Basin by Gray et al., 2021) was buried and heated older rocks until at  
26 444 least ~40 Ma, when it was finally inverted. This inversion caused quick erosion of the basin, providing  
27 445 detrital material first eastward into the Gulf of Mexico, then southward toward the Tampico–Misantla  
28 446 Basin. The youngest (Oligocene–Miocene, post-Mexican Orogeny) compressional features affected  
29 447 pre-Miocene sedimentary units and are mainly observed in the adjacent foreland region (not in the  
30 448 interior parts of the fold belt; Gray et al., 2001). An interpreted northward-younging diachronous uplift  
31 449 and deformation during Oligocene–Miocene time along the length of the Sierra Madre Oriental is  
32 450 plausible from the thermochronological data (Gray et al., 2001).

33 451  
34 452 Farther to the south, in the northern Cuicateco Belt (the Sierra de Zongolica s.s./Córdoba platform)  
35 453 only two AFT ages have been published (Gray et al., 2001). The AFT pooled ages were obtained  
36 454 from Santonian–Campanian sediments and yielded a partially reset age of  $74 \pm 7$  Ma and a fully reset  
37 455 age of  $33 \pm 2$  Ma. Fluid-inclusion homogenization temperatures suggest that the sample with the  
38 456 younger age was buried and heated above  $130^\circ\text{C}$ , due to burial, prior to final exhumation. The older  
39 457 aged sample was probably not buried enough and recorded detrital AFT information (Gray et al.,  
40 458 2001).

## 41 459 42 460 **4 New geochronological and thermochronological data**

43 461  
44 462 We have obtained 15 new geochronological ages (zircon U–Pb), two new K-feldspar  $^{40}\text{Ar}/^{39}\text{Ar}$  ages,  
45 463 13 new AFT ages, one new ZFT age, four new apatite (U–Th)/He and 14 new zircon (U–Th)/He ages  
46 464 (**Figure 3** and **Tables 1–6**). We have also reinterpreted AFT age data from four samples in the  
47 465 Tampico–Misantla Basin and 17 samples in the Cuicateco Belt published by Gray et al. (2021),  
48 466 considering the new geo and thermochronological data obtained in this work. The details of the  
49 467 methodologies used in this study are shown in **Appendix 2**. All the age results are shown in **Tables**  
50 468 **1–6** and are grouped according to the litho-tectonic units described in **Figure 3**.

51 469  
52 470 We have also run a controlled random search procedure (HeFTy; Ketcham, 2012) to identify thermal  
53 471 histories that closely match our medium- and low-temperature thermochronological analytical data  
54 472 within certain statistical parameters by using an inverse modelling procedure (Ketcham, 2005;  
55 473 Ketcham et al., 2007). By doing so, we have created time–Temperature paths (**Figures 4a and 4b**)  
56 474 that help us to identify periods of cooling and heating in southern Mexico described below.

### 57 475 58 476 **4.1 Mixteca and Oaxaca blocks**

59 477  
60  
61  
62  
63  
64  
65

478 We have obtained a few AFT ages in western Mixteca Block ranging from 62.4 Ma and 83.2 Ma  
1 479 (**Figure 3; Table 3**). Dated lithologies include low-grade metamorphosed and deformed sediments of  
2 480 the Cosoltepec Fm. of the Paleozoic Acatlán Complex (DH-23-12-3-11; DH-24-12-3-11) and fine-  
3 481 grained volcanoclastic sandstones of the Upper Paleozoic Olinalá Fm. (DH-22-12-3-11). Although the  
4 482 rocks did not yield enough AFT length information required for thermal modelling, consistent  
5 483 Campanian to early Paleocene AFT ages suggest that western Mixteca experienced cooling during  
6 484 the Mexican Orogeny.

7 485  
8 486 Samples located farther to the east and close to the Oaxaca Fault (gneiss 18-01-18-01 covered by  
9 487 Jaltepetongo Fm.) record continuous heating from Early Cretaceous through the latest Cretaceous  
10 488 with cooling starting only at about 60 Ma (**Figure 4a**). We have also obtained zircon U–Pb from  
11 489 intrusive and volcanic rocks in central Oaxaca (samples 17-01-18-01, 17-01-18-04, 17-01-18-05, 17-  
12 490 01-18-06; **Table 1**). These crystallization ages span 33 Ma to 23 Ma, which attest to a continued  
13 491 Oligocene–early Miocene magmatism that has undoubtedly affected the Miocene paleo-geothermal  
14 492 gradient south of Oaxaca City (**Figure 3**). Thermal models from one Jaltepetongo Fm. sandstone (17-  
15 493 01-18-03) intruded by the Oligo–Miocene granites yielded middle Miocene elevated cooling rates  
16 494 (**Figure 4a**).

#### 17 495 18 496 **4.2 Sierra Juárez Complex (high and medium temperature data)**

19 497  
20 498 Alkali-feldspar from two orthogneiss samples 5-11-11-02A (zircon U–Pb age of  $158 \pm 13$  Ma, Pindell et  
21 499 al., 2020a) and 5-11-11-03A (zircon U–Pb age of  $137.2 \pm 2.2$ ; Coombs, 2016) collected approximately  
22 500 50 km SE of the city of Tehuacán (**Figure 3**) were dated by  $^{40}\text{Ar}/^{39}\text{Ar}$ . Both samples present excess  
23 501  $^{40}\text{Ar}$  at the initial steps (sample 5-11-11-03A presents higher percentage of excess  $^{40}\text{Ar}$  based on a  
24 502 more defined U-shaped spectrum; **Figure 5a**). Alkali-feldspar from sample 5-11-11-03A consequently  
25 503 presents a more disturbed spectrum with one hump at approximately 40% of the  $^{39}\text{Ar}$  released. In  
26 504 contrast, sample 5-11-11-02A shows a more consistent stair-like spectrum with the younger reliable  
27 505 single step ages ranging from  $90 \pm 9$  Ma to  $133 \pm 5$  Ma (2-sigma error; **Figure 5a; Table 2**). We  
28 506 consider the latter as a more representative and less disturbed sample.

29 507  
30 508 Higher temperature domains (closure temperature of  $\sim 350^\circ\text{C}$ ) within the K-feldspar yielded a single-  
31 509 step age of  $133 \pm 5$  Ma (5-11-11-02A), which overlaps within error with muscovite and hornblende  
32 510  $^{40}\text{Ar}/^{39}\text{Ar}$  ages of 134–130 Ma, previously reported by Ángeles-Moreno (2006) and Delgado-Argote et  
33 511 al. (1992). This reinforces the idea that the K-feldspar age data successfully complement the thermal  
34 512 history of the region at least since  $\sim 130$  Ma.

35 513  
36 514 Alkali-feldspars degassed by step heating with a  $\text{CO}_2$ –IR laser arguably provide a semi-quantitative  
37 515 thermal history of the sample within the zone of partial  $^{40}\text{Ar}$  retention (see discussion in Villagómez et  
38 516 al., 2019). Age spectra show that there might be some excess  $^{40}\text{Ar}$  at the initial steps, but alkali-  
39 517 feldspar from crystalline samples from the Sierra de Juárez Complex record a slow protracted cooling  
40 518 from  $\sim 130$  Ma to  $\sim 90$  Ma (**Figure 5a**).

#### 41 519 42 520 **4.3 Sierra Juárez Complex (low-temperature data)**

43 521  
44 522 Orthogneiss 5-11-11-02A and migmatitic orthogneiss 5-11-11-03A from the Teotitlán Migmatitic  
45 523 Complex (northern Sierra de Juárez Complex) were also dated by AFT yielding indistinguishable ages  
46 524 within error ( $51.9 \pm 5.6$  Ma and  $57.2 \pm 6.0$  Ma, respectively; **Table 3**). Apatite (U–Th)/He was obtained  
47 525 from one sample (5-11-11-02A) and yielded a weighted mean age of  $16.4 \pm 0.5$  Ma (**Table 4**). Inverse  
48 526 thermal modelling using AFT data and Apatite (U–Th)/He in both samples shows similar patterns. The  
49 527 good solutions and best-fitting thermal models (**Figure 4a**) show: i) an onset of moderate cooling in  
50 528 the latest Cretaceous–Paleocene, lasting until about 50 Ma as observed in the best constrained  
51 529 model; ii) that there is no evidence of significant late Eocene–early Miocene cooling in those rocks;  
52 530 and iii) a renewed cooling at about 10 Ma.

#### 53 531 54 532 **4.4 Cuicateco Belt**

##### 55 533 56 534 4.4.1 West of Villa Alta and Aloapán faults, East of Siempre Viva Fault

57 535 We dated a number of samples for thermochronology including deformed/low-grade metamorphosed  
58 536 Jurassic sediments (Todos Santos-like units) and Cretaceous sedimentary rocks (Jaltepetongo Fm.),  
59 537 which are conspicuously intruded by Oligo–early Miocene plutons. In order to precisely determine the  
60 538

538 timing of Cenozoic magmatism, we dated two San Juan Juquila plutons, which yielded U–Pb zircon  
539 crystallization ages of 17.3–17.5 Ma (**Table 1**). We also dated by zircon U–Th/He an undeformed  
540 dacitic porphyry (26Feb16-6B) collected near the locality of Las Animas, which gave a middle  
541 Miocene crystallization age (15.7 Ma; **Table 5**).

542  
543 All the thermal models show that the Jurassic and Cretaceous rocks (16-01-18-05A; 16-01-18-08A;  
544 16-01-18-09A; 18-01-18-03; 26Feb16-7A) were continuously heated after deposition to temperatures  
545 above ~120°C until about 30–20 Ma, after which they were finally cooled (**Figure 4a**).

#### 547 4.4.2 Between Villa Alta/Aloapán and Vista Hermosa faults (Mazateco Complex)

548 We modelled AFT age data published by Gray et al. (2021), including new apatite and zircon U–  
549 Th/He data (**Tables 3–5**). The new thermal models from Paleozoic metamorphic rocks, as well as  
550 from Todos Santos red beds, show cooling starting at 45 Ma and continuing through the latest  
551 Miocene (**Figure 4a**). The best constrained sample is a low-grade Paleozoic metamorphic rock (21-  
552 01-18-01), which included AFT, apatite and zircon U–Th/He constraints. Its thermal model shows that  
553 the rocks experienced continuous cooling possibly from 45 Ma, with probable pulses after 10 Ma. The  
554 late Eocene onset of cooling is also supported by a different Paleozoic sample (21-01-18-04), which  
555 yielded a ZFT age of 40.6 Ma (**Table 6**). This continuous cooling starting in the middle Eocene is also  
556 recorded in red beds from the Todos Santos Fm. (27Feb16-3B), which yielded early Oligocene zircon  
557 U–Th/He cooling ages (**Table 5**).

#### 559 4.4.3 Between Vista Hermosa and Valle Nacional faults

560 Two Jurassic sandstones from the Todos Santos (20-01-18-08 and 19-01-18-10) and a Cretaceous  
561 litharenite from the Xonamanca Fm. (19-01-18-06) yielded AFT ages of 27.6 Ma and 19.7 Ma.  
562 Samples of similar lithologies (27Feb16-4B and 27Feb16-5B) were dated by zircon U–Th/He but they  
563 yielded partial reset ages with uninterpretable discordant single grain ages (**Table 5**). This points out  
564 that the region never reached sufficient temperatures to fully reset the zircon U–Th/He system  
565 (~200°C). Nonetheless, the AFT modelling suggests that samples were heated since deposition until  
566 about 35 Ma, when they were subsequently cooled (**Figure 4a**).

### 568 **4.4 Remodelling of published data from the Tampico–Misantla Basin**

569 We have dated detrital zircons (DZ) for U–Pb from a number of Chicontepec sandstones (COAP17-1,  
570 SANT17-2A, SANT17-2B, SFRAN17-1; **Table 1**) and our results consistently indicate that the basal  
571 Chicontepec has a Paleocene maximum depositional age, while middle and upper Chicontepec  
572 members have lower Eocene maximum depositional ages. We modelled the Time–temperature  
573 history from key samples (COAP17-1, ACAT17, SANT17-1, ALTO17-2; **Figure 3**) also reported in  
574 Gray et al. (2021). Our models (**Figure 4b**) show an eastward younging trend in both heating and  
575 cooling in the region, in line with Gray et al. (2021) interpretation. The most relevant samples are  
576 described below.

#### 579 4.4.1. Samples located close to the Sierra Madre Oriental fold-thrust-belt

580 Lower Chicontepec samples located close to the Sierra Madre Oriental fold-thrust-belt were heated  
581 after deposition to 100°C (probably even to 120°C) and started cooling between 45 Ma and 25 Ma  
582 according to Gray et al. (2021). The middle Chicontepec sample ACAT17 shows minor reworking and  
583 includes sub-angular carbonate and volcanic clasts rich in euhedral zircons, which suggests that a  
584 large component of the grains were sourced from a proximal, contemporaneous volcanic source. It is  
585 very likely that the middle Chicontepec units experienced only some partial thermal resetting  
586 (temperatures above 60°C but below ~120°C) after deposition based on its AFT length distribution.  
587 Since then, the sample underwent final cooling in mid Miocene time, as suggested by the U–Th/He  
588 data.

#### 590 4.4.2 Samples from more central regions of the Tampico–Misantla Basin

591 Thermal models from basal Chicontepec samples (COAP17-1), as well as older samples, such as a  
592 Cretaceous breccia straddling the K/T boundary (SANT17-1) and the Jurassic Cahuasas red-beds  
593 (ALTO17-2) show cooling in the late Oligocene–Miocene. The pre-Chicontepec units were heated  
594 enough to reset the AFT system (temperatures above 120°C) but not enough to reset the zircon U–  
595 Th/He age (temperatures below ~200°C; see sample SANT17-1).

### 597 **4.5 Guichicovi and Mixtequita blocks**

598

1 599 We dated one Mixtequita Permian granitoid (27Mar17-3A) by a number of methods in order to unravel  
2 600 the thermal history of this block. The granitoid yielded a zircon U–Th/He age of 108.6 Ma, AFT age of  
3 601 42 Ma, and apatite U–Th/He age of 8.2 Ma. The Jurassic Todos Santos Fm. was deposited on the  
4 602 flanks of the Guichicovi and Mixtequita blocks, indicating that this sample was located near the  
5 603 surface in the Jurassic. The composite thermal models (**Figure 4b**) suggest that the rocks reached  
6 604 temperatures of around 180°C prior to mid Cretaceous. The Mixtequita granitoid was subsequently  
7 605 cooled from ~70 Ma through 30 Ma, with increased cooling rates from 10 Ma to Present.  
8 606

9 607 On the other hand, samples from the Guichicovi Block experienced a different Cenozoic thermal  
10 608 history than that of the Mixtequita Block. Precambrian Guichicovi metasediments (26Mar17-3A and  
11 609 26Mar17-5A) yielded zircon U–Th/He cooling ages ranging from 31 Ma and 43 Ma. A different  
12 610 Guichicovi sample (Precambrian granulitic gneiss 19-07-04-1) yielded an AFT age of 23 Ma. All U–  
13 611 Th/He ages and the AFT thermal model (**Figure 4b**) suggest that the Guichicovi samples were heated  
14 612 prior to Middle Eocene and it was subsequently cooled during the late Eocene–Miocene (with  
15 613 increased rates from ~27 Ma till ~16 Ma).  
16 614

#### 17 615 **4.6 Chontal Complex (Western Tehuantepec)**

18 616  
19 617 We sampled for AFT (**Table 3**) a few middle Miocene plutons (U–Pb crystallization ages presented in  
20 618 Pindell et al., 2020b) in the western Tehuantepec region, as well as one Cretaceous phyllite (19-07-  
21 619 03-2B) from a complex lithodeme south of the Chivela Nappe. The thermal modelling systematically  
22 620 shows that all samples in Western Tehuantepec were cooled from ~15 Ma with increased rates of  
23 621 cooling from ~10–7 Ma to the Present (**Figure 4b**).  
24 622

#### 25 623 **4.7 Chiapas Massif**

26 624  
27 625 One porphyritic granite (19-07-05-4) located in westernmost Chiapas Massif yielded an AFT age of  
28 626 8.3 Ma (**Table 3**), attesting to late Miocene–Recent cooling. Moreover, one Triassic migmatite  
29 627 (25Mar17-1A) and one Triassic granitoid (27Mar17-2A) yielded a zircon U–Th/He and apatite U–  
30 628 Th/He age of 7.7 Ma and 13.3 Ma, respectively (**Table 5**). The two samples are located approximately  
31 629 150 km apart (**Figure 3**), and these ages suggest an important middle to late Miocene cooling event.  
32 630

### 33 631 **5 Interpretation and discussion**

34 632  
35 633 Heating and cooling periods constrained by our data are related to burial and exhumation (either  
36 634 erosional or tectonic) or to advective heat transfer (e.g., thermal relaxation due to in-situ or nearby  
37 635 magmatism). We use the term erosional exhumation to mean vertical upward movement of rocks with  
38 636 respect to the Earth's surface, representing a reduction of overburden due to erosion (England and  
39 637 Molnar, 1990; Braun et al., 2006).  
40 638

41 639 Several regions, such as the easternmost outcrops of the Oaxaca Block and the westernmost  
42 640 Cuicateco sub-belts (south of Villa Alta and Aloapán faults) are extensively intruded by Oligo–  
43 641 Miocene magmatic rocks and affected by hydrothermal fluids (Camprubí et al., 2019; and references  
44 642 therein). We consider the Cenozoic heating observed in some host rocks in the previously mentioned  
45 643 regions to be a consequence of advective heat transfer from the plutons, leaving the pre-Oligocene  
46 644 thermal history nearly completely erased. Similarly, we treat the observed cooling from these two  
47 645 regions with a degree of scepticism, as Miocene cooling might record sub-solidus thermal relaxation  
48 646 following the emplacement of the plutons (see for instances sample 17-01-18-06 Ejutla pluton, which  
49 647 yielded zircon U–Pb and apatite fission track ages that are similar within error).  
50 648

#### 51 649 **5.1 Sierra de Juárez Complex and the Cuicateco Belt**

##### 52 650 **5.1.1 Pre-Mexican Orogeny**

53 651  
54 652  
55 653 Muscovite and hornblende  $^{40}\text{Ar}/^{39}\text{Ar}$  data suggests that the migmatitic–mylonitic rocks of the Sierra de  
56 654 Juárez Complex were cooled at extremely fast rates during Hauterivian (~134–130 Ma) until ~350–  
57 655 300°C. Alkali-feldspar  $^{40}\text{Ar}/^{39}\text{Ar}$  data show that migmatites subsequently cooled slowly from the  
58 656 Barremian and reached temperatures of ~150°C by ~90 Ma. This indicates that the migmatites were  
59 657  
60  
61  
62  
63  
64  
65

657 not exposed at surface levels when the Lower Cretaceous Chivillas Fm. was deposited in the northern  
1 658 Cuicateco Belt.

2 659  
3 660 Any model on the tectonics of Sierra de Juárez Belt should explain the existence of these mid-crustal  
4 661 rocks (migmatites and mylonites) and their emplacement into higher crustal levels at extremely fast  
5 662 rates during the Hauterivian. The two existing models, Ángeles-Moreno (2006) and Mendoza-Rosales  
6 663 et al. (2010), do not explain the quick exhumation of mid-crustal rocks of the Sierra de Juárez  
7 664 Complex. It would be unlikely for mid-crustal rocks to be elevated in multiple small pull-apart basins  
8 665 (Ángeles-Moreno 2006), or along a transform margin (Mendoza-Rosales et al., 2010) to expose the  
9 666 migmatites and mylonites to nearly the surface, while allowing the deposition of the overlying Lower  
10 667 Cretaceous Chivillas Fm. in such a short period. Our K-feldspar  $^{40}\text{Ar}/^{39}\text{Ar}$  data show, in fact, that the  
11 668 migmatites from the Sierra de Juárez Complex only reached the 150°C-isotherm (~5 km depth) in the  
12 669 Late Cretaceous (~90 Ma), meaning that these rocks were not close to the surface during most of the  
13 670 Cretaceous.

14 671  
15 672 The Hauterivian cooling in migmatitic rocks cannot be solely a consequence of magmatic cooling  
16 673 because there was an ongoing tectonic deformation (shearing and deformation D2 of Ángeles-  
17 674 Moreno, 2006), along with a decrease of the metamorphic grade (amphibolitic to greenschist facies;  
18 675 Ángeles-Moreno, 2006). The only mechanism fast enough to allow quick cooling (from ~550°C to  
19 676 350°C, during ~134–130 Ma) concurrent with the observed deformation is tectonic unroofing on low-  
20 677 angle detachment faults during regional-scale extension, perhaps in a similar way to metamorphic  
21 678 core complexes (Lister and Davis, 1989). However, the orientation of the stretching lineation in the  
22 679 mylonites indicates N–S shear on west-dipping planes, pointing to sinistral transtension as the driver  
23 680 (Graham et al., 2020). The fast cooling (from ~134 Ma through ~130 Ma) indicates large-scale hyper-  
24 681 transtension possibly accompanied with retrograde metamorphism (**Figures 5b and 6**).

25 682  
26 683 Syn-extensional supra-detachment basins usually develop above the exposed detachment surface  
27 684 (Friedmann and Burbank, 1995; Gawthorpe and Leeder, 2000), and they are probably represented by  
28 685 the Jaltepetongo Fm. and possibly by the basal units of the Chivillas Fm. (Graham et al., 2020). While  
29 686 the migmatitic rocks exposed in the north possibly did not reach the surface during the stretching  
30 687 process, our field evidence suggests that the mylonitic rocks (mainly proto-mylonites) exposed in the  
31 688 south possibly reached surface levels in the Early Cretaceous, based on clasts observed in the  
32 689 Jaltepetongo Fm. Nevertheless, it appears that the quick stretching process decelerated drastically by  
33 690 ~130 Ma (**Figures 5b and 6**).

34 691  
35 692 Subsequently, slower but protracted cooling from ~130 Ma to ~90 Ma in the Sierra Juárez Complex  
36 693 was contemporaneous with more stable platform and basinal depositional conditions in the northern  
37 694 Cuicateco area, and in particular the Córdoba Platform. This precludes any possibility of an important  
38 695 exhumation phase between ~130 Ma and ~90 Ma. We propose that the thermal relaxation of the crust  
39 696 (lowering of the geothermal gradients) that followed the high thermal (migmatization at ~147–134 Ma)  
40 697 and the rapid extensional (~134–130 Ma) events was responsible for overall basement cooling  
41 698 (**Figure 5b and 6**). This cooling accompanied long wavelength thermal subsidence of the Cuicateco  
42 699 Belt and probably the neighbouring Oaxaca Block during the middle and Late Cretaceous. Thermal  
43 700 relaxation and cooling probably lasted >40 My (as shown by the feldspar  $^{40}\text{Ar}/^{39}\text{Ar}$  data) and reflect a  
44 701 slow decay of geothermal gradients in the mid–upper crust. Net cooling was not greatly affected by  
45 702 the moderate sediment burial that accompanied the subsidence itself in quasi-stable conditions  
46 703 (maximum thickness of 2 km of middle–Upper Cretaceous carbonate platform). Depositional burial  
47 704 lasted until the Maastrichtian, when samples from the Sierra de Juárez Complex began to be cooled  
48 705 further during Mexican Orogeny-related exhumation.

### 50 706 51 707 **5.1.2 Syn-Mexican Orogeny**

52 708  
53 709 Thermochronological data from the basement rocks of the Sierra de Juárez Complex show that  
54 710 cooling probably started as early as Maastrichtian (**Figure 4a**) with increased rates (~5°C/My)  
55 711 observed during ~60–50 Ma. Cooling was likely driven by erosional exhumation and this produced  
56 712 contemporaneous foredeep sediments that were deposited to the east and fed the Veracruz Basin. If  
57 713 we convert cooling into exhumation assuming a normal geothermal gradient of 30°C/km, then it is  
58 714 estimated that this hinterland region exhumed at low rates of ~0.2 km/My during the early Paleocene–  
59 715 middle Eocene.

717 There is no evidence of the late Eocene exhumation within the Sierra de Juárez Complex (**Figure 6**),  
718 in contrast to the Mazateco Complex (this work) and the foreland Veracruz Basin (Gray et al., 2001).  
719 This may suggest that the deformation and exhumation migrated in-sequence as thrusting propagated  
720 eastwards, away from the Sierra de Juárez Complex.

721  
722 Mexican Orogeny-related thrusting and deformation in the Sierra de Juárez Complex appears to have  
723 continued to slightly younger times (early Paleocene–middle Eocene) than compressional  
724 deformation observed in other regions (**Figure 6**) such as in the Mixteca and Oaxaca blocks  
725 (Campanian–early Paleocene; this work) and the Guerrero–Morelos platform (Latest Cretaceous;  
726 Nieto-Samaniego et al., 2006; Ruiz-Arriaga, 2018). Although the direction of shortening during the  
727 Mexican Orogeny may be variable (E–W in the Guerrero–Morelos platform and NE–SW in the  
728 Zongolica fold-and-thrust belt), there is a slight eastward migration of the deformation as proposed by  
729 Nieto-Samaniego et al. (2006). It seems that regional deformation was preferentially partitioned along  
730 the main basement structures within the Cuicateco Belt.

731  
732 Exhumation of the Mazateco Complex (sub-belt 4b in **Figure 1**) from samples near the Vista Hermosa  
733 Fault began in the middle Eocene (~45 Ma) and lasted through the latest Miocene. This exhumation  
734 phase is not observed in the hinterland region (Sierra de Juárez Complex). This delayed cooling  
735 compared with the western hinterland regions supports the idea that Mexican Orogeny related-  
736 exhumation propagated eastwards.

737  
738 Rocks from the easternmost Cuicateco belt (sub-belt 4c in **Figure 1**) were most likely heated due to  
739 sedimentary burial (possibly in a foredeep setting) and/or thrust imbrication until about 35 Ma, when  
740 they were finally cooled (due to tectonic uplift and erosional exhumation) and brought to present-day  
741 surface levels. We envisage that the Cenozoic heating of sub-belt 4b and 4c (**Figure 4b**) involved  
742 development of piggy-back basins and imbrication of nappes as a consequence of the Mexican  
743 Orogeny compressional deformation, mostly eroded today. Most of the Cretaceous–Paleogene  
744 sedimentary pile was eroded from ~35 Ma onwards in sub-belt 4c (**Figure 4b**). This suggests that the  
745 first stages of the Mexican orogenesis in the Cuicateco Belt led to the development of a topography  
746 dominated by folding, thrusting and nappe piling, while the erosional exhumation phase in the  
747 easternmost Cuicateco sub-belt came at the very end of the Mexican Orogeny (**Figure 6**) and it was  
748 probably renewed in Miocene times (see below).

749  
750 Cretaceous sediments from the Córdoba Platform (sub-belt 4d) record Oligocene AFT ages that are  
751 fully reset (reaching  $T > 130^{\circ}\text{C}$ , Gray et al., 2001). This resetting suggests that either sediment  
752 accumulation in the foreland was thicker than the present-day preserved section or, alternatively,  
753 thrust stacking provided significant tectonic burial prior to the Oligocene. It is likely that migration of  
754 deformation towards the Zongolica foreland occurred only after the Eocene and was possibly  
755 responsible for partial erosion of the early Mexican Orogeny molasse (Gray et al., 2001).

756  
757 It is worth noting that the amount of exhumation in the Mazateco Complex (sub-belts 4b and c) was  
758 higher than in the northern regions of the Cuicateco Belt such as the Zongolica Belt/Córdoba platform  
759 (sub-belt 4d). This might imply steeper thrust ramps or greater shortening toward the south, the latter  
760 of which could suggest minor anti-clockwise rotation of the thrusts during shortening.

### 761 762 **5.1.3 Post Mexican Orogeny**

763  
764 The high-angle Oaxaca (normal) Fault (**Figure 1**) started to grow and propagate in the Oligocene  
765 (Nieto-Samaniego et al., 2006; Dávalos-Álvarez et al. 2007) down-dropping the Oaxaca Block as a  
766 hanging-wall relative to the Cuicateco Belt. This extension also formed several grabens on the  
767 Oaxaca Complex during the Oligo–Miocene (Nieto-Samaniego et al., 2006). It is impossible to  
768 quantitatively determine the amount of exhumation experienced in the westernmost sub-belt of the  
769 Cuicateco (sub-belt 4a) during Oligo–Miocene times given the conspicuous presence of Oligocene–  
770 early Miocene plutons in the region (Camprubí et al., 2019; and references therein). Given that these  
771 plutons east and south of Oaxaca City are currently exposed at surface, we estimate that this region  
772 experienced at least 4–5 km (plausible pluton emplacement depths) of exhumation since the middle  
773 Miocene (approx. 16 Ma).

774  
775 On the other hand, the easternmost Cuicateco Belt (sub-belt 4c) underwent exhumation since the  
776 early Oligocene, probably peaking in the early–middle Miocene. This was contemporaneous with

777 rapid exhumation in the Xolapa–Oaxaca blocks (Villagómez and Pindell, 2020b). We estimate that  
1 778 exhumation was a consequence of establishing Farallon/Cocos flat-slab subduction behind the  
2 779 Chortis Block, with interplate coupling at the position of Cuicateco such that Cuicateco was uplifted  
3 780 rather than Oaxaca being downdropped (Pindell and Kennan, 2009; Pindell and Miranda 2011;  
4 781 Graham et al. 2020; Molina-Garza et al., 2020b). Given the geometry of some of the faults involved in  
5 782 this post-Mexican Orogeny deformation (e.g., Vista Hermosa Fault and Valle Nacional faults) it is  
6 783 plausible that some back-stepped high-angle faulting occurred after the thin-skinned process  
7 784 (Graham et al., 2020).

8 785  
9 786 The Oligocene–early Miocene magmatism in the Cuicateco Belt is arc-related, documenting the  
10 787 flattening of the Farallon/Cocos slab as SW Mexico overthrust its own Benioff Zone. We interpret the  
11 788 early–middle Miocene cooling and exhumation of the Cuicateco Belt as a whole relate to this slab  
12 789 flattening.

## 13 790 **5.2 Mixteca/Oaxaca, the Sierra Madre Oriental and the Tampico–Misantla Basin**

### 14 791 **5.2.1 Syn-Mexican Orogeny**

15 792  
16 793  
17 794  
18 795 The earliest record of deformation and exhumation related to the Mexican Orogeny is dated as  
19 796 Campanian and is found in rocks located in the vicinities of the western border of the Mixteca Block  
20 797 (Ruiz-Arriaga, 2018). Similarly, our samples within the Mixteca and Oaxaca blocks (those located  
21 798 away from the influence of Cenozoic plutons) record cooling starting in Campanian times. Their  
22 799 thermal history paths (**Figure 4a**) and geological record might suggest that Mixteca/Oaxaca were  
23 800 heated (probably due to burial) throughout most of the Cretaceous and its overburden was partially  
24 801 exhumed from the latest Cretaceous through the early Paleocene due to the Mexican Orogeny. As for  
25 802 the southernmost extension of the Sierra Madre Oriental fold-thrust-belt (Mexican Orogeny), Gray et  
26 803 al. (2021) demonstrated that some regions in the central part of the belt also record this earliest stage  
27 804 of the orogeny.

28 805  
29 806 In general, the Time–temperature history paths of sedimentary samples from the Tampico–Misantla  
30 807 Basin show consistent patterns, with post-depositional heating and subsequent Oligocene–Miocene  
31 808 cooling (**Figure 4b**). We ascribe heating and cooling to be due to burial and exhumation, respectively.  
32 809 There is an along- and across-strike variation in the amount of burial and subsequent exhumation  
33 810 within the basin. Cooling due to erosional exhumation shows an eastward-younging trend, with late  
34 811 Eocene–Oligocene cooling in the foothills of the Sierra Madre Oriental fold-and-thrust belt (Gray et al.,  
35 812 2021) and Oligocene–Miocene cooling in the lower coastal plains of the Tampico–Misantla Basin.

## 36 813 **5.3 Chontal, Guichicovi and Mixtequita blocks**

### 37 814 **5.3.1 Mexican Orogeny phase**

38 815  
39 816  
40 817  
41 818 The Mixtequita and the Guichicovi blocks experienced heating during the Cretaceous. We assume  
42 819 that this heating was due burial by continental and then marine deposits (akin to the evolution of the  
43 820 neighbouring Chiapas Massif and Basin). The thermal models (**Figure 4b**) show that, unlike the  
44 821 Mixtequita Block, the Guichicovi Block underwent continuous heating through Paleocene to Middle  
45 822 Eocene.

46 823  
47 824 Field observations and geophysical data indicate that some Guichicovi-like rocks are partially buried  
48 825 by the Chontal Complex (Pérez-Gutiérrez et al., 2009; Molina-Garza et al., 2020a). Molina-Garza et  
49 826 al. (2020a) argued that Paleocene–middle Eocene is the time when slices from the Chontal litho-  
50 827 tectonic unit and the Jurassic Todos Santos Fm. were overthrust above the Guichicovi along the  
51 828 Chivela Nappe front, now deeply eroded, forming a thin-skinned Mexican Orogeny thrust front above  
52 829 the Guichicovi. We therefore assume that the continuous Paleocene–middle Eocene heating  
53 830 observed in the Guichicovi Block was a consequence of overthrusting and tectonic burial from the  
54 831 south or southwest.

55 832  
56 833 The allochthonous Chontal litho-tectonic unit has a maximum depositional age of 77 Ma (Pérez-  
57 834 Gutiérrez et al., 2009) and was deformed and metamorphosed prior to the Oligocene, given that it is  
58 835 unconformably covered by the Eocene–Oligocene Huamelula conglomerates (Tectonic Analysis Ltd.,  
59 836 pers. comm., 2022, unpublished data). It is therefore plausible that i) low-grade metamorphism of the

837 Chontal Complex, and ii) the main period of exhumation of the Chontal occurred from Paleocene  
1 838 through Eocene. This is exactly the time when the Guichicovi Block was heated, arguably  
2 839 corroborating its overthrusting by the Chontal along the Chivela Nappes proposed by Pérez-Gutiérrez  
3 840 et al. (2009) and Molina-Garza et al. (2020a).

4 841  
5 842 The Guichicovi and Mixtequita blocks record distinct cooling histories during the Cenozoic, at least  
6 843 until the late Miocene (see **Figure 6**). Cooling was likely due to erosional exhumation. While the  
7 844 Mixtequita Block underwent exhumation from Paleocene through early Oligocene, the Guichicovi  
8 845 Block experienced exhumation from the late Eocene through late Miocene (**Figure 6**). Summing up,  
9 846 exhumation seems to be younger and of higher magnitudes in the Guichicovi Block (late Eocene–late  
10 847 Miocene) compared to the Mixtequita Block (Paleocene–early Oligocene). This difference on the  
11 848 timing and magnitude of the exhumation between the two blocks (or between the northern and  
12 849 southern ends of a composite block behaving as one) might be the result of northward propagation of  
13 850 minor thrusting (and uplift) of the Mixtequita portion of the composite massif, with the Todos Santos  
14 851 and Chivela nappes riding piggy-back on the Guichicovi prior to erosion.

## 16 853 **5.4 Chiapas and Chortis areas**

### 18 855 **5.4.1. Syn and post-Mexican Orogeny**

20 857 The Tonalá Shear Zone represents one of the primary fault strands of the North America–Chortis  
21 858 (Caribbean) plate boundary zone (Molina-Garza et al., 2015), at least since early Miocene times  
22 859 (Graham et al., 2020). However, the long-lived sinistral displacement of Chortis involved a number of  
23 860 other faults during and prior to the Miocene, including “paleo-Motagua” faults possibly encompassing  
24 861 the Jocotán–Chamelecón and Baja Verapaz faults (**Figure 7a**). All the post-mid Miocene magmatic,  
25 862 hydrothermal, and tectonic events along the Tonalá Shear Zone constrained by Villagómez et al.  
26 863 (2020a), Witt et al. (2011), and Ratschbacher et al. (2009) have unfortunately overprinted older (Late  
27 864 Cretaceous–mid Miocene) thermal histories that could have potentially been recorded by higher  
28 865 temperature thermochronometers.

29 866  
30 867 The southernmost tip of the Chiapas Massif (the Huixtla Block of Villagómez and Pindell, 2020a)  
31 868 located south of the Polochic and Tonalá Shear Zone records an earlier onset of exhumation (middle  
32 869 Miocene). Moreover, rocks located away from the Polochic Fault in the Chortis Block, including the  
33 870 Chuacús and Las Ovejas complexes, also record continued middle Eocene to late Miocene  
34 871 exhumation (Simon-Labric et al., 2013; Ratschbacher et al., 2009). We believe that the northern  
35 872 Chortis Block has consequently experienced exhumation since at least the Paleocene and most of  
36 873 this exhumation occurred long before the arrival of the Chortis Block at its present-day position  
37 874 (Villagómez and Pindell, 2020b). Thus, the Chortis Block has very likely supplied detrital material to  
38 875 the Chiapas Basin while located south of the Chiapas Massif since the Paleocene, and prior to the  
39 876 late Miocene uplift of the massif.

40 877  
41 878 The Chiapanecan folding event that created the Chiapas fold-and-thrust belt started in middle  
42 879 Miocene times (Mandujano-Velázquez and Keppie, 2009), prior to the main period of uplift observed  
43 880 in the Chiapas Massif itself (<10 Ma). The folding event was driven by the onset of subduction  
44 881 beneath Chiapas in the wake of the eastwardly migrating Chortis Block, and the younger uplift of the  
45 882 massif pertains to the encroachment of slab flattening into Chiapas from Oaxaca (Pindell and  
46 883 Miranda, 2011; Pindell et al., 2020b; Graham et al., 2020; Molina-Garza et al., 2020b). The Chiapas  
47 884 Massif has become an effective topographic barrier starting at around 10 Ma (Pindell et al., 2020b).

48 885  
49 886 Such a mechanism for the younger exhumation of the Chiapas Massif is also validated by the  
50 887 northward sweep of arc magmatism, from about 15 Ma in western Tehuantepec (Damon and  
51 888 Montesinos, 1978; Pindell et al., 2020b), 9–11 Ma along the Tonalá Fault Zone (Molina-Garza et al.,  
52 889 2015), and Pliocene to Recent times within the Chiapas fold-and-thrust belt (Mora et al., 2012;  
53 890 Garduño-Monroy et al., 2015). Similarly, the Chontal Block has been cooling since the late Miocene,  
54 891 and this also probably pertains to the increasingly flat subduction of the Cocos slab beneath the  
55 892 Tehuantepec area.

## 57 893 **6 Paleogeographic reconstructions and sediment delivery pathways to the foreland basins and** 58 894 **Gulf of Mexico**

59 895  
60 896



897 We present a detailed description of the source-to-sink interpretation and the evolution of southern  
1 898 Mexico from the Late Cretaceous at eight different times (**Figures 7b–i**). These reconstruction maps  
2 899 are based on the models of Pindell and Kennan (2009), Villagómez and Pindell (2020b) and Graham  
3 900 et al. (2020), within the context of the approximate relative displacement history of the Chortis Block.  
4 901 Our reconstructions include the block rotations as indicated by the paleomagnetic data of Molina-  
5 902 Garza et al. (2019a) for the core of Chortis and Molina-Garza et al. (2020b) for the Chiapas Massif.  
6 903

7 904 The sediment source terrains (active exhumation and presumed erosion) are represented by the  
8 905 horizontal ruled pattern in **Figures 7a–i**. In general, hinterland uplift and exhumation becomes  
9 906 progressively younger from west to east along the southern Mexican margin, with uplift of the Xolapa  
10 907 and Mixteca/Oaxaca blocks beginning in the earliest Cretaceous, uplift of the Mixtequita in Paleocene  
11 908 and uplift of the Guichicovi and Chiapas Massif possibly beginning in the Eocene–Oligocene but with  
12 909 greatly increased rates since the middle Miocene. We complement the maps with information from  
13 910 key wells drilled by the state-owned petroleum company (Pemex) and other international operators in  
14 911 onshore and offshore areas, as further described in Section 7.  
15 912

16 913 Various Paleogene and Neogene depositional systems in the southern Gulf of Mexico, as described  
17 914 by Ambrose et al. (2003), Arreguín-López et al. (2011), Escalera-Alcocer (2010), CNH (2014, 2015,  
18 915 2017a, 2017b, 2019), González and Medrano (2014), Snedden and Galloway (2019), Brito and  
19 916 Luysterburg (2019), Shann et al. (2020), and Davison (2021) have been integrated with the uplift and  
20 917 exhumation data presented here (**Figure 6**). Our analysis is also supported by incorporating  
21 918 additional geochronological evidence, such as detrital zircon and heavy mineral analyses (Beltrán-  
22 919 Triviño et al., 2021). Our aim is to build an initial framework for connecting the primary sediment  
23 920 source terrains with their respective depositional systems (transport routes and sinks).  
24 921

25 922 The locations of the present-day drainage system entry points (**Figure 7a**) into the southern Gulf of  
26 923 Mexico are probably largely representative of the main entry points throughout the Paleogene and  
27 924 Neogene in the region (Shann et al., 2020). Accepting this, and looking at current drainage basins, it  
28 925 is possible to identify three main entry points that likely delivered sediment into the Gulf of Mexico  
29 926 from the Veracruz and Sureste basins during those times. Similarly, the Tampico–Misantla Basin was  
30 927 fed during the Eocene by channels that flowed southwards (Cantú-Chapa, 2001; Cossey et al., 2021),  
31 928 and which potentially originated in the Tamaulipas or Río Grande embayment area (Gray et al.,  
32 929 2021). Considering the impact of the Mexican Orogeny and later morphologic and tectonic  
33 930 development, the drainage basins associated with those entry points could have been as much as  
34 931 30% larger prior to final compressional deformation, thus increasing the potential sediment input  
35 932 significantly, especially during the earlier part of the Paleogene. Also, the potential contribution from  
36 933 the Chortis Block across the plate boundary during relative displacement along the southern Mexico  
37 934 could add significantly more drainage area to the hinterland south of the Sureste basins and the  
38 935 Chiapas Massif (see also Snedden et al., 2021; Stockli et al., 2021).  
39 936

40 937 Deposition into the southern Gulf of Mexico during the Paleogene and Neogene occurred primarily via  
41 938 deep water (bathyal) channel and fan (turbidite) depositional systems (e.g., Snedden and Galloway,  
42 939 2019), which in most cases developed in response to hinterland tectonics and further influenced by  
43 940 structured slope and basinal topography (e.g., Mayall et al., 2010) and active volcanism. Cenozoic  
44 941 depositional environments in the Veracruz Basin, for instance, are dominantly upper slope. The shelf  
45 942 and coastal environments have been eroded due to continued uplift and erosion of the Cuicateco and  
46 943 Zongolica belts (González and Medrano, 2014). The same can be said for the Paleogene sequences  
47 944 in the onshore Sureste Basin, although Neogene fluvial and deltaic (coastal) depositional  
48 945 environments have been encountered in numerous wells (Chávez-Valois et al., 2009).  
49 946

50 947 Sedimentary reworking is a fundamental aspect that should be taken into consideration when  
51 948 determining provenance and reservoir quality. The Eocene–Oligocene foreland in the Sureste Basin  
52 949 is involved in the middle Miocene to recent Chiapas folding, implying the potential for recycling those  
53 950 sediments into younger (post-middle Miocene) deposits. Such “second cycle” sediments are more  
54 951 texturally and compositionally mature once they are re-deposited farther out into younger basins.  
55 952

## 56 953 **6.1 Latest Cretaceous–Eocene (Figures 7b and 7c)**

### 57 954 Source

58 955

956 Our data from the Mixteca and Oaxaca blocks suggest that uplift and exhumation in those areas  
1 957 started as early as the Campanian. This may coincide with the Mexican Orogeny deformation (i.e.,  
2 958 uplift of the Oaxaquian region) which propagated eastwards to form the southern Sierra Madre  
3 959 Oriental Belt (Cuicateco). Our first evidence for exhumation in the southern Sierra Madre Oriental belt  
4 960 dates to the Maastrichtian, although the northern region of the Sierra Madre Oriental possibly started  
5 961 to deform and exhume earlier in Coniacian times (Fitz-Díaz et al., 2018; Gray et al., 2021).

6 962  
7 963 As the Sierra Madre Oriental Belt developed into a topographic high, it also started to provide  
8 964 carbonate clastic debris to the foreland basins. Whether or not the Sierra Madre Oriental was uplifted  
9 965 in discrete pulses (Fitz-Díaz et al., 2018), several intra-orogenic basins developed throughout the  
10 966 belt's Mexican Orogeny history (Gray et al., 2021).

11 967  
12 968 Deformation during the Mexican Orogeny also appears to be younger to the south. The Cretaceous  
13 969 sedimentary cover of the Oaxaca and Sierra de Juárez Complex started to erode in the Maastrichtian  
14 970 and delivered the first clastic carbonate material (Méndez Fm.) to the nascent Veracruz foredeep  
15 971 basin (Sierra-Rojas et al., 2020).

16 972  
17 973 As deformation continued throughout the Paleocene, some intra-orogenic basins of the Sierra Madre  
18 974 Oriental began to be eroded (Gray et al., 2021) and this material also contributed to the Paleocene–  
19 975 Eocene synorogenic turbidites of the Chicontepec Fm. deposited in foredeep depocenters of the  
20 976 Tampico–Misantla Basin (**Figure 7b**). Similarly, the Paleocene–lower Eocene denudation of  
21 977 Cretaceous sediments capping the Oaxaca Block and the Sierra de Juárez Complex continued  
22 978 providing material to the Veracruz Basin along submarine fans (González and Medrano, 2014).

23 979  
24 980 “In-sequence” propagation of thrusts and exhumation is observed in the Oaxaca and Cuicateco  
25 981 regions throughout the Paleogene. Unroofing of the Oaxaca Complex and the Mazateco Complex in  
26 982 the Cuicateco Belt continued in the middle Eocene and led to a continuous supply of material toward  
27 983 the foreland basin (Chapopote, Aragón and Guayabal formations.; **Figure 7c**). The detrital material  
28 984 initially consisted of the Cretaceous sedimentary cover. Graham et al., (2020) postulate that Oaxacan  
29 985 basement formed the uppermost nappe of the western Cuicateco Belt, the erosion of which may have  
30 986 potentially contributed to Eocene some clastic supply reaching the Veracruz Basin and Gulf of  
31 987 Mexico. It is very likely that the southern Veracruz Basin also received material coming from the  
32 988 denudation of the Mixtequita Massif during most of the Eocene (González and Medrano, 2014). We  
33 989 estimate that the source material coming from Mixtequita consisted of Cretaceous marine deposits  
34 990 and arguably northwardly-vergent overthrust Jurassic Todos Santos siliciclastics that once covered  
35 991 the Mixtequita Massif. The late Eocene marks the culmination of the Sierra Madre Oriental thrusting  
36 992 (Fitz-Díaz et al., 2018), concurrent with strong transpression along the Chortis–Southern Mexico plate  
37 993 boundary zone.

38 994  
39 995 Farther south, our analyses suggest that the allochthonous Chontal litho-unit (present-day western  
40 996 Tehuantepec area) cooled in the Paleocene–Eocene, possibly during final emplacement onto the  
41 997 southern Mexican margin. Although many of the rocks and detritus of Chontal may require a  
42 998 Maastrichtian arrival of the Greater Antilles arc along the margin, the cooling data suggest that the  
43 999 final emplacement onto the margin was more likely due to Mérida Andes-style transpression between  
44 1000 Chortis and Mexico once displacement was underway (Graham et al., 2020). The Chontal rocks were  
45 1001 eroded and provided material of oceanic affinity to the western Sureste and Chiapas basins, such as  
46 1002 that seen in the Maastrichtian Cerebro Mb. of the Ocozocuahtla Fm., the Paleocene Soyaló Fm., the  
47 1003 Eocene Uzpanapa conglomerate (Michaud and Fourcade, 1987; Molina-Garza et al., 2019b, 2020b),  
48 1004 and the Eocene El Bosque Fm. (Tectonic Analysis Ltd., pers. comm., 2022, unpublished data; **Figure**  
49 1005 **7b**),

50 1006  
51 1007 The continental core of Chortis migrated towards the east in a highly transpressive setting due to  
52 1008 rapid Farallon–North America convergence rates and the westward drift of North America over the  
53 1009 mantle (e.g., Engebretson et al., 1984). The erosional exhumation of the Chortis metamorphic  
54 1010 complexes during the Paleogene (Simon-Labric et al., 2013) probably provided quartz-rich and  
55 1011 metamorphic lithic-rich material to the Chiapas Basin through marine turbiditic channels. We believe,  
56 1012 however, that an important proportion of material feeding the Chiapas Basin's Soyaló/Sepúr and El  
57 1013 Bosque formations derived from the denudation of Cretaceous (Sierra Madre Fm.) and Jurassic units  
58 1014 (Todos Santos Fm.) that once covered the Chiapas Massif and were possibly involved in thrusting on  
59 1015 the massif's southern flank. This partial denudation of the sedimentary cover of the Chiapas Massif is

60  
61  
62  
63  
64  
65

1016 suggested by the initial cooling history of its basement (Witt et al., 2012; Villagómez and Pindell,  
1 1017 2020b) as a very slow and restricted late Eocene–early Oligocene exhumation pulse, possibly related  
2 1018 the passage of the Chortis Block (Villagómez and Pindell, 2020b).

3 1019  
4 1020 The Late Cretaceous–Eocene magmatic arc that bordered both western and eastern Chortis after arc  
5 1021 collision also provided volcanic and pyroclastic rocks to the Paleogene Soyaló/Sepúr and Eocene El  
6 1022 Bosque formations of the Chiapas Basin, as shown in **Figure 7b**.

#### 7 1023 Sink

8 1024  
9 1025 The Chortis Block was actively migrating east at this time coincident with the advance of the Sierra  
10 1026 Madre Oriental, generating robust depositional systems that fed sediment eroded from the impinging  
11 1027 highlands directly into the Gulf of Mexico across a narrow foreland shelf and into deep water.

12 1028  
13 1029 In the Tampico–Misantla Basin, the Bejuco–La Laja, Chicontepec and Nautla (also known as San  
14 1030 Andrés) paleo-canyons were channels for submarine fan systems coming from the erosion of the  
15 1031 Sierra Madre Oriental (Cantú-Chapa, 2001; Rosenfeld and Pindell, 2003; Graham et al., 2020). The  
16 1032 fans propagated into deep water, depositing turbiditic sandstones and shales throughout the Eocene.  
17 1033 Within the submarine facies that reached deep water zones, it is possible to observe meandering  
18 1034 channels, crevasse splays, lobes, basin floor fans, as well as mass transport complexes (CNH, 2019).

19 1035  
20 1036 In the Veracruz and Chiapas basins, bathyal water conditions prevailed during the Paleocene–  
21 1037 Eocene (Velasco, Chicontepec and Guayabal formations in Veracruz; Soyaló Fm. in Chiapas), in  
22 1038 continental slope and rise environments, ultimately connecting the developing foreland basins with the  
23 1039 Gulf of Mexico. This allowed the deposition of material derived from the sedimentary cover of the  
24 1040 uplifting blocks to be deposited as calcareous and siliciclastic lithic-rich turbidites interbedded with  
25 1041 deep marine shales farther out in the basin (Pemex, 2013a, 2013b; Martens et al., 2021).

26 1042  
27 1043 Sedimentary reworking played a major role in the Paleocene–Eocene depositional systems. As  
28 1044 mentioned previously, in the Chiapas Basin, one of the main sources of material feeding the  
29 1045 Paleocene Soyaló/Sepúr were derived from the denudation of Cretaceous (Sierra Madre carbonates)  
30 1046 and Jurassic (Todos Santos siliciclastic) units that once covered the Chiapas Massif and were actively  
31 1047 deforming along the massif's southern flank.

32 1048  
33 1049 Similarly, the erosion of the Soyaló/Sepúr foredeep units also provided second/third-cycle siliciclastic  
34 1050 sediments (e.g., into the Eocene El Bosque Fm. and the Nanchital shale) from the southeast,  
35 1051 delivered across a somewhat broader coastal and shelfal region in the Chiapas and Sureste area. El  
36 1052 Bosque Fm. sandstones (deposited in fluvial, littoral and possibly bathyal environments; García-  
37 1053 Molina, 1994; Meneses-Rocha, 2001) were originally transported from the south across the Chiapas  
38 1054 Massif to the Chiapas foredeep, the accommodation space for which was possibly aided by  
39 1055 northwardly evacuating salt. This siliciclastic fairway was northwest trending towards the western  
40 1056 Sureste basins (Isthmus Saline Basin, s.s.), promoting the formation of an early salt canopy.

41 1057  
42 1058 Large Eocene channel systems have been mapped from seismic data, extending far into the  
43 1059 Campeche Salt Basin mainly along the western margin of the basin (CNH, 2015; **Figure 7c**). These  
44 1060 channels consist of deep water turbidite system sandstones. Seismic interpretations allow for the  
45 1061 identification of sedimentary fairways related to turbidite deposition and include elements such as  
46 1062 amalgamated channels, crevasse splays and channelized lobes oriented southwest to northeast.  
47 1063 Outboard of the Campeche Salt Basin, these amalgamated/anastomosed channel systems are  
48 1064 largely straight and unconfined but tend to turn eastward towards the distal end of the salt province  
49 1065 (**Figure 7c**), where deposition is controlled by incipient halo-kinetic activity (CNH, 2019). In addition to  
50 1066 these robust depositional systems, intrusive volcanic bodies (of undetermined age) within the Eocene  
51 1067 section have been locally identified on industry seismic images, particularly in the northwest Isthmus  
52 1068 Saline Basin.

53 1069  
54 1070 Towards the east of the Campeche Salt Basin, calcarenite flows shed from the Yucatán shelf margin  
55 1071 (**Figure 7c**) were deposited in a slope apron adjacent to the platform (middle Eocene Kumaza: the  
56 1072 Ku, Maloob, Zaap fields; Ríos-López and Cantú-Chapa, 2009).

## 57 1073 **6.2 Oligocene–middle Miocene (Figures 7d, 7e and 7f)**

58 1074  
59 1075  
60 1076  
61  
62  
63  
64  
65

1076 Source

1 1077 New and published data show that deformation (e.g., Fitz-Díaz and Van der Pluijm, 2013) and  
2 1078 exhumation in the western and central portions of the southern Sierra Madre Oriental waned by the  
3 1079 latest Eocene. However, our thermochronological and detrital geochronological data suggest that the  
4 1080 westernmost regions of the Tampico–Misantla Basin remained tectonically active during the  
5 1081 Oligocene–Miocene. In fact, some of the former Paleogene foredeep deposits from the Sierra Madre  
6 1082 Oriental thrust front were probably eroded and reworked, feeding more easterly depocenters and  
7 1083 possibly the Gulf of Mexico during the Oligocene–Miocene.

8 1084  
9 1085 Subduction beneath southern Mexico in the migrating wake of the Chortis Block led to the onset of  
10 1086 arc-magmatism first in Guerrero and western Oaxaca states (Martiny et al., 2000) and later in eastern  
11 1087 Oaxaca/western Cuicateco in late Oligocene–Miocene times (Morán-Zenteno et al., 2005, 2018). This  
12 1088 was concurrent with uplift and erosional exhumation of the eastern Cuicateco sub-belts, the  
13 1089 Guichicovi, and the Mixtequita blocks that resulted in a continued supply of sediment directly into the  
14 1090 Veracruz Basin (**Figure 7d**). Oligocene onset of motion on the high-angle Oaxaca Fault, which cut  
15 1091 pre-existing low-angle detachment faults in the Sierra de Juárez Complex (Dávalos-Álvarez et al.,  
16 1092 2007; Graham et al., 2020), as well as initial movement on the left-lateral Chacalapa Fault (Tolson,  
17 1093 2005) downdropped the Oaxaca Block relative to the neighbouring blocks (**Figure 7d**).

18 1094  
19 1095 The Oligocene material that entered the Veracruz Basin (Horcones Fm.) mostly consisted of the  
20 1096 (presently eroded) Cretaceous platform that had still covered the Cuicateco Belt (remains of the  
21 1097 platform are preserved north of the Valle Nacional Fault). We estimate that by the earliest Miocene,  
22 1098 the eastern Cuicateco sub-belts had had much of their Cretaceous carbonate cover fully removed;  
23 1099 therefore, their Lower Cretaceous and Jurassic siliciclastic cover and metamorphic core were finally  
24 1100 becoming exposed. This might have important implications for reservoir quality especially in the  
25 1101 Veracruz Basin because the early Miocene was probably the time when feldspar and quartz clastics,  
26 1102 possibly derived from the Todos Santos and Xonamanca formations, were first delivered to the basin  
27 1103 from the west (Martínez-Medrano et al., 2009).

28 1104  
29 1105 The volcanic arc jumped northward to the Trans-Mexican Volcanic Belt in the latest early Miocene  
30 1106 (~20 Ma; Ferrari et al., 2012; **Figure 7e**), with the first volcanoclastic detritus feeding the northern  
31 1107 Veracruz Basin in the middle Miocene (Martínez-Medrano et al., 2009). It is worth noting that the  
32 1108 Cordoba Platform was not deeply exhumed during the Neogene based on its current preservation;  
33 1109 therefore, its detrital input towards the northern Veracruz Basin was limited. The southern Veracruz  
34 1110 Basin probably continued to receive siliciclastic material from the exhumation of the Guichicovi and  
35 1111 Mixtequita massifs throughout the Miocene (CNH, 2017a).

36 1112  
37 1113 Exhumation of the Chontal litho-tectonic unit, as well as exhumation of some metamorphic complexes  
38 1114 within Chortis, continued during the Oligocene–middle Miocene (Ratschbacher et al., 2009; Simon-  
39 1115 Labric et al., 2013). We believe that these regions located south of the Chiapas Massif were important  
40 1116 sources of material for the Oligocene La Laja, the lower Miocene Depósito Fm., and the mid-Miocene  
41 1117 Encanto Fm. (including the Nanchital conglomerate; Pindell et al., 2020b) in the Chiapas Basin  
42 1118 (**Figure 7d–f**), suggesting low relief for the Chiapas Massif at those times.

43 1119  
44 1120 As explained previously, the amount of material reworked from older sedimentary units should not be  
45 1121 underestimated, and it is probably the main reason why mineral detrital provenance studies have led  
46 1122 to disparate interpretations in the Chiapas Basin (Ortega-Flores et al., 2018, 2020; Molina-Garza et  
47 1123 al., 2019b). Moreover, Oligocene–Miocene arc magmatism along the southern Mexican margin  
48 1124 provided contemporaneous volcanic material to sedimentary units in the Chiapas Basin as well,  
49 1125 contributing to the different detrital zircon populations.

50 1126  
51 1127 The main deformational event in the Chiapas Basin (Chiapanecan orogeny) began in the middle  
52 1128 Miocene (Ángeles-Aquino et al., 1994; Mandujano-Velázquez and Keppie, 2009). The deformation  
53 1129 was driven by the clockwise rotation of the Chiapas Massif, which acted as an indenter prior to the  
54 1130 late Miocene (Molina-Garza et al., 2020b), and ultimately was a consequence of the onset of  
55 1131 subduction beneath Chiapas. Folding and thrusting of the Chiapas Basin provided, therefore, a  
56 1132 proximal source for second-cycle sediments.

57 1133  
58 1134 Sink

60  
61  
62  
63  
64  
65

1135 Fine-grained sandstones continued to be transported to deep water settings through submarine fan  
1136 systems. The most observed sedimentary facies in the Oligo–middle Miocene turbiditic system in the  
1137 Tampico–Misantla Basin include channels, crevasse splays, and basin floor fans (CNH, 2019).

1138  
1139 The Oligo–Middle Miocene sediments in the Veracruz Basin were deposited as basin-floor fans that  
1140 were fed from multiple areas. In onshore Veracruz Basin, the high-energy upper Oligocene–Miocene  
1141 deposits usually contain subangular to rounded clasts of Cretaceous carbonates with minor presence  
1142 of metamorphic and igneous rock fragments in a sandy or shaly matrix (IHS, 2010; Sánchez-  
1143 Hernández, 2013).

1144  
1145 In the Veracruz Basin, volcanic material derived from the Trans-Mexican Volcanic Belt started to  
1146 become important by the middle Miocene (Martínez-Medrano et al., 2009). Similarly, volcanic activity  
1147 in the Los Tuxtlas and Aneгада volcanic centers probably started in the middle Miocene (Ferrari et  
1148 al., 2005), providing volcanoclastic material to the neighbouring areas. Moreover, the Los Tuxtlas and  
1149 Aneгада centers became bathymetric highs that resulted in a constriction of sedimentary entry points  
1150 into the Gulf of Mexico from the Veracruz Basin (Winter, 2018), as shown in **Figure 7f**.

1151  
1152 Sandstone-prone submarine channel complexes up to 10 km wide fed these deep-water deposits that  
1153 comprise turbidites and debrites (Winter, 2018). For instance, middle Miocene reservoirs (Encanto  
1154 Fm.) have been described as deltaic and turbiditic sandstone with minor conglomerate lenses that  
1155 were confined to submarine canyons (Martínez-Medrano et al., 2009). In addition, shale diapirism and  
1156 deformation continued offshore Veracruz, enhancing the structure of the slope environment and  
1157 having a dramatic impact on sediment dispersal patterns throughout the Neogene.

1158  
1159 In the Campeche Salt Basin and the Catemaco Foldbelt, the lower–middle Miocene sandstones and  
1160 shales include high-density deep-water turbidites, debris flow deposits, low-density turbidites, slumps,  
1161 tuff-rich debrites and distal volcanoclastic turbidites (Sosa-Patrón et al., 2009; Sánchez-Hernández,  
1162 2013). The lower Miocene high-density turbidity currents have been encountered unconfined outboard  
1163 (to the west) of the Campeche salt, but their distribution is controlled by salt tectonics in mini-basins  
1164 within the salt province itself (CNH, 2017a, 2019).

1165  
1166 Middle Miocene deposition in the Campeche Basin was very similar to that of the lower Miocene, with  
1167 perhaps more robust systems delivering coarse sands and conglomerates even farther out into the  
1168 different basins due to increased hinterland deformation. Confined and unconfined fans and channels  
1169 of varying thickness have been encountered, likely reflecting the fact that many wells have been  
1170 drilled on anticlinal highs that were actively growing during the time of deposition (particularly in the  
1171 Catemaco Foldbelt). Contemporaneous salt movement also played an important role in  
1172 sedimentation, locally restricting flow and impacting direction of sediment fairways (CNH, 2019).

1173  
1174 Recent studies in the Campeche Salt Basin have delineated extensive Oligo–Miocene fans sourced  
1175 from the southern Veracruz Basin (Brito and Luysterburg, 2019) and arguably also from the Chiapas  
1176 basin (Clark et al., 2019) extending across the deep water Gulf of Mexico and reaching as far north as  
1177 U.S. waters. Deposition of these compensating fan systems began in the upper Oligocene (**Figure  
1178 7d**), peaked during the middle Miocene (**Figure 7f**), and ceased by the late Miocene (**Figure 7g**), as  
1179 documented in Winter (2018). Detrital zircon U–Pb ages derived from DSDP cores tie these  
1180 sediments to southern continental Mexico (Clark et al., 2019), implying that the sediments were  
1181 delivered more than 600 km northward into the basin. DSDP Leg 10 Sites 87, 90, and 91 (**Figure 7f  
1182 and Table 7**) encountered middle Miocene aged turbidite sands and gravels ranging in thickness from  
1183 20cm (Site 87) to more than 10m (Site 91). The turbidite sandstones from the DSDP sites are coarse-  
1184 grained and they are characterized by high percentages of quartz, plagioclase and a diverse heavy  
1185 mineral assemblage including biotite and hornblende. They also have a minor and fine gravel  
1186 component of carbonate rock fragments, volcanic rock fragments and chert (Worzel et al., 1973).  
1187 While such large volumes of sediment being derived from drainage areas potentially limited in scale  
1188 may seem counter-intuitive, earlier research has shown that tectonics and climate, among other  
1189 things, can be significant controlling factors in such short-runoff systems as were present throughout  
1190 the Cenozoic in the Veracruz and Sureste Basin areas (Sømme et al., 2009; Covault and Graham,  
1191 2010).

### 1192 1193 **6.3 Late Miocene–Present (Figures 7g, 7h and 7i)**

1194

61  
62  
63  
64  
65

1195 Source  
11196 Several regions of Southern Mexico experienced variable amounts of uplift and exhumation during the  
21197 late Miocene–Pliocene, and they, along with widespread volcanic centers located along Gulf of  
31198 Mexico margin, provided a continued supply of detrital material to the basins.  
41199  
51200 By the late Miocene there was a major reorganization of drainage patterns in the southern margin  
61201 because the Chiapas Massif had become a positive topographic high (Pindell et al., 2020b). The early  
71202 late Miocene marks then the onset of material coming directly from the crystalline basement of the  
81203 Chiapas Massif towards the Chiapas Basin and the Sureste basins. Upper Miocene turbidite  
91204 sandstones from the offshore Zama discovery (**Figure 7g**) also exhibit a major input from the Chiapas  
101205 mountainous areas (Stockli et al., 2021).  
111206  
121207 In the absence of high-resolution 3D seismic data, it is difficult to establish whether the late Miocene  
131208 exhumation of the Guichicovi and Mixtequita massifs sourced fluvial channels towards the Veracruz  
141209 Basin, the Sureste/Chiapas basins, or to all of them. However, our data record an important erosional  
151210 exhumation of both massifs; therefore, quartz-rich material sourced from these areas should have  
161211 been distributed generally towards the Gulf of Mexico.  
171212  
181213 The Veracruz Basin was surrounded by active volcanic centres including Los Tuxtlas, which  
191214 continued providing volcanoclastic material to the offshore basin (**Figure 7g**). The southern Veracruz  
201215 Basin continued to receive siliciclastic and metamorphic detritus from the erosion of the easternmost  
211216 Cuicateco sub-belts (the primary outlet for fluvial flow was possibly the original river that is now  
221217 dammed as the Lake Miguel Alemán). However, the volcanic lithic component became dominant in  
231218 the upper Miocene sequences and took over the plutonic and metamorphic provenance (Gutiérrez-  
241219 Paredes et al., 2009).  
251220  
261221 Sink  
271222 The upper Miocene sandstones in the Veracruz Basin were deposited as basin-floor progradational  
281223 submarine fans, which formed channels and over-bank deposits. Subsequent Pliocene submarine  
291224 fans were dominated by meandering channels (Martínez-Medrano et al., 2009) and they are more  
301225 limited in extent than the Miocene fans (Jennette et al., 2003a, 2003b).  
311226  
321227 Although the erosion of the Cuicateco Belt continued to provide sediment to depositional systems in  
331228 the Veracruz basin during the late Miocene, the basin experienced a significant change in  
341229 depositional patterns during this time. Prior to the middle Miocene (**Figure 7e**), the Cenozoic  
351230 depositional fairways fed directly into the deeper Gulf of Mexico Basin in a dip-oriented sense, i.e.,  
361231 running southwest to northeast. With the emergence of the Anegada and Los Tuxtlas volcanic centers  
371232 in the latest middle Miocene, entry points into the Gulf of Mexico became restricted, and depositional  
381233 systems in the Veracruz Basin became axially oriented, running northwest–southeast before exiting  
391234 the basin between the volcanic highs (**Figures 7f–7g**; Martínez-Medrano et al., 2009).  
401235  
411236 In the Isthmus Saline Basin, the upper Miocene sequences are characterized by lateral and vertical  
421237 facies variations, which evolved from deeper to shallower waters (Sosa-Patrón et al., 2009). This  
431238 progradation accelerated in the lower Pliocene with the shelf margin advancing towards the  
441239 northwest. The upper Miocene–Pleistocene sandstones of the Reforma–Comalcalco–Macuspana  
451240 depocenters were deposited mostly in proximal turbidite, prograding transitionally into deltaic  
461241 environments. The shelf margin migrated progressively northward in the Sureste basins throughout  
471242 the Miocene, making particularly substantial advancement during the late Miocene and Pliocene.  
481243 Upper Miocene fine-grained sandstones are interbedded with siltstones and shales in very thin layers  
491244 and were deposited in a relatively confined depositional environment (Chávez-Valois et al., 2009).  
501245  
511246 The upper Miocene–Pleistocene sandstones in the Sureste basins are distributed along NE–SW  
521247 trends (**Figures 7g–7h**) controlled by normal growth faults (Pemex, 2013c). Development and growth  
531248 of the Macuspana supra-salt extensional basin (beginning in the latest middle Miocene; Pindell and  
541249 Miranda, 2011) and the Comalcalco–Pescadores extensional system (mainly Pliocene) appears to  
551250 have captured a considerable amount of siliciclastic sediment derived from the south/southeast.  
561251 When underfilled, the two basins likely inhibited the coarsest detrital fractions of south-derived  
571252 material from reaching farther north into the Campeche salt province.  
581253  
59  
60  
61  
62  
63  
64  
65

1254 Considering the constriction of depositional fairways in the Veracruz Basin and that near-coast  
1 1255 Comalcalco and Pescadores extensional systems in Sureste were actively growing during the  
2 1256 Pliocene, it is not surprising that there is little evidence of robust Pliocene reservoir deposition in deep  
3 1257 water tests to date. However, Pliocene sands are encountered inboard of these extensional systems  
4 1258 and can be good reservoirs. Further entrapment of sediment may have occurred due to continued  
5 1259 anticlinal growth in the Chiapas fold-and-thrust belt onshore and concurrent salt deformation offshore,  
6 1260 creating paleobathymetric relief. Pliocene deposits in the Campeche Salt Basin appear to be  
7 1261 dominated by deposition of mass transport deposits (Sickmann and Snedden, 2021). Pliocene sands  
8 1262 tend to be rich in carbonate lithic grains and quartz (Hessler et al., 2018), with reservoirs developed in  
9 1263 amalgamated channels, crevasse splays, and channelized lobe facies possibly also associated with  
10 1264 turbidite depositional systems.

11 1265  
12 1266 Within the Chiapas Basin, the transtensional Ixtapa Graben captured a significant volume of littoral  
13 1267 and deltaic coarse-grained sediments (Ixtapa Fm.) during the latest middle Miocene to the earliest  
14 1268 Pliocene, derived from acidic plutonic, metamorphic and volcanic rocks (Meneses-Rocha, 2001;  
15 1269 Sánchez-Hernández, 2013).

## 16 1270 17 1271 **7. Clastic reservoir characteristics**

18 1272  
19 1273 Oil and gas have been under production from Cenozoic reservoirs in southern Mexico for decades,  
20 1274 both onshore and in the shallow offshore. Pemex and other international operators have stepped out  
21 1275 into water depths exceeding 500m since the reform of the Mexican petroleum industry in 2013. New  
22 1276 wells have provided additional data and evidence for the extension of the Cenozoic depositional  
23 1277 systems farther out into the Gulf of Mexico.

24 1278  
25 1279 We have integrated these wells into the interpretations of both provenance and potential reservoir  
26 1280 quality presented below. Many of these wells have discovered hydrocarbons. The most important  
27 1281 Cenozoic wells that have proven important prospects are listed in **Table 7**.

### 28 1282 29 1283 **7.1 Eocene clastic reservoirs**

30 1284  
31 1285 Tampico–Misantla Basin: The Chicontepec sandstones are considered immature and contain a  
32 1286 predominance of lithic clasts. The majority of the lithic clasts are reportedly fragments of limestones,  
33 1287 with a lesser proportion of siliciclastic fragments (Bitter, 1993; Santillán-Pina and Aguayo-Camargo,  
34 1288 2011).

35 1289  
36 1290 Veracruz Basin: Porosity preservation in Eocene sediments seems to be relatively good (porosities  
37 1291 vary between 10% and 25%; González and Medrano, 2014) even at burial depths approaching  
38 1292 5,000m, as observed in the Tepaxtli-1EXP (deep pools in Perdiz Field) and Heim-1 wells, onshore  
39 1293 Veracruz Basin (**Figure 7g**). The impact of varying sediment source terrains could be significant with  
40 1294 respect to compositional and textural make-up of Eocene sediment offshore and in deep water. Core  
41 1295 descriptions of middle Eocene conglomerates and breccias in the onshore Perdiz Field include  
42 1296 carbonate and igneous rock fragments supported in a calcareous clay matrix and cemented with  
43 1297 calcite (industry reports). Small gas and condensate accumulations are also reportedly found in mass  
44 1298 flow deposits of the upper Eocene Chapopote Fm. in the Mata Espino-2 onshore well (IHS, 2010).

45 1299  
46 1300 Campeche Salt Basin and Chiapas Basin: Recently, the deep water Bukma-1SON well discovered  
47 1301 gas and condensate in middle Eocene siliciclastic reservoirs. In the Chiapas Basin, the Eocene  
48 1302 sediments include fine to coarse conglomeratic sandstones of the El Bosque Fm., which are  
49 1303 conspicuously found in onshore outcrops (García-Molina, 1994).

### 50 1304 51 1305 **7.2 Oligo–middle Miocene reservoirs**

52 1306  
53 1307 Veracruz Basin: Oligocene reservoirs are represented by deep water turbidite system deposits,  
54 1308 although they have not received considerable attention as an exploration target. Oligocene deep  
55 1309 clastic reservoirs have been reported in several wells in the offshore Catemaco Foldbelt (Shann,  
56 1309 2021). Oligocene potential reservoirs in the onshore region of the Veracruz Basin show porosity  
57 1310 values between 15% and 20% (González and Medrano, 2014).

58 1311  
59 1312

60  
61  
62  
63  
64  
65

1313 Lower Miocene conglomerates and sandstones are reportedly rich in calcareous clasts. The samples  
1 1314 also show the onset of quartz and feldspar delivery to the basin, and an increased presence of  
2 1315 metamorphic and plutonic rock fragments (Martínez-Medrano et al., 2009; Sánchez-Hernández  
3 1316 2013). Gas is reportedly produced from five clastic Miocene sequences. Some lower Miocene  
4 1317 producing horizons (La Laja Fm.) show average porosity ranging from 6–8% (IHS, 2010) to 23%  
5 1318 (Martínez-Medrano et al., 2009). The middle Miocene reservoirs show maximum porosity values of  
6 1319 29% (Martínez-Medrano et al., 2009). Summing up, lower and middle Miocene sandstones average  
7 1320 porosity in the range of 6 to 29%.

8 1321  
9 1322 As observed in several onshore fields in the Veracruz Basin (Playuela, Apertura–Madera), the onset  
10 1323 of delivery of quartz and feldspar was in the early Miocene, reaching a period of maximum supply in  
11 1324 the middle Miocene (Martínez-Medrano et al., 2009). Middle Miocene was also the time when  
12 1325 sediments in the northern Veracruz Basin started to receive the first volcanoclastic input coming from  
13 1326 the Trans-Mexican Volcanic Belt (Martínez-Medrano et al., 2009), although the main contribution to  
14 1327 the sandstones still came from the erosion of the Cuicateco sub-belts (carbonates, metamorphic and  
15 1328 siliciclastic clasts).

16 1329  
17 1330 Campeche Salt Basin: In general, Neogene sediments are poorly sorted and mineralogically  
18 1331 immature. They correspond to feldspathic litharenites with abundant volcanic lithics, feldspar, quartz,  
19 1332 metamorphic and sedimentary fragments (CNH, 2019). The lower Miocene play is considered to be  
20 1333 the most prospective in the deep-water region of Campeche Salt Basin and has been the focus of  
21 1334 many wells drilled in recent years (e.g., Kabili-1, Labay-1, Leek-1, Polok-1EXP, Tabscoob-101 and  
22 1335 Yoka-1 wells). Well logs and cores reveal upward-fining stacking patterns of massive coarse-grained  
23 1336 sandstones, plus siltstone and shale, with some channels exhibiting erosive bases and basal  
24 1337 conglomerates.

### 25 1338 **7.3 Upper Miocene–Pliocene reservoirs**

#### 26 1339 Veracruz

27 1340  
28 1341 Upper Miocene–Pliocene reservoirs show an increased contribution of mafic and felsic volcanic lithics  
29 1342 at expenses of carbonate and metamorphic lithics (Martínez-Medrano et al., 2009; Jennette et al.,  
30 1343 2003a; Gutiérrez-Paredes et al., 2009). The same is observed in the Catemaco Foldbelt, where most  
31 1344 of the detrital material was supplied by Los Tuxtlas Volcanic Complex. Maximum porosity determined  
32 1345 in upper Miocene–Pliocene sandstones in the Veracruz Basin reach up to 34% (Martínez-Medrano et  
33 1346 al., 2009).

#### 34 1347 Sureste and Campeche Salt Basins

35 1348  
36 1349 The Upper Miocene–Pleistocene sandstones of the Reforma–Comalcalco–Macuspana are classified  
37 1350 as arkoses and subarkoses, with a lesser proportion of litharenites (Pemex, 2013c). The main  
38 1351 constituents of the sandstones are quartz, feldspars, and rock fragments of igneous and metamorphic  
39 1352 provenance according to Pemex (2013c).

40 1353 Reservoir quality highly depends on the depositional facies and the depth of burial (Chávez-Valois et  
41 1354 al., 2009). In the Isthmus Saline Basin (onshore) porosity values in upper Miocene reservoirs range  
42 1355 from 10% to 30% (Sosa-Patrón et al., 2009), similarly as in the Reforma–Comalcalco–Macuspana  
43 1356 region, where porosity reaches up to 30% in the coarsest upper Miocene–Pleistocene horizons  
44 1357 (Chávez-Valois et al., 2009).

45 1358 The percentage of volcanic rocks fragments in sandstones from offshore wells (e.g., Chuktah-1,  
46 1359 Chuktah-201, Tibil-1, Lakmay-1, Lakach-1, Kunah-1; CNH, 2019; Beltrán-Triviño et al., 2021)  
47 1360 indicates the increased presence of a significant calc-alkaline volcanic source likely sourced from the  
48 1361 Los Tuxtlas Volcanic Complex and the scattered arc-related volcanoes and domes present in the  
49 1362 Chiapas Basin. Nevertheless, the Upper Miocene–Pliocene reservoirs are deemed good (CNH,  
50 1363 2019). Eni's Sayulita-1EXP discovery in shallow waters contains 150–200 mmboc reportedly in good  
51 1364 quality upper Miocene sands approximately 70km from the coast. The Tabscoob-1 discovery located  
52 1365 near the transition from shallow to deep water produces gas and condensate from middle Pliocene  
53 1366 sandstones (CNH, 2019).



#### 1373 **7.4 Summary on reservoir potential**

1374  
1375 Cenozoic siliciclastic reservoir quality tends to improve from older to younger units due to progressive  
1376 exposure of basement rocks following the erosion of their overlying sedimentary cover (mainly  
1377 Cretaceous carbonates). Cenozoic siliciclastic reservoirs are typically classified as litharenites or  
1378 feldspathic litharenites due to the abundance of lithic fragments contained in the sediments (often  
1379 exceeding 50% of constituent grains; Shann et al., 2020). Porosity types identified include  
1380 intergranular porosity, secondary porosity (due to the dissolution of unstable lithic grains, feldspars,  
1381 and bioclasts), fracturing, and microporosity (Gutiérrez-Paredes et al., 2018). Analyses of core data  
1382 indicates that a 10% porosity cutoff for reservoir effectiveness is appropriate for these rocks; porosity-  
1383 depth relationships thereby suggest a reservoir floor of approximately 4,000m below mud line (Shann  
1384 et al., 2020). Quartz cementation does not seem to be a significant contributor to porosity reduction,  
1385 but rather the high lithic content of most of these sands can result in substantial porosity loss due to  
1386 compaction of ductile lithics with burial (Mousavi and Bryant, 2013).

#### 1388 **8 Conclusions**

1389  
1390 The extensive geo- and thermo-chronological data set that we have generated allows us to determine  
1391 with confidence all areas in southern Mexico that have potentially provided carbonate and clastic  
1392 material towards the onshore and offshore foreland basins of southern Mexico and the Gulf of Mexico,  
1393 including the Tampico–Misantla, Veracruz, Sureste and Chiapas basins.

1394  
1395 We outline an Early Cretaceous rapid low-angle extensional event in the Sierra de Juárez Complex  
1396 that was followed by cooling from ~130 Ma to ~90 Ma, as well as platform and basinal depositional  
1397 conditions in the Cuicateco Belt. Subsequently, the onset of the Mexican Orogeny deformation in  
1398 Mixteca/Oaxaca blocks and the Sierra Madre Oriental occurred from the Campanian–Maastrichtian  
1399 through the early Oligocene and propagated eastward and southward towards the foreland regions  
1400 and the Cuicateco Belt. Erosional exhumation of these regions provided carbonate detrital material to  
1401 the Tampico–Misantla and Veracruz basins.

1402  
1403 Although relatively local sources such as the Mixtequita and Guichicovi Blocks possibly provided first-  
1404 order quartz-rich material to the southernmost Veracruz Basin from the Eocene, most of the quartz-  
1405 rich and metamorphic-rich material feeding the Veracruz basins came from the Cuicateco sub-belts  
1406 and was only supplied from the earliest Miocene. This clastic material has been subsequently  
1407 overtaken by volcanoclastic material derived from the Trans-Mexican Volcanic Belt since the middle  
1408 Miocene.

1409  
1410 During most of the Cenozoic, the Chiapas Basin and the Sureste basins were sourced from the  
1411 Chontal Complex (western Tehuantepec), the mobile Chortis Block, as well as volcanic-arc rocks that  
1412 bordered Chortis during the Cenozoic. Moreover, older sedimentary material covering the Chiapas  
1413 Massif and Basin has been partially eroded throughout the Cenozoic and provided second-cycle  
1414 material to the Chiapas and the Sureste basins.

1415  
1416 Our results highlight the importance of understanding relative block and plate boundary  
1417 displacements and ponder the role of major faults when interpreting source-to-sink relationships in the  
1418 area. This work documents how foredeep deposits in the Mexican foreland basins have been involved  
1419 in late deformational events, and how those sediments are very often re-incorporated into younger  
1420 deposition. This has traditionally led to incorrect detrital provenance conclusions. This synthesis  
1421 should help to predict the physical nature and lithologic characteristics of turbidites and fluvial  
1422 channels from several Late Cretaceous–Cenozoic fairways along the southern Gulf of Mexico rim.

1423  
1424 Future work should seek an improved determination of the offshore limits of the Chortis Block, such  
1425 as along the Pacific margin and the Honduras Shelf regions because they were source areas for  
1426 Mexican basins throughout most of the Cenozoic. Also, more robust determinations of the thermal  
1427 histories in onshore regions of the Chortis Block will not only aid exploration in Central America, but  
1428 will impact our understanding of potential provision of detritus to Mexico, as well.

#### 1430 **Acknowledgments**

1431  
60  
61  
62  
63  
64  
65

1432 This work is dedicated to our dear colleague and friend Roberto Molina Garza, whose life was taken  
1433 from us too soon. His memory will last forever in our hearts. We thank Elisa Fitz Díaz (Universidad  
1434 Nacional Autónoma de México, UNAM), Goran Andjic (Utrecht University) and Editor Douwe van  
1435 Hinsbergen (Utrecht University) for a thorough and enriching review of this manuscript. We also thank  
1436 the sponsors of the 11-year Cordilleran (Mexico) Research Program, in particular Phase 3 corporate  
1437 sponsors (BHP, Chevron, Equinor and ExxonMobil). We wish to acknowledge the contribution and  
1438 knowledge shared with us by Uwe Martens (UNAM). We also thank Juliana Estrada Carmona and  
1439 María Isabel Sierra Rojas (UNAM) for processing some of the samples presented herein.

## Figure captions

### Figure 1

Tectonic map of southern Mexico modified from Reed et al. (2004) showing the main litho-tectonic units defined in this work. Inset shows the extent of the Mexican Orogen (after Fitz-Díaz et al., 2018). Abbreviations: AF, Aloapán Fault (possibly a reactivated subvertical structure) ; BGB, Barranca Grande Backthrust ; CB, Cuicateco Belt ; ChT, Chivela Thrust ; CF, Caltepec Fault ; CP, Córdoba Platform ; OF, Oaxaca Fault (steep westerly dipping structure of Tertiary age) ; PF, Papalutla Fault ; PeF : Petapa Fault ; SF, Soyaltepec Fault ; SVF, Siempre Viva Fault (thrust carrying basement rocks of the Sierra de Juárez Complex over the Cuicateco Belt) ; TF, Tehuantepec Fault ; TV, Tehuacán valley (a Tertiary half-graben) ; VAF, Villa Alta Fault (possibly a reactivated subvertical structure) ; VHF, Vista Hermosa Fault (thrust); VNF, Valle Nacional Fault (oblique inversion structure). Geographic Coordinate System: Mexico ITRF2008; Projection: Lambert Conformal Conic.

### Figure 2 a,b

a) Oaxaca cross section A1–A4; b) Chiapas cross section B1–B5 (lines shown on Figure 1). Modified from Graham et al. (2020, figures 7b and 15b).

### Figure 3

Tectonic map of southern Mexico modified from Reed et al. (2004) showing the main litho-tectonic units and new samples analysed in this work for geo- and thermochronology (red squares). We also include sample locations with published thermochronological data (blue squares) used in our interpretations. Published data include Villagómez et al. (2019); Villagómez and Pindell (2020a, 2000b) and Gray et al. (2021). Geographic Coordinate System: Mexico ITRF2008; Projection: Lambert Conformal Conic.

### Figures 4 a,b

Thermal history models for the different litho-tectonic units using HeFTy© software. Input data included AFT age, track length data, and Dpar (a proxy for chemical composition), as well as apatite and zircon U–Th/He when available. The good-fit envelope of solutions (all solutions with a goodness of fit of 0.5 and higher) are shown in pink. Acceptable solutions (goodness of fit between 0.05 and 0.5) are shown in green. For more details on the dating methods and thermal modelling see **Appendix 2**. Most thermal models are unpublished although input AFT data in the Tampico–Misantla and the Cuicateco models include data from Gray et al. (2021) and Villagómez (2014).

### Figure 5 a, b

a) New K-feldspar  $^{40}\text{Ar}/^{39}\text{Ar}$  ages from the Sierra de Juárez Complex. b) Cooling history of the Sierra de Juárez Complex and interpretation.

### Figure 6

Stratigraphic columns and post-Jurassic rock cooling periods observed in southern Mexico, as well as an interpretation of the causes of cooling. Geologic time scale used is the International Chronostratigraphic Chart of the International Commission on Stratigraphy, version 2013/01 (Cohen et al., 2013). Sources are listed in the text and in **Appendix 1**. For more details on the stratigraphy see **Appendix 1**.

### Figures 7 a–i

Present-day configuration (**Figure 7a**) and Late Cretaceous to Recent (**Figures 7b–i**) reconstruction of southern Mexico and Chortis. Litho-tectonic units represented using the same colours as in **Figure 1**. Areas that were potentially eroded are colour filled. The horizontal line patterns represent litho-

1492 tectonic units which experienced known erosional exhumation for a given map. The maps show the  
1 1493 present-day outline of continental core of Chortis (Chortis s.s.) according Andjic et al. (2018) and  
2 1494 Romito and Mann (2020), as well as our preferred outline based on onshore geology. Key wells drilled  
3 1495 offshore Chortis are also shown on the present-day configuration. Paleo-position of Chortis and  
4 1496 movement relative to North America are from Pindell and Kennan (2009), Villagómez and Pindell  
5 1497 (2020b), Graham et al. (2020). Our reconstruction maps include basic palinspastic corrections that  
6 1498 account for possible rigid and nonrigid deformation of the different block boundaries. Rotation of  
7 1499 Chortis since early Paleocene is about 40° counter-clockwise, in line with data from Molina-Garza et  
8 1500 al. (2019a). Rotation (and translation) of Chiapas is about 15° clockwise (possible moving pole at  
9 1501 around 14.7°N/92.7°W) between early and mid-Miocene (Molina-Garza et al., 2020b). Paleogene  
10 1502 channels are based on Rosenfeld and Pindell (2003). Depositional axes of the most relevant fairways  
11 1503 are shown with coloured arrows and are compiled from Arreguín-López et al., 2011; Ambrose et al.,  
12 1504 2003; Escalera-Alcocer, 2010; CNH, 2014, 2015, 2017a, 2017b, 2019, González and Medrano, 2014;  
13 1505 Snedden and Galloway, 2019; Brito and Luysterburg, 2019; Shann et al., 2020; Davidson, 2021 and  
14 1506 unpublished industry data. The depositional facies areas are based on multiple published  
15 1507 interpretations (*incl.* Quezada-Muñetón, 1987; Meneses-Rocha, 2001; Witt et al., 2012; CNH, 2017b)  
16 1508 and our own fieldwork observations.

17 1509  
18 1510 Geographic Coordinate System and datum used in this map are WGS84. Abbreviations: BVF: Baja  
19 1511 Verapaz Fault; JChF: Jocotán–Chamelecón Fault; MF: Motagua Fault; PFZ: Polochic Fault Zone.  
20 1512 Figure 7a. Inset: Modern river drainage system of southern Mexico, indicating the extent of drainage  
21 1513 into the Gulf of Mexico. These drainage systems were probably considerably larger prior to  
22 1514 compressional deformation (possibly as early as Eocene but peaking in middle Miocene) and could  
23 1515 deliver vast volumes of sediment to offshore areas.

## 24 1516 **Appendixes**

25 1517  
26 1518  
27 1519 **Appendix 1**  
28 1520 Litho-tectonic unit details

29 1521  
30 1522 **Appendix 2**  
31 1523 Methodologies

32 1524  
33 1525 **Appendix 3**  
34 1526 Analytical data

## 35 1527 **References**

36 1528  
37 1529  
38 1530 Alaniz-Álvarez, S.A., van der Heyden, P., Nieto-Samaniego, A.F. and Ortega-Gutiérrez, F. 1996.  
39 1531 Radiometric and kinematic evidence for Middle Jurassic strike-slip faulting in southern Mexico related  
40 1532 to the opening of the Gulf of Mexico. *Geology*, 24(5), pp. 443–446. [https://doi.org/10.1130/0091-](https://doi.org/10.1130/0091-7613(1996)024%3C0443:RAKEFM%3E2.3.CO;2)  
41 1533 [7613\(1996\)024%3C0443:RAKEFM%3E2.3.CO;2](https://doi.org/10.1130/0091-7613(1996)024%3C0443:RAKEFM%3E2.3.CO;2)

42 1534  
43 1535 Allen, P.A. 2017. *Sediment routing systems: The fate of sediment from source to sink*. Cambridge  
44 1536 University Press. 442 pp.

45 1537  
46 1538 Allen, P.A. and Allen, J.R., 2013. *Basin analysis: Principles and application to petroleum play*  
47 1539 *assessment*. John Wiley & Sons.

48 1540  
49 1541 Ambrose, W.A., Wawrzyniec, T.F., Fouad, K., Talukdar, S.C., Jones, R.H., Jennette, D.C., Holtz,  
50 1542 M.H., Sakurai, S., Dutton, S.P., Dunlap, D.B. and Guevara, E.H., 2003. Geologic framework of upper  
51 1543 Miocene and Pliocene gas plays of the Macuspana Basin, southeastern Mexico. *AAPG bulletin*, 87(9),  
52 1544 pp.1411–1435.

53 1545  
54 1546 Andjić, G., Baumgartner, P.O. and Baumgartner- Mora, C., 2018. Rapid vertical motions and  
55 1547 formation of volcanic arc gaps: Plateau collision recorded in the forearc geological evolution (Costa  
56 1548 Rica margin). *Basin Research*, 30(5), pp.863–894.

57 1549  
58 1550 Ángeles-Aquino, F.J., Reyes-Nunez, J., Quezada-Muneton, J.M. and Meneses-Rocha, J.J., 1994.  
59 1551 Tectonic evolution, structural styles, and oil habitat in Campeche sound, Mexico.

60 1551  
61  
62  
63  
64  
65

- 1552  
1 1553 Ángeles-Moreno, E., 2006. *Petrografía, geología estructural y geocronología del borde noroccidental*  
2 1554 *del terreno Cuicateco, Sierra Mazateca, estado de Oaxaca, México*. Universidad Nacional Autónoma  
3 1555 de México, Posgrado en Ciencias de la Tierra, Instituto de Geología, unpublished M. Sc. Thesis.  
4 1556  
5 1557 Ángeles-Moreno E., Elías-Herrera M, Macías-Romo C, Sánchez-Zavala JL, Ortega-Gutiérrez F. 2012.  
6 1558 Geological Map of the Western Border of Cuicateco Terrane, Southern Mexico. *Geological Society of*  
7 1559 *America*, Map & Chart Series MCH102.  
8 1560  
9 1561 Armstrong, P.A., 2005. Thermochronometers in sedimentary basins. *Reviews in Mineralogy and*  
10 1562 *Geochemistry*, 58(1), pp.499–525.  
11 1563  
12 1564 Arreguín-López, M.A., Reyna-Martinez, G., Sanchez-Hernandez, H., Escamilla-Herrera, A. and  
13 1565 Gutierrez-Araiza, A., 2011. Tertiary Turbidite Systems in the Southwestern Gulf of Mexico. *Gulf Coast*  
14 1566 *Association of Geological Societies Transactions*, v. 61, p. 45–53.  
15 1567  
16 1568 Beltrán-Triviño, A., U. Martens, and A. von Quadr, 2021, Siliciclastic provenance of the Cenozoic  
17 1569 stratigraphic succession in the southern Gulf of Mexico: insights from U-Pb detrital zircon  
18 1570 geochronology and heavy minerals analysis. In: Martens, U. and Molina-Garza, R.S. (eds) Southern  
19 1571 and Central Mexico: Basement Framework, Tectonic Evolution, and Provenance of Mesozoic–  
20 1572 Cenozoic Basins. Geological Society of America, Special Papers, 546.  
21 1573  
22 1574 Bernet, M., Garver, J. I., 2005. Fission-track Analysis of Detrital Zircon. *Reviews in Mineralogy and*  
23 1575 *Geochemistry* 58, 205–237.  
24 1576  
25 1577 Bitter, M.R., 1993. Sedimentation and provenance of Chicontepec sandstones with implications for  
26 1578 uplift of the Sierra Madre Oriental and Teziutlan Massif, east-central Mexico. Mesozoic and Early  
27 1579 Cenozoic Development of the Gulf of Mexico and Caribbean Region—A Context for Hydrocarbon  
28 1580 Exploration, James L. Pindell, Bob F. Perkins. p. 155–172. <https://doi.org/10.5724/gcs.92.13.0155>  
29 1581  
30 1582 Braun, J., Van der Beek, P. and Batt, G., 2006. *Quantitative thermochronology: numerical methods*  
31 1583 *for the interpretation of thermochronological data*. Cambridge University Press. 254 pp.  
32 1584  
33 1585 Brito, M. and Luysterburg, C., 2019, April. Evaluation of Sediment Fairways Along the Western Margin  
34 1586 of the Saline Basin. In Second EAGE (European Association of Geoscientists & Engineers) *Workshop*  
35 1587 *on Deepwater Exploration in Mexico: Knowledge transfer and collaboration from shelf to deepwater*.  
36 1588 Vol. 2019, No. 1, pp. 1–5.  
37 1589  
38 1589 Brocard, G.Y., Willenbring, J.K., Salles, T., Cosca, M., Gutiérrez-Orrego, A., Cacao-Chiquín, N.,  
39 1590 Morán-Ical, S. and Teyssier, C., 2020. Top-down and bottom-up controls on mountain-hopping  
40 1591 erosion: insights from detrital 10 Be and river profile analysis in Central Guatemala. *Earth Surface*  
41 1592 *Dynamics Discussions*, pp.1–46.  
42 1593  
43 1594 Campa-Uranga, M.F., and Coney P.J. 1983. Tectono-stratigraphic terranes and mineral resource  
44 1595 distribution in Mexico: Canadian Journal of Earth Sciences, v. 20, pp. 1040–1051.  
45 1596  
46 1597 Campos-Madrigal, E., Centeno-García, E., Mendoza-Rosales, C.C. and Silva-Romo, G., 2013.  
47 1598 Sedimentología, reconstrucción paleoambiental y significado tectónico de las sucesiones clásticas del  
48 1599 Jurásico Medio en el área de Texcalapa, Puebla-Huajuapán de León, Oaxaca: Revisión de las  
49 1600 formaciones Ayuquila y Tecmazúchil. *Revista mexicana de ciencias geológicas*, 30(1), pp.24–50.  
50 1601 24–50. ISSN 2007-2902.  
51 1602  
52 1603 Camprubí, A., Cabrera-Roa, M.Á., González-Partida, E. and López-Martínez, M., 2019.  
53 1604 Geochronology of Mexican mineral deposits. VIII: the Zacatepec polymetallic skarn, Oaxaca. *Boletín*  
54 1605 *de la Sociedad Geológica Mexicana*, 71(1), pp.207–218.  
55 1606  
56 1607 Cantú-Chapa, A. 2001, Paleocanyons in the subsurface of eastern Mexico: Facts and uncertainties, in  
57 1608 C. Bartolini, R. T. Buffler, and A. Cantú-Chapa, eds., The western Gulf of Mexico Basin: Tectonics,  
58 1609 sedimentary basins, and petroleum systems: AAPG Memoir 75, p. 421–430.  
59 1610  
60 1611

61  
62  
63  
64  
65

- 1612 Carfantán, J.C., 1981. Evolución estructural del sureste de México, Paleogeografía e historia  
1613 tectónica de las zonas internas mesozoicas. *Revista mexicana de Ciencias Geológicas*, 5(2), pp.207–  
1614 216.
- 1615
- 1616 Carfantán, J.C. 1985. Du Système Cordilleran nord-américain au domaine Caraïbe. Etude Géologique  
1617 du Mexique Méridional. PhD thesis, Université de Savoie, France.
- 1618
- 1619 Carrillo-Bravo, J.C., 1980. Paleocanones terciarios de la planicie costera del Golfo de México. *Boletín*  
1620 *de la Asociación Mexicana de Geólogos Petroleros*, 32(1), pp.27–55. <https://shar.es/aWxtC1>
- 1621
- 1622 Chávez-Valois, V. M., M. d. L. C. Valdés, J. I. Juárez-Placencia, I. A. Ortiz, M. M. Jurado, R. V.  
1623 Yanez, M. G. Tristan, and S. Ghosh. 2009. A new multidisciplinary focus in the study of the tertiary  
1624 plays in the Sureste Basin, Mexico, in C. Bartolini and J. R. Romá- Ramos, eds., *Petroleum systems*  
1625 *in the southern Gulf of Mexico: AAPG Memoir 90*, p. 155–190.
- 1626
- 1627 Clark, J., Ochoa, J., Stockli, D., Fildani, A., Gerber, T., Covault, J., Guzman, J., Vinnels, J. and  
1628 Marshall, J., 2019. Provenance and Morphology of Extensive Oligocene-Miocene Deep-Water Fan  
1629 Systems Sourced from Chiapas-Veracruz and Sierra Madre Oriental, Gulf of Mexico. In *2019 AAPG*  
1630 *Annual Convention and Exhibition*.
- 1631
- 1632 CNH. 2014. Cuencas del Sureste Aguas Someras - Síntesis Geológica Petrolera. Comisión Nacional  
1633 de Hidrocarburos (CNH), Mexico City, 64 p. <https://www.rondasmexico.gob.mx/media/1418/atlas.pdf>
- 1634
- 1635 CNH. 2015. Saline Basin - Petroleum Geological Synthesis. Comisión Nacional de Hidrocarburos  
1636 (CNH), Mexico City, 47p. <https://rondasmexico.gob.mx/media/1557/geological-atlas-cs.pdf>
- 1637
- 1638 CNH. 2017a. Atlas Geológico Cuenca Veracruz. Comisión Nacional de Hidrocarburos (CNH), Mexico  
1639 City, 57p. [https://hidrocarburos.gob.mx/media/3092/atlas\\_geologico\\_cuenca\\_veracruz\\_v3.pdf](https://hidrocarburos.gob.mx/media/3092/atlas_geologico_cuenca_veracruz_v3.pdf)
- 1640
- 1641 CNH. 2017b. Atlas Geológico Cuencas Del Sureste - Cinturón Plegado de la Sierra de Chiapas..  
1642 Comisión Nacional de Hidrocarburos (CNH), Mexico City, 54p.  
1643 [https://hidrocarburos.gob.mx/media/3094/atlas\\_geologico\\_cuencas\\_sureste\\_v3.pdf](https://hidrocarburos.gob.mx/media/3094/atlas_geologico_cuencas_sureste_v3.pdf)
- 1644
- 1645 CNH. 2019. Prospective Resources of Mexico: Perdido Area, Mexican Ridges and Saline Basin,  
1646 deepwater Gulf of Mexico. Comisión Nacional de Hidrocarburos (CNH),  
1647 160p. [https://www.gob.mx/cms/uploads/attachment/file/527025/Deepwater\\_Prospective\\_Resources\\_of\\_Mexico\\_Publishing\\_2019\\_DGPEPP\\_low.pdf](https://www.gob.mx/cms/uploads/attachment/file/527025/Deepwater_Prospective_Resources_of_Mexico_Publishing_2019_DGPEPP_low.pdf)
- 1648
- 1649
- 1650 Cohen, K.M., Finney, S.C., Gibbard, P.L. and Fan, J.-X. 2013. The ICS International  
1651 Chronostratigraphic Chart. *Episodes*, 36, 199–204,  
1652 <http://www.stratigraphy.org/ICSchart/ChronostratChart2018-07.pdf>;  
1653 <https://doi.org/10.18814/epiiugs/2013/v36i3/002>
- 1654
- 1655 Coombs, H. 2016. Geochemical and geochronological constraints on terrane definition in Mexico.  
1656 PhD thesis. Cardiff University, 378 p.
- 1657
- 1658 Cossey, S., Rosenfeld, J., Bitter, M., and Pindell, J., 2021. Update on the Paleogene Water-Level  
1659 Drawdown Hypothesis, Gulf of Mexico. *Gulf Coast Association of Geological Societies Journal*, 10,  
1660 pp.123-141.
- 1661
- 1662 Covault, J.A. and Graham, S.A., 2010. Submarine fans at all sea-level stands: Tectono-morphologic  
1663 and climatic controls on terrigenous sediment delivery to the deep sea. *Geology*, 38(10), pp.939–942.
- 1664
- 1665 Damon, P. and Montesinos, E., 1978. Late Cenozoic volcanism and metallogenesis over an active  
1666 Benioff zone in Chiapas, Mexico. *Arizona Geological Society Digest*, 11, pp.155–168.
- 1667
- 1668 Dávalos-Álvarez, O.G., Nieto-Samaniego, Á.F., Alaniz-Álvarez, S.A., Martínez-Hernández, E. and  
1669 Ramírez-Arriaga, E., 2007. Estratigrafía cenozoica de la región de Tehuacán y su relación con el  
1670 sector norte de la falla de Oaxaca. *Revista mexicana de ciencias geológicas*, 24(2), pp.197–215.
- 1671

61  
62  
63  
64  
65

- 1672 Davison, I., 2021. Salt tectonics in the Sureste Basin, SE Mexico: some implications for hydrocarbon  
1 1673 exploration. *Geological Society, London, Special Publications*, 504(1), pp.147–165.  
2 1674 <https://doi.org/10.1144/SP504-2019-227>  
3 1675
- 4 1676 Delgado-Argote, L.A., López-Martínez, M., York, D. and Hall, C.M. 1992. Geologic framework and  
5 1677 geochronology of ultramafic complexes of the southern México. *Canadian Journal of Earth Sciences*  
6 1678 29(7), 1590–1604, <https://doi.org/10.1139/e92-125>  
7 1679
- 8 1680 Delgado-Argote, L.A., 1988. Geología preliminar de la secuencia volcanosedimentaria y serpentinitas  
9 1681 asociadas del Jurásico (?) del área de Cuicatlán–Concepción Pápalo, Oaxaca. *Rev. - Inst. Geol.,*  
10 1682 *UNAM* 7, 127–135.  
11 1683
- 12 1684 Dodson, M.H., 1973. Closure temperature in cooling geochronological and petrological systems.  
13 1685 *Contributions to Mineralogy and Petrology*, 40(3), pp.259–274.  
14 1686
- 15 1687 Ducea, M.N., Valencia, V.A., Shoemaker, S., Reiners, P.W., DeCelles, P.G., Campa, M.F., Morán-  
16 1688 Zenteno, D., and Ruiz, J., 2004, Rates of sediment recycling beneath the Acapulco trench:  
17 1689 Constraints from (U-Th)/He thermochronology: *Journal of Geophysical Research*, v. 109, B09404,  
18 1690 <https://doi.org/10.1029/2004JB003112>.  
19 1691
- 20 1692 Elías- Herrera, M. and Ortega- Gutiérrez, F., 2002. Caltepec fault zone: An Early Permian dextral  
21 1693 transpressional boundary between the Proterozoic Oaxacan and Paleozoic Acatlán complexes,  
22 1694 southern Mexico, and regional tectonic implications. *Tectonics*, 21(3), pp. 1–18.  
23 1695
- 24 1696 Engebretson, D.C., Cox, A. and Gordon, R.G. 1984. Relative motions between oceanic plates of the  
25 1697 Pacific Basin. *Journal of Geophysical Research*, 89, 10291–10310,  
26 1698 <https://doi.org/10.1029/JB089iB12p10291>  
27 1699
- 28 1700 England, P. and Molnar, P., 1990. Surface uplift, uplift of rocks, and exhumation of rocks. *Geology*,  
29 1701 18(12), pp.1173–1177.  
30 1702
- 31 1703 Escalera-Alcocer, J.A., 2010. Estrategia, Logros y desafíos de la exploración petrolera en  
32 1704 Mexico. *Trabajo de Ingreso a la Academia de Ingeniería México. Especialidad: Ingeniería Geológica.*  
33 1705 70 p.  
34 1706
- 35 1707 Espejo-Bautista, G., Ortega-Gutiérrez, F., Solari, L.A., Maldonado, R. and Valencia-Morales, Y.T.,  
36 1708 2021. The Sierra de Juárez Complex: a new Gondwanan Neoproterozoic-early Palaeozoic  
37 1709 metamorphic terrane in southern Mexico. *International Geology Review*, pp.1-23.  
38 1710 <https://doi.org/10.1080/00206814.2020.1870172>  
39 1711
- 40 1712 Farley, K.A., 2002, (U-Th)/He dating: Techniques, calibrations, and applications: *Reviews in*  
41 1713 *Mineralogy and Geochemistry*, v. 47, no. 1, p. 819–844, <https://doi.org/10.2138/rmg.2002.47.18>.  
42 1714
- 43 1715 Ferrari, L., Tagami, T., Eguchi, M., Orozco-Esquivel, M.T., Petrone, C.M., Jacobo-Albarrán, J. and  
44 1716 López-Martínez, M. 2005. Geology, geochronology and tectonic setting of late Cenozoic volcanism  
45 1717 along the southwestern Gulf of Mexico: The Eastern Alkaline Province revisited. *Journal of*  
46 1718 *Volcanology and Geothermal Research*, 146(4), pp.284–306.  
47 1719 <https://doi.org/10.1016/j.jvolgeores.2005.02.004>  
48 1720
- 49 1721 Ferrari, L., Orozco-Esquivel, T., Manea, V. and Manea, M., 2012. The dynamic history of the Trans-  
50 1722 Mexican Volcanic Belt and the Mexico subduction zone. *Tectonophysics*, 522, pp.122-149.  
51 1723 <https://doi.org/10.1016/j.tecto.2011.09.018>  
52 1724
- 53 1725 Fitz-Díaz, E. and van der Pluijm, B., 2013. Fold dating: A new Ar/Ar illite dating application to  
54 1726 constrain the age of deformation in shallow crustal rocks. *Journal of Structural Geology*, 54, pp.174–  
55 1727 179. <https://doi.org/10.1016/j.jsg.2013.05.011>  
56 1728
- 57 1729 Fitz- Díaz, E., Hudleston, P., Tolson, G. and Van Der Pluijm, B., 2014. Progressive, episodic  
58 1730 deformation in the Mexican Fold–Thrust Belt (Central Mexico): evidence from isotopic dating of folds  
59 1731 and faults. *International Geology Review*, 56(6), pp.734–755.  
60 1731

61  
62  
63  
64  
65

- 1732  
1 1733 Fitz-Díaz, E., Lawton, T.F., Juárez-Arriaga, E. and Chávez-Cabello, G., 2018. The Cretaceous-  
2 1734 Paleogene Mexican orogen: Structure, basin development, magmatism and tectonics. *Earth-Science*  
3 1735 *Reviews*, 183, pp.56–84.  
4 1736  
5 1737 Fitz-Díaz, E., Hernández-Vergara, R., Ortega-Gutiérrez, F., Sanz-Valencia, J. Albarrán-Santos, M.A.,  
6 1738 Pi-Puig, T., 2022. Kinematics and Ar–Ar illite age of deformation in the late Paleozoic Chicomuselo  
7 1739 Fold-Thrust Belt (CFTB), Chiapas, Mexico and tectonic implications. *Journal of South American Earth*  
8 1740 *Sciences*, 113, p.103648.  
9 1741  
10 1742 Friedmann, S.J., and Burbank, D.W., 1995, Rift basins and supra detachment basins: Intracontinental  
11 1743 extensional end-members. *Basin Research*, v. 7, p. 109–127  
12 1744 Galloway, W.E., Whiteaker, T.L. and Ganey-Curry, P. 2011. History of Cenozoic North American  
13 1745 drainage basin evolution, sediment yield, and accumulation in the Gulf of Mexico  
14 1746 basin. *Geosphere*, 7(4), pp.938–973.  
15 1747  
16 1748 García-Molina, G., 1994. *Structural evolution of SE Mexico (Chiapas-Tabasco-Campeche) offshore*  
17 1749 *and onshore*. Doctoral dissertation, Rice University. 494 pp.  
18 1750  
19 1751 Garduño-Monroy, V.H., Macías, J.L. and Garza, R.M., 2015. Geodynamic setting and pre-volcanic  
20 1752 geology of active volcanism in Chiapas. In *Active Volcanoes of Chiapas (Mexico): El Chichón and*  
21 1753 *Tacaná* (pp. 1-23). Springer, Berlin, Heidelberg.  
22 1754  
23 1755 Gawthorpe, R.L., and Leeder, M.R., 2000, Tectonosedimentary evolution of active extensional basins.  
24 1756 *Basin Research*, v. 12, p. 195–218.  
25 1757  
26 1758 González, E. and Medrano, M. 2014. Structural slope fans resulting from Palaeogene compression in  
27 1759 the Veracruz Basin, Mexico. AAPG Search and Discovery Article #50963, AAPG 2014 Annual  
28 1760 Convention and Exhibition, April 6–9, 2014, Houston, Texas, USA,  
29 1761 [http://www.searchanddiscovery.com/pdfz/documents/2014/50963gonzalez/ndx\\_gonzalez.pdf.html](http://www.searchanddiscovery.com/pdfz/documents/2014/50963gonzalez/ndx_gonzalez.pdf.html)  
30 1762  
31 1763 Graham, R., Pindell, J., Villagómez, D., Molina-Garza, R., Granath, J. and Sierra-Rojas, M., 2020.  
32 1764 Integrated Cretaceous–Cenozoic plate tectonics and structural geology in Southern Mexico.  
33 1765 *Geological Society, London, Special Publications*, 504(1), pp. 285–314.  
34 1766 <https://doi.org/10.1144/SP504-2020-70>  
35 1767  
36 1768 Gray, G.G., Pottorf, R.J., Yurewicz, D.A., Mahon, K.I., Pevear, D.R., Chuchla, R.J., 2001, Thermal  
37 1769 and chronological record of syn- to post-Laramide burial and exhumation, Sierra Madre Oriental,  
38 1770 Mexico, in Bartolini, C., Buffler, R.T., Cantú-Chapa, A. (eds.), *The western Gulf of Mexico Basin:*  
39 1771 *Tectonics, sedimentary basins, and petroleum systems*: American Association of Petroleum  
40 1772 *Geologists Memoir*, 75, 159–181.  
41 1773  
42 1774 Gray, G., Villagómez, D., Pindell, J., Molina-Garza, R., O'Sullivan, P., Stockli, D., Farrell, W., Blank,  
43 1775 D. and Schuba, J. 2021. Late Mesozoic and Cenozoic thermotectonic history of eastern, central and  
44 1776 southern Mexico as determined through integrated thermochronology, with implications for sediment  
45 1777 delivery to the Gulf of Mexico. *Geological Society of London Special Publications* 504, no.1. 255–  
46 1778 283. <https://doi.org/10.1144/SP504-2019-243>  
47 1779  
48 1780 Gutiérrez Paredes, H. C., Martínez Medrano, M. and Sessarego, H. L. 2009, Provenance for the  
49 1781 middle and upper Miocene sandstones of the Veracruz Basin, Mexico, in C. Bartolini and J. R. Roman  
50 1782 Ramos, eds., *Petroleum systems in the southern Gulf of Mexico*: AAPG Memoir 90, p. 397–407.  
51 1783 <https://doi.org/10.1016/j.jsames.2017.10.007>  
52 1784  
53 1785 Gutiérrez-Paredes, H. C., O. Catuneanu, and U. Hernandez Romano. 2018. Controls on the quality of  
54 1786 Miocene reservoirs, southern Gulf of Mexico. *Journal of South American Earth Sciences*, 81, pp.45–  
55 1787 65.  
56 1788  
57 1789 Harrison, T.M., Célérier, J., Aikman, A.B., Hermann, J. and Heizler, M.T., 2009. Diffusion of <sup>40</sup>Ar in  
58 1790 muscovite. *Geochimica et Cosmochimica Acta* 73, 1039–1051.  
59 1791  
60  
61  
62  
63  
64  
65

- 1792 Helland-Hansen, W., Sømme, T.O., Martinsen, O.J., Lunt, I. and Thurmond, J. 2016. Deciphering  
1 1793 Earth's natural hourglasses: perspectives on source-to-sink analysis. *Journal of Sedimentary*  
2 1794 *Research*, 86(9), pp.1008–1033.
- 3 1795  
4 1796 Hernández-Vergara, R., Fitz-Díaz, E., Brocard, G. and Morán-Zenteno, D.J., 2021. Illite 40Ar–39Ar  
5 1797 dating of Eocene deformation in the Chiapas Fold and Thrust Belt, southern Mexico. *Geological*  
6 1798 *Society*, London, Special Publications, 504(1), pp.315–341.
- 7 1799  
8 1800 Herrmann, U.R., Nelson, B.K. and Ratschbacher, L., 1994. The origin of a terrane: U/Pb zircon  
9 1801 geochronology and tectonic evolution of the Xolapa complex (southern Mexico). *Tectonics*, 13(2),  
10 1802 pp.455-474. <https://doi.org/10.1029/93TC02465>
- 11 1803  
12 1804 Hessler, A.M., Covault, J.A., Stockli, D.F. and Fildani, A., 2018. Late Cenozoic cooling favored glacial  
13 1805 over tectonic controls on sediment supply to the western Gulf of Mexico. *Geology*, 46(11), pp.995–  
14 1806 998. <https://doi.org/10.1130/G45528.1>
- 15 1807  
16 1808 Horbury, A.D., Gonzalez-P, S.H.F., Rodriguez-F, D., Reyes-F, A., Ortiz-G, P., Martinez-M, M. and  
17 1809 Quintanilla-R, G. 2003, Tectonic sequence stratigraphy of the western margin of the Gulf of Mexico in  
18 1810 the late Mesozoic and Cenozoic: Less passive than previously imagined, in C. Bartolini, R. T. Buffler,  
19 1811 and J. Blickwede, eds., *The Circum-Gulf of Mexico and the Caribbean: Hydrocarbon habitats, basin*  
20 1812 *formation, and plate tectonics: AAPG Memoir 79*, p. 184–245.
- 21 1813  
22 1814 IHS. 2010. Basin Monitor – Veracruz Basin, IHS Markit Basin Dataset. Mexico.  
23 1815 <https://ihsmarkit.com/Info/en/a/mexico/e-p-data.html>
- 24 1816  
25 1817 Jennette, D.C., Fouad, K., Wawrzyniec, T., Dunlap, D., Muñoz, R. and Meneses-Rocha, J. 2003a.  
26 1818 Slope and basin-floor reservoirs from the Miocene and Pliocene of the Veracruz Basin, southeastern  
27 1819 Mexico. *Marine and Petroleum Geology*, 20(6-8), pp.587–600.  
28 1820 <https://doi.org/10.1016/j.marpetgeo.2003.01.001>
- 29 1821  
30 1822 Jennette, D., Wawrzyniec, T., Fouad, K., Dunlap, D.B., Meneses-Rocha, J., Grimaldo, F., Muñoz, R.,  
31 1823 Barrera, D., Williams-Rojas, C.T. and Escamilla-Herrera, A., 2003. Traps and turbidite reservoir  
32 1824 characteristics from a complex and evolving tectonic setting, Veracruz Basin, southeastern  
33 1825 Mexico. *AAPG bulletin*, 87(10), pp.1599–1622. <https://doi.org/10.1306/05130302010>
- 34 1826  
35 1827 Kazachkina, E., Kostoglodov, V., Cotte, N., Walpersdorf, A., Ramirez-Herrera, M.T., Gaidzik, K.,  
36 1828 Husker, A. and Santiago, J.A., 2020. Active 650-km long fault system and Xolapa siver in Southern  
37 1829 Mexico. *Frontiers in Earth Science*, 8, p.155. <https://doi.org/10.3389/feart.2020.00155>
- 38 1830  
39 1831 Keppie, J.D., Dostal, J., Cameron, K.L., Solari, L.A., Ortega-Gutiérrez, F., and López, R., 2003,  
40 1832 Geochronology and geochemistry of Grenvillian igneous suites in the northern Oaxacan Complex,  
41 1833 southern Mexico: Tectonic implications: *Precambrian Research*, v. 120, p. 365–389,  
42 1834 [https://doi.org/10.1016/S0301-9268\(02\)00166-3](https://doi.org/10.1016/S0301-9268(02)00166-3).
- 43 1835  
44 1836 Ketcham, R.A., 2005, Forward and inverse modelling of low-temperature thermochronometry data:  
45 1837 *Reviews in Mineralogy and Geochemistry*, v. 58, p. 275–314.
- 46 1838  
47 1839 Ketcham, R.A., 2012. User's manual for HeFTy Version 1.7.5.
- 48 1840  
49 1841 Ketcham, R.A., Carter, A., Donelick, R.A., Barbarand, J., and Hurford, A.J., 2007, Improved modeling  
50 1842 of fission-track annealing in apatite: *The American Mineralogist*, v. 92, no. 5–6, p. 799–810,  
51 1843 <https://doi.org/10.2138/am.2007.2281>.
- 52 1844  
53 1845 Kirsch, M., Helbig, M., Keppie, J.D., Murphy, J.B., Lee, J.K.W., Solari, L.A., 2014. A Late Triassic  
54 1846 tectonothermal event in the eastern Acatlán Complex, southern Mexico, synchronous with a  
55 1847 magmatic arc hiatus: the result of flat-slab subduction? *Lithosphere* 6, 63–79.
- 56 1848  
57 1849 Lawton, T.F., Sierra-Rojas, M.I. and Martens, U., 2020. Stratigraphic correlation chart of  
58 1850 Carboniferous–Paleogene rocks of Mexico, adjacent southwestern United States, Central America,  
59 1851 and Colombia. *Southern and Central Mexico: Basement Framework, Tectonic Evolution, and*

61  
62  
63  
64  
65



- 1852 *Provenance of Mesozoic–Cenozoic Basins. Geological Society of America, Special Papers, 546,*  
1 1853 p.28.  
2 1854
- 3 1855 Lister, G., and Davis, A.G., 1989, The origin of metamorphic core complexes and detachment faults  
4 1856 formed during Tertiary continental extension in the northern Colorado River region, USA: *Journal of*  
5 1857 *Structural Geology*, v. 11, p. 65–94.  
6 1858
- 7 1859 Lovera, O. M., Richter, F. M., Harrison, T. M., 1991. Diffusion Domains Determined by <sup>39</sup>Ar Released  
8 1860 During Step Heating. *Journal of Geophysical Research* 96, 2057–2069.  
9 1861
- 10 1862 Mandujano-Velázquez, J.J. and Keppie, J.D., 2009. Middle Miocene Chiapas fold and thrust belt of  
11 1863 Mexico: a result of collision of the Tehuantepec Transform/Ridge with the Middle America  
12 1864 Trench. *Geological Society, London, Special Publications*, 327(1), pp.55–69.  
13 1865
- 14 1866 Martens, U. and Molina-Garza, R., 2021. Mexico: Basement Framework and pre-Cretaceous  
15 1867 Stratigraphy. *Southern and Central Mexico: Basement Framework, Tectonic Evolution, and*  
16 1868 *Provenance of Mesozoic–Cenozoic Basins. Geological Society of America, Special Papers, 546.*  
17 1869 [https://doi.org/10.1130/2021.2546\(01\)](https://doi.org/10.1130/2021.2546(01))  
18 1870
- 19 1871 Martini, M. and Ortega-Gutiérrez, F., 2018. Tectono-stratigraphic evolution of eastern Mexico during  
20 1872 the break-up of Pangea: A review, in Gómez-Tuena, A. and Ortega-Gutiérrez, F., *Tectonic Systems of*  
21 1873 *Mexico. Origin and Evolution. Earth-Sciences Reviews*, 183, 1–182.  
22 1874
- 23 1875 Martiny, B., Martínez-Serrano, R.G., Morán-Zenteno, D.J., Macías-Romo, C. and Ayuso, R.A., 2000.  
24 1876 Stratigraphy, geochemistry and tectonic significance of the Oligocene magmatic rocks of western  
25 1877 Oaxaca, southern Mexico. *Tectonophysics*, 318(1-4), pp.71–98. [https://doi.org/10.1016/S0040-](https://doi.org/10.1016/S0040-1951(99)00307-8)  
26 1878 [1951\(99\)00307-8](https://doi.org/10.1016/S0040-1951(99)00307-8)  
27 1879
- 28 1880 Martínez-Medrano, M., Vega-Escobar, R., Flores-Cruz, F., Angeles-Marin, D. and Lopez-Martinez, C.,  
29 1881 2009. Integrated seismic and petrographic analyses of the sandstone reservoirs of the Tertiary  
30 1882 Veracruz Basin, Mexico. in C. Bartolini and J. R. Roman Ramos, eds., *Petroleum systems in the*  
31 1883 *southern Gulf of Mexico: AAPG Memoir 90*, p. 217–235. DOI:10.1306/13191085M903335  
32 1884
- 33 1885 Martön, G.L. and Buffler, R.T. 1994. Jurassic reconstruction of the Gulf of Mexico Basin. *International*  
34 1886 *Geology Review*, 36, 545–586, <https://doi.org/10.1080/00206819409465475>  
35 1887
- 36 1888 Mayall, M., Lonergan, L., Bowman, A., James, S., Mills, K., Primmer, T., Pope, D., Rogers, L. and  
37 1889 Skeene, R., 2010. The response of turbidite slope channels to growth-induced seabed  
38 1890 topography. *AAPG Bulletin*, 94(7), pp.1011–1030. <https://doi.org/10.1306/01051009117>  
39 1891
- 40 1892 McDougall, I., and Harrison, T., 1999, *Geochronology and Thermochronology by the 40Ar/39Ar*  
41 1893 *Method.*: Oxford University Press, New York, v. 2nd ed.  
42 1894
- 43 1895 Mendoza-Rosales, C.C., Centeno-García, E., Silva-Romo, G., Campos-Madrugal, E., and Bernal, J.P.,  
44 1896 2010. Barremian rift-related turbidites and alkaline volcanism in southern Mexico and their role in the  
45 1897 opening of the Gulf of Mexico: *Earth and Planetary Science Letters*, 295, 419–434,  
46 1898 <https://doi.org/10.1016/j.epsl.2010.04.020>.  
47 1899
- 48 1900 Meneses-Rocha, J. J., 2001, Tectonic evolution of the Ixtapa graben, an example of a strike-slip basin  
49 1901 in southeastern Mexico: Implications for regional petroleum systems, in C. Bartolini, R. T. Buffler, and  
50 1902 A. Cantú-Chapa, eds., *The western Gulf of Mexico Basin: Tectonics, sedimentary basins, and*  
51 1903 *petroleum systems: AAPG Memoir 75*, p. 183–216.  
52 1904
- 53 1905 Michaud, F. and Fourcade, E.R.I.C., 1989. Stratigraphie et paléogéographie du Jurassique et du  
54 1906 Crétacé du Chiapas (Sud-Est du Mexique). *Bulletin de la Société géologique de France*, (3), pp.639-  
55 1907 650. <https://doi.org/10.2113/gssgfbull.V.3.639>  
56 1908
- 57 1908 Molina-Garza, R.S., Van der Voo, R. and Urrutia-Fucugauchi, J., 1992. Paleomagnetism of the  
58 1909 Chiapas Massif, southern Mexico: Evidence for rotation of the Maya Block and implications for the  
59 1910 opening of the Gulf of Mexico. *Geological Society of America Bulletin*, 104(9), pp.1156–1168.  
60 1911

61  
62  
63  
64  
65

- 1912
- 1 1913 Molina-Garza, R.S., Geissman, J.W., Wawrzyniec, T.F., Pena Alonso, T.A., Iriondo, A., Weber, B. and
- 2 1914 Aranda-Gómez, J., 2015. Geology of the coastal Chiapas (Mexico) Miocene plutons and the Tonalá
- 3 1915 shear zone: Syntectonic emplacement and rapid exhumation during sinistral
- 4 1916 transpression. *Lithosphere*, 7(3), pp.257–274.
- 5 1917
- 6 1918 Molina-Garza, R.S., van Hinsbergen, D.J., Boschman, L.M., Rogers, R.D. and Ganerød, M., 2019a.
- 7 1919 Large-scale rotations of the Chortis Block (Honduras) at the southern termination of the Laramide flat
- 8 1920 slab. *Tectonophysics*, 760, pp.36-57.
- 9 1921
- 10 1922 Molina-Garza, R.S., Pindell, J. and Villagómez, D. 2019b. Discussion of Ortega-Flores et al. (2018)
- 11 1923 'Provenance analysis of Oligocene sandstone from Cerro Pelón area, southern Gulf of Mexico'.
- 12 1924 *International Geology Review*, 62, 415–420, <https://doi.org/10.1080/00206814.2019.1616620>
- 13 1925
- 14 1926 Molina-Garza, R.S., Pindell, J., Coombs, H., Weber, B., Peña Alonso, T. 2020a. Definition of tectonic
- 15 1927 elements in Tehuantepec, southeast Mexico: An integrated geophysical, geochronological, and
- 16 1928 stratigraphic perspective. *Southern and Central Mexico: Basement Framework, Tectonic Evolution,*
- 17 1929 *and Provenance of Mesozoic–Cenozoic Basins. Geological Society of America, Special Papers*, 546.
- 18 1930
- 19 1931 Molina-Garza, R.S., Pindell, J. and Cortés, P.C.M., 2020b. Slab flattening and tractional coupling
- 20 1932 drove Neogene clockwise rotation of Chiapas Massif, Mexico: Paleomagnetism of the Eocene El
- 21 1933 Bosque Formation. *Journal of South American Earth Sciences*, 104, p.102932.
- 22 1934
- 23 1935 Molina Garza, R.S., Geissman, J.W., Peña Alonso, T., Aranda Gómez, J. and Wawrzyniec, T., 2021.
- 24 1936 Structural Setting, Paleomagnetism, and Magnetic Fabric of Miocene Plutons in a Transpressional
- 25 1937 Sinistral Shear Zone, Tonalá, Chiapas, Mexico: Evidence of Shortening During Magma
- 26 1938 Emplacement. *Tectonics*, 40(2), p.e2020TC006559. <https://doi.org/10.1029/2020TC006559>
- 27 1939
- 28 1940 Mora, J.C., Layer, P.W. and Jaimes-Viera, M.D.C., 2012. New 40Ar/39Ar ages from the central part of
- 29 1941 the Chiapanecan Volcanic Arc, Chiapas, México. *Geofísica internacional*, 51(1), pp.39–49.
- 30 1942
- 31 1943 Morán-Zenteno, D.J., Corona-Chávez, P., and Tolson, G., 1996, Uplift and subduction erosion in
- 32 1944 southwestern Mexico since the Oligocene: Pluton geobarometry constraints: Earth and Planetary
- 33 1945 Science Letters, v. 141, p. 51–65, [https://doi.org/10.1016/0012-821X\(96\)00067-2](https://doi.org/10.1016/0012-821X(96)00067-2).
- 34 1946
- 35 1947 Morán-Zenteno, D.J., Cerca, M. and Keppie, J.D., 2005. La evolución tectónica y magmática
- 36 1948 cenozoica del suroeste de México: avances y problemas de interpretación. *Boletín de la Sociedad*
- 37 1949 *Geológica Mexicana*, 57(3), pp.319–341. <https://doi.org/10.18268/bsgm2005v57n3a4>
- 38 1950
- 39 1951 Morán-Zenteno, D.J., Martiny, B.M., Solari, L., Mori, L., Luna-González, L. and González-Torres,
- 40 1952 E.A., 2018. Cenozoic magmatism of the Sierra Madre del Sur and tectonic truncation of the Pacific
- 41 1953 margin of southern Mexico. *Earth-Science Reviews*, 183, pp.85-114.
- 42 1954 <https://doi.org/10.1016/j.earscirev.2017.01.010>
- 43 1955
- 44 1956 Mousavi, M.A. and Bryant, S.L., 2013. Geometric models of porosity reduction by ductile grain
- 45 1957 compaction and cementation. *AAPG Bulletin*, 97(12), pp.2129–2148.
- 46 1958 <https://doi.org/10.1306/05171311165>
- 47 1959
- 48 1960 Nguyen, L.C. and Mann, P. 2016. Gravity and magnetic constraints on the Jurassic opening of the
- 49 1961 oceanic Gulf of Mexico and the location and tectonic history of the Western Main transform fault along
- 50 1962 the eastern continental margin of Mexico. *Interpretation*, 4, SC23–SC33, [https://doi.org/10.1190/INT-](https://doi.org/10.1190/INT-2015-0110.1)
- 51 1963 [2015-0110.1](https://doi.org/10.1190/INT-2015-0110.1)
- 52 1964
- 53 1965 Nieto-Samaniego, A.F., Alaniz-Álvarez, S.A., Silva-Romo, G., Eguiza-Castro, M.H. and Mendoza-
- 54 1966 Rosales, C.C., 2006. Latest Cretaceous to Miocene deformation events in the eastern Sierra Madre
- 55 1967 del Sur, Mexico, inferred from the geometry and age of major structures. *Geological Society of*
- 56 1968 *America Bulletin*, 118(1-2), pp.238–252.
- 57 1969
- 58 1970 Ortega-Flores, B., Martini, M., Solari, L., Colás, V., Guerrero-Moreno, S., Centeno-García, E., Silva-
- 59 1971 Romo, G., Grajales-Nishimura, M. 2018. Provenance analysis of Oligocene sandstone from the Cerro
- 60 1971

61  
62  
63  
64  
65

- 1972 Pelón area, southern Gulf of Mexico. *International Geology Review*, 61, 915–935,  
1 1973 <https://doi.org/10.1080/00206814.2018.1476922>  
2 1974  
3 1975 Ortega-Flores, B., Martini, M., Solari, L., Colás, V., Guerrero-Moreno, S., Centeno-García, E., Silva-  
4 1976 Romo, G., Grajales-Nishimura, M. 2020. Reply to Molina- Garza et al. (2019) ‘Discussion of: Ortega-  
5 1977 Flores et al. (2018) “Provenance analysis of Oligocene sandstone from the Cerro Pelón area,  
6 1978 southern Gulf of Mexico”. *International Geology Review*, 62, 421–427,  
7 1979 <https://doi.org/10.1080/00206814.2019.1616621>  
8 1980  
9 1981 Ortuño-Arzate, S., Ferket, H., Cacas, M.-C., Swennen, R., and Roure, F. 2003. Late Cretaceous  
10 1982 carbonate reservoirs in the Cordoba Platform and Veracruz Basin (eastern Mexico). In C. Bartolini, R.  
11 1983 T. Buffler, and J. Blickwede, eds., *The Circum-Gulf of Mexico and the Caribbean: Hydrocarbon*  
12 1984 *habitats, basin formation, and plate tectonics*, AAPG Memoir 79, p. 476–514.  
13 1985 <https://doi.org/10.1306/M79877C22>  
14 1986  
15 1987 Pemex. 2013a. Provincia Petrolera Veracruz. Petróleos Mexicanos (Pemex). Exploración y  
16 1988 Producción Subdirección de Exploración Versión 2.0, 2013. 38p.  
17 1989  
18 1990 Pemex. 2013b. Provincia Petrolera Cinturón Plegado de Chiapas. Petróleos Mexicanos (Pemex).  
19 1991 Exploración y Producción Subdirección de Exploración Versión 2.0, 2013. 33p.  
20 1992  
21 1993 Pemex. 2013c. Provincia Petrolera Sureste (Salina del Istmo, Reforma-Akal y Macuspana). Petróleos  
22 1994 Mexicanos (Pemex). Exploración y Producción Subdirección de Exploración Versión 2.0, 2013. 57p.  
23 1995  
24 1996 Peña-Alonso, T.A., Estrada-Carmona, J., Molina-Garza, R.S., Solari, L., Levresse, G., and Latorre,  
25 1997 C., 2017, Lateral spreading of the middle to lower crust inferred from Paleocene migmatites in the  
26 1998 Xolapa Complex (Puerto Escondido, Mexico): Gravitational collapse of a Laramide orogen?.  
27 1999 *Tectonophysics*, v. 706–707, p. 143–163, <https://doi.org/10.1016/j.tecto.2017.04.010>.  
28 2000  
29 2001 Peña-Alonso, T.A., Molina-Garza, R.S., Villalobos-Escobar, G., Estrada-Carmona, J., Levresse, G.  
30 2002 and Solari, L., 2018. The opening and closure of the Jurassic-Cretaceous Xolapa basin, southern  
31 2003 Mexico. *Journal of South American Earth Sciences*, 88, pp.599–620.  
32 2004  
33 2005 Peña-Alonso, T.A., Latorre, C., Estrada-Carmona, J., Molina-Garza, R.S., Solari, L. 2021. Multi-stage,  
34 2006 Upper Eocene-Oligocene anatexis in the Xolapa metamorphic belt (Puerto Escondido, Mexico):  
35 2007 Dynamics of the Xolapa Complex as the decoupled lower crust of the Chortís Block upper crust  
36 2008 during its tectonic migration. *Tectonophysics*. <https://doi.org/10.1016/j.tecto.2021.229004>  
37 2009  
38 2010 Pérez-Gutiérrez, R., Solari, L.A., Gómez-Tuena, A., and Valencia, V.A., 2009, The Cuicateco terrane:  
39 2011 Upper Cretaceous oceanic basin with subduction influence in southern Mexico? New structural,  
40 2012 geochemical and geochronological data: *Revista Mexicana de Ciencias Geológicas*, v. 26, p. 222–  
41 2013 242.  
42 2014  
43 2015 Pindell, J.L. 1985. Alleghanian reconstruction and the subsequent evolution of the Gulf of Mexico,  
44 2016 Bahamas, and Proto-Caribbean Sea. *Tectonics*, 4, 1–39, <https://doi.org/10.1029/TC004i001p00001>  
45 2017  
46 2018 Pindell, J.L. and Kennan, L. 2001. Kinematic evolution of the Gulf of Mexico and Caribbean. In: Fillon,  
47 2019 R.H., Rosen, N.C. et al. (eds) *Petroleum Systems of Deep-Water Basins: Global and Gulf of Mexico*  
48 2020 *Experience*. Transactions of the 21st Annual GCSSEPM Foundation Bob F. Perkins Research  
49 2021 Conference. Gulf Coast Section SEPM, Houston, TX, 193–220.  
50 2022  
51 2023 Pindell, J.L. and Kennan, L. 2009. Tectonic evolution of the Gulf of Mexico, Caribbean and northern  
52 2024 South America in the mantle reference frame: an update. *Geological Society, London, Special*  
53 2025 *Publications*, 328, 1–55, <https://doi.org/10.1144/SP328.1>.  
54 2026  
55 2027 Pindell, J.L. and Miranda, E. 2011. Linked kinematic histories of the Macuspana, Akal-Reforma,  
56 2028 Comalcalco, and deepwater Campeche Basin tectonic elements, southern Gulf of Mexico. *Gulf Coast*  
57 2029 *Association of Geological Societies Transactions*, 61, 353–361.  
58 2030  
59 2030  
60  
61  
62  
63  
64  
65

- 2031 Pindell, J., Maresch, W.V., Martens, U. and Stanek, K., 2011. The Greater Antillean Arc: Early  
12032 Cretaceous origin and proposed relationship to Central American subduction mélanges: implications  
22033 for models of Caribbean evolution. *International Geology Review*, 54(2), pp.131-143.  
32034 <https://doi.org/10.1080/00206814.2010.510008>  
42035
- 52036 Pindell, J., Miranda E., Cerón, A., and Hernandez, L. 2016. Aeromagnetic Map Constrains Jurassic-  
62037 Early Cretaceous Synrift, Breakup, and Rotational Seafloor Spreading History in the Gulf of Mexico. *In*  
72038 Lowery, C.M., Snedden, J.W., and Rosen, N. (eds.). *Mesozoic of the Gulf Rim and Beyond: New*  
82039 *progress in Science and Exploration of the Gulf of Mexico Basin. Transactions 35th Annual Gulf*  
92040 *Coast Section of the Society of Economic and Paleontological Mineralogists Foundation*, Perkins-  
102041 Rosen Research Conference, Houston, Texas, p. 123–153.  
112042
- 122043 Pindell, J., Villagómez, D., Molina-Garza, R., Graham, R., Weber, B. 2020a. A revised synthesis of  
132044 the rift and drift history of the Gulf of Mexico and surrounding regions in the light of improved age  
142045 dating of the Middle Jurassic salt. In: Davidson I., Pindell J. (eds). *The Geology and Hydrocarbon*  
152046 *Potential of Mexico and the Northern Caribbean*. Geological Society of London Special Publication.  
162047
- 172048 Pindell, J., Molina-Garza, R., Villagómez, D., Martens, U., Graham, R., Stockli, D., Weber, B., Sierra-  
182049 Rojas, M.I. 2020b. Provenance of the Miocene Nanchital Conglomerate, western Chiapas Foldbelt,  
192050 Mexico: implications for reservoir sands in the Sureste Basin, greater Campeche Province. In:  
202051 Davidson I., Pindell J. (eds). *The Geology and Hydrocarbon Potential of Mexico and the Northern*  
212052 *Caribbean*. Geological Society of London Special Publication.  
222053
- 232054 Pindell, J., Martens, U., Molina Garza, R., Villagomez, D., Beltrán, A., Stockli, D., Wildman, M., Solari,  
242055 L., 2022 (submitted). Late Cretaceous–Paleogene depositional evolution of Chiapas, Mexico: a  
252056 foreland controlled by collision of Greater Antilles Arc and the subsequent relative migration of the  
262057 Chortís Block.  
272058
- 282059 Prost, G., and Aranda, M. 2001, Tectonics and hydrocarbon systems of the Veracruz Basin, Mexico,  
292060 *in* C. Bartolini, R. T. Buffler, and A. Cantú-Chapa, eds., *The western Gulf of Mexico Basin: Tectonics,*  
302061 *sedimentary basins, and petroleum systems: AAPG Memoir 75*, p. 271–291. <https://shar.es/aWwoHn>  
312062
- 322063 Quezada-Muñetón, J.Q., 1987. El Cretacico Medio–Superior, y el limite Cretacico Superior–Terciario  
332064 Inferior en la Sierra de Chiapas. *Boletín de la Asociación Mexicana de Geólogos Petroleros (AMGP)*,  
342065 *vol. 39*, pp.3–98. <https://shar.es/aWYHmk>  
352066
- 362067 Ratschbacher, L., Franz, L., Min, M., Bachmann, R., Martens, U., Stanek, K., Stübner, K., Nelson,  
372068 B.K., Herrmann, U., Weber, B., López-Martínez, M., Jonckheere, R., Sperner, B., Tichomirowa, M.,  
382069 McWilliams, M.O., Gordon, M., and Meschede, M. 2009. The North American-Caribbean plate  
392070 boundary in Mexico-Guatemala-Honduras. *In* James, K., Lorente, M.A., and Pindell, J., eds., *Origin*  
402071 *and evolution of the Caribbean Region: Geological Society of London, Special Publication*, **328**, p.  
412072 219–293. <https://doi.org/10.1144/SP328.11>  
422073
- 432074 Reed, J.C., Wheeler, J.O., Tucholke, B.E. and Compilers. 2004. Geological Map of North America:  
442075 Decade of North American Geology. Continental Scale Map 001. Geological Society of America,  
452076 Boulder, CO. Scale 1:5 000 000, 1 sheet.  
462077
- 472078 Riller, U., Ratschbacher, L. and Frisch, W., 1992. Left-lateral transtension along the Tierra Colorada  
482079 deformation zone, northern margin of the Xolapa magmatic arc of southern Mexico. *Journal of South*  
492080 *American Earth Sciences*, 5(3–4), pp.237–249.  
502081
- 512082
- 522083 Ríos-López, J. J., and A. Cantu-Chapa, 2009, Stratigraphy and sedimentology of Middle Eocene  
532084 Kumaza Calcarenites Member in the Ku, Maloob, and Zaap oil fields, offshore Campeche,  
542085 Mexico, in C. Bartolini and J. R. Roman Ramos, eds., *Petroleum systems in the southern Gulf of*  
552086 *Mexico: AAPG Memoir 90*, p. 257–277. Doi:10.1306/13191087M903336  
562087
- 572088 Romito, S. and Mann, P. 2020. Tectonic terranes underlying the present-day Caribbean plate: their  
582089 tectonic origin, sedimentary thickness, subsidence histories and regional controls on hydrocarbon  
592089

60  
61  
62  
63  
64  
65

- 2090 resources. Geological Society, London, Special Publications, 504, 343–377.  
12091 <https://doi.org/10.1144/SP504-2019-221>
- 22092
- 32093 Rosenfeld, J., and J. Pindell, 2003, Early Paleogene isolation of the Gulf of Mexico from the world's  
42094 oceans? Implications for hydrocarbon exploration and eustasy, in C. Bartolini, R. T. Buffler, and J.  
52095 Blickwede, eds., *The Circum-Gulf of Mexico and the Caribbean: Hydrocarbon habitats, basin*  
62096 *formation, and plate tectonics: AAPG Memoir 79*, p. 89–103.
- 72097
- 82098 Ruiz-Arriaga, D., 2018. *Historia de deformación de la margen Oriental de la Plataforma Morelos-*  
92099 *Guerrero*. Msc Thesis. Universidad Nacional Autónoma de México. 132 pp.
- 102100
- 112101 Sanchez-Barreda, L.A., 1981. *Geologic evolution of the continental margin of the Gulf of Tehuantepec*  
122102 *in Southwestern Mexico*. Doctoral dissertation, The University of Texas at Austin. 272 pp.
- 132103
- 142104 Sánchez Hernández, H., 2013. Stratigraphic characterization and evolution of a Mid-tertiary age deep  
152105 water system, Holok area, SW Gulf of Mexico. Doctoral dissertation, University of Aberdeen, 358 pp.
- 162106
- 172107 Santillán-Piña, N. and Aguayo-Camargo, J.E. 2011. Facies sedimentarias turbidíticas del Terciario  
182108 Inferior en la cuenca de Chicontepec, centro-oriente de México. *Ingeniería, Investigación y*  
192109 *Tecnología*, 12(3), pp.337–352.
- 202110
- 212111 Shann, M.V., 2021. The Sureste Basin of Mexico: its framework, future oil exploration opportunities  
222112 and key challenges ahead. *Geological Society, London, Special Publications*, 504(1), pp.119–146.  
232113 <https://doi.org/10.1144/SP504-2019-214>
- 242114
- 252115 Shann, M.V., Vazquez-Reyes, K., Ali, H.M. and Horbury, A.D. 2020. The Sureste Super Basin of  
262116 southern Mexico. *AAPG Bulletin*, 104(12), pp.2643-2700. <https://doi.org/10.1306/09172020081>
- 272117
- 282118 Shoemaker, S., Ducea, M., Reiners, P.W., Garver, J.I., and Campa, M.F. 2002. Cenozoic plate  
292119 tectonic history of southwestern Mexico: Constraints from low temperature thermochronology:  
302120 *Geotemas*, v. 4, p. 137–138.
- 312121
- 322122 Sickmann, Z.T. and Snedden, J.W. 2021. Neogene to recent evolution of the Southern Gulf of Mexico  
332123 basin: Tectonic controls on deep- water sediment dispersal systems. *Basin Research*, 33(2),  
342124 pp.1240–1265. <https://doi.org/10.1111/bre.12512>
- 352125
- 362126 Sierra-Rojas, M.I., Molina-Garza, R.S. and Lawton, T.F., 2016. The Lower Cretaceous Atzompa  
372127 Formation in south-central Mexico: record of evolution from extensional backarc basin margin to  
382128 carbonate platform. *Journal of Sedimentary Research*, 86(6), pp.712–733.
- 392129
- 402130 Sierra-Rojas, M.I., Lawton, T.F., Martens, U., von Quadt, A., Beltrán-Triviño, A., Coombs, H., and  
412131 Stockli, D.F. 2020. Early Cretaceous to Paleogene sandstone provenance and sediment-dispersal  
422132 systems of the Cuicateco terrane, Mexico. *In Southern and Central Mexico: Basement Framework,*  
432133 *Tectonic Evolution, and Provenance of Mesozoic–Cenozoic Basins*, Geological Society of America,  
442134 doi:10.1130/2020.2546(10).
- 452135
- 462136 Simon-Labric, T., Brocard, G.Y., Teyssier, C., Beek, P.A., Fellin, M.G., Reiners, P.W., and  
472137 Authemayou, C., 2013, Preservation of contrasting geothermal gradients across the Caribbean–North  
482138 America plate boundary (Motagua fault, Guatemala): *Tectonics*, v. 32, no. 4, p. 993–1010,  
492139 <https://doi.org/10.1002/tect.20060>.
- 502140
- 512141 Snedden, J.W. and Galloway, W.E., 2019. *The Gulf of Mexico sedimentary basin: Depositional*  
522142 *evolution and petroleum applications*. Cambridge University Press. 351 p.
- 532143
- 542144 Snedden, J.W., Stockli, D.F., and Pasley, J. 2021. Reconstructing the Zama (Mexico) Discovery  
552145 Source to Sink Story, Part II. Implications for and predictions within the depositional sink.  
562146 *Transactions of the GeoGulf2021 Conference*, October 27–29, 2021. Austin, TX.
- 572147
- 582148 Solari, L.A., Torres de León, R., Hernández-Pineda, G., Solé, J., Solís-Pichardo, G., and Hernández-  
592149 Treviño, T., 2007, Tectonic significance of Cretaceous–Tertiary magmatic and structural evolution of

61  
62  
63  
64  
65

- 2150 the northern margin of the Xolapa Complex: Tierra Colorada area, southern Mexico: Geological  
12151 Society of America Bulletin, v. 119, p. 1265–1279, <https://doi.org/10.1130/B26023.1>.
- 22152
- 32153 Solari, L.A., García-Casco, A., Martens, U., Lee, J.K. and Ortega-Rivera, A., 2013. Late Cretaceous  
42154 subduction of the continental basement of the Maya block (Rabinal Granite, central Guatemala):  
52155 Tectonic implications for the geodynamic evolution of Central America. *Bulletin*, 125(3-4), pp.625–  
62156 639.
- 72157
- 82158 Sømme, T.O., Helland- Hansen, W., Martinsen, O.J. and Thurmond, J.B. 2009. Relationships  
92159 between morphological and sedimentological parameters in source- to- sink systems: a basis for  
102160 predicting semi- quantitative characteristics in subsurface systems. *Basin Research*, 21(4), pp. 361–  
112161 387.
- 122162
- 132163 Sosa-Patrón, A. A., J. G. Cardenas Lopez, C. Cardenas Lara, O. Pinto Gomez, M. E. Guzzy  
142164 Arredondo, M. E. Monroy Audelo, and R. Castellanos Calvo, 2009, Integrated geological  
152165 interpretation and impact on the definition of Neogene plays in the Isthmus Saline Basin, Mexico, *in*C.  
162166 Bartolini, and J. R. Roman Ramos, eds., *Petroleum systems in the southern Gulf of Mexico: AAPG*  
172167 *Memoir* 90, p. 29–47. DOI:10.1306/13191076M903330
- 182168
- 192169 Stockli, D.F., Snedden, J., and Pasley, J. - Reconstructing the Zama (Mexico) Discovery Source to  
202170 Sink Story, Part I. Detrital Zircon U-Pb Provenance Analysis and Implications for Sediment Source  
212171 Dynamics. Transactions of the GeoGulf2021 Conference, October 27–29, 2021. Austin, TX.
- 222172
- 232173 Talavera-Mendoza, O., Ruiz, J., Corona-Chavez, P., Gehrels, G.E., Sarmiento-Villagrana, A., García-  
242174 Díaz, J.L. and Salgado-Souto, S.A., 2013. Origin and provenance of basement metasedimentary  
252175 rocks from the Xolapa Complex: New constraints on the Chortis–southern Mexico connection. *Earth*  
262176 *and Planetary Science Letters*, 369, pp.188–199.
- 272177
- 282178 Tolson, G., 2005. La falla Chacalapa en el sur de Oaxaca. *Boletín de la Sociedad Geológica*  
292179 *Mexicana*, 57(1), pp.111–122.
- 302180
- 312181 Vega-Granillo, R., Talavera-Mendoza, O., Meza-Figueroa, D., Ruiz, J., Gehrels, G.E., López-  
322182 Martínez, M. and de la Cruz-Vargas, J.C., 2007. Pressure-temperature-time evolution of Paleozoic  
332183 high-pressure rocks of the Acatlán Complex (southern Mexico): implications for the evolution of the  
342184 Iapetus and Rheic Oceans. *Geological Society of America Bulletin*, 119(9-10), pp.1249–1264.
- 352185
- 362186 Villagómez, D. 2014. The Northern Cuicateco Terrane from a thermochronological perspective and its  
372187 implications on the pre-, syn- and post-Laramide deformation. Tectonic Analysis Ltd, West Sussex,  
382188 UK, Cordillera Program Phase 1 technical report, 20. <https://doi.org/10.13140/RG.2.2.22814.43840>
- 392189
- 402190 Villagómez, D., Pindell, J.L. and Spikings, R. 2019. Thermal history of the crystalline basement from  
412191 the western and southern Gulf of Mexico: Implications for rifting and later events. *Geological Society*  
422192 *of America Special Papers*, 546, 1–18, [https://doi.org/10.1130/2019.2546\(16\)](https://doi.org/10.1130/2019.2546(16))
- 432193
- 442194 Villagómez, D. and Pindell, J. 2020a. Cooling and uplift history of the Chiapas Massif and its influence  
452195 on sedimentation and deformation in the adjacent Sierra de Chiapas Basin. In: Martens, U. and  
462196 Molina-Garza, R.S. (eds) *Southern and Central Mexico: Basement Framework, Tectonic Evolution,*  
472197 *and Provenance of Mesozoic–Cenozoic Basins*. Geological Society of America, Special Papers, 546,  
482198 [https://doi.org/10.1130/2020.2546\(17\)](https://doi.org/10.1130/2020.2546(17))
- 492199
- 502200 Villagómez, D. and Pindell, J. 2020b. Thermochronology of the southern Mexican margin (Xolapa  
512201 belt), Acapulco to Puerto Angel: Crustal dynamics of a trench–trench–transform triple junction. In:  
522202 Martens, U. and Molina-Garza, R.S. (eds) *Southern and Central Mexico: Basement Framework,*  
532203 *Tectonic Evolution, and Provenance of Mesozoic–Cenozoic Basins*. Geological Society of America,  
542204 *Special Papers*, 546, [https://doi.org/10.1130/2020.2546\(14\)](https://doi.org/10.1130/2020.2546(14))
- 552205
- 562206 Walsh, J.P., Wiberg, P.L., Aalto, R., Nittrouer, C.A. and Kuehl, S.A. 2016. Source-to-sink research:  
572207 economy of the Earth's surface and its strata. *Earth Science Reviews*, 153, pp.1–6.
- 582208
- 59
- 60
- 61
- 62
- 63
- 64
- 65

2209 Weber, B. and Hecht, L., 2003. Petrology and geochemistry of metaigneous rocks from a Grenvillian  
12210 basement fragment in the Maya block: the Guichicovi complex, Oaxaca, southern Mexico.  
22211 *Precambrian Research*, 124(1), pp.41–67. [https://doi.org/10.1016/S0301-9268\(03\)00078-0](https://doi.org/10.1016/S0301-9268(03)00078-0)  
32212  
42213 Weber, B., Iriondo, A., Premo, W.R., Hecht, L. and Schaaf, P., 2007. New insights into the history and  
52214 origin of the southern Maya block, SE México: U–Pb–SHRIMP zircon geochronology from  
62215 metamorphic rocks of the Chiapas massif. *International Journal of Earth Sciences*, 96(2), pp.253–269.  
72216 <https://doi.org/10.1007/s00531-006-0093-7>  
82217  
92218 Weber, B., Scherer, E.E., Schulze, C., Valencia, V.A., Montecinos, P., Mezger, K. and Ruiz, J. 2010.  
102219 U–Pb and Lu–Hf isotope systematics of lower crust from central-southern Mexico—Geodynamic  
112220 significance of Oaxaquia in a Rodinia Realm. *Precambrian Research*, 182, 149–162,  
122221 <https://doi.org/10.1016/j.precamres.2010.07.007>  
132222  
142223 Winker, C.D. and Buffler, R.T., 1988. Paleogeographic evolution of early deep-water Gulf of Mexico  
152224 and margins, Jurassic to Middle Cretaceous (Comanchean). *AAPG bulletin*, 72(3), pp.318-346.  
162225 <https://doi.org/10.1306/703C8C22-1707-11D7-8645000102C1865D>  
172226  
182227 Winter, R., 2018, Coarse-grained deep water, slope, and basin-floor systems: Influence of tectonic  
192228 processes on internal and external architecture: University of Texas PhD Dissertation, 163 pp.  
202229  
212230 Witt, C., Brichau, S. and Carter, A., 2012. New constraints on the origin of the Sierra Madre de  
222231 Chiapas (south Mexico) from sediment provenance and apatite thermochronometry. *Tectonics*, 31(6).  
232232 <https://doi.org/10.1029/2012TC003141>  
242233  
252234 Wolfe, M.R. and Stockli, D.F., 2010. Zircon (U–Th)/He thermochronometry in the KTB drill hole,  
262235 Germany, and its implications for bulk He diffusion kinetics in zircon. *Earth and Planetary Science*  
272236 *Letters*, 295(1-2), pp.69–82.  
282237  
292238 Worzel, J. L., Bryant, W., Beall, A. O. R. Jr, Capo, R., Dickinson, K., Foreman, H. P., Laury, R.,  
302239 McNeely, B. W., & Smith, L. A., 1973, Initial reports of the deep sea drilling project v. 10. Deep Sea  
312240 Drilling Project Reports and Publications, p.1–748.  
322241  
332242 Zepeda-Martínez, M., Martini, M., Solari, L.A. and Mendoza-Rosales, C.C., 2021. Reconstructing the  
342243 tectono-sedimentary evolution of the Early–Middle Jurassic Tlaxiaco Basin in southern Mexico: New  
352244 insights into the crustal attenuation history of southern North America during Pangea  
362245 breakup. *Geosphere* 17 (4): 1294–1317.

37  
38  
39  
40  
41  
42  
43  
44  
45  
46  
47  
48  
49  
50  
51  
52  
53  
54  
55  
56  
57  
58  
59  
60  
61  
62  
63  
64  
65

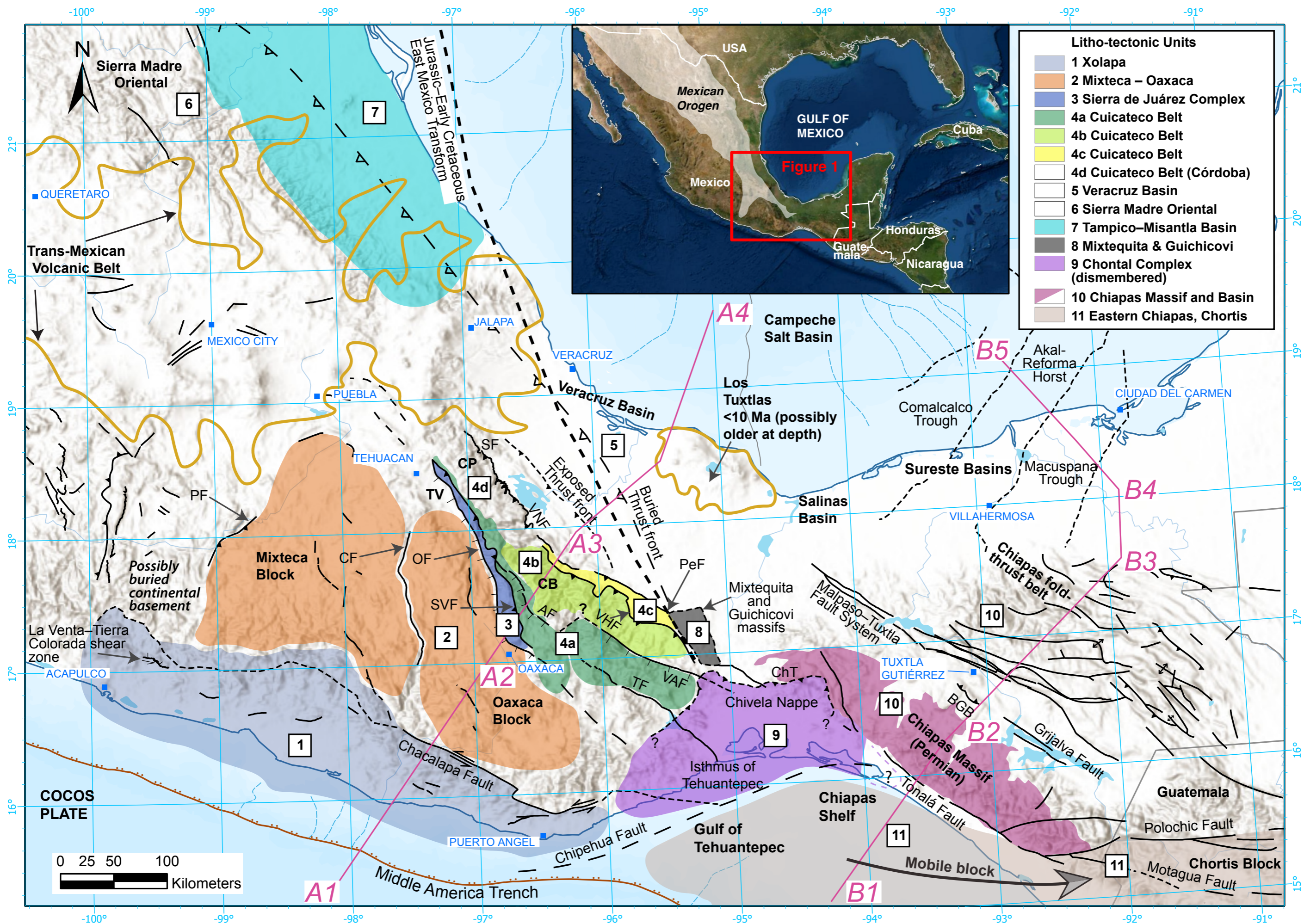


Figure 1



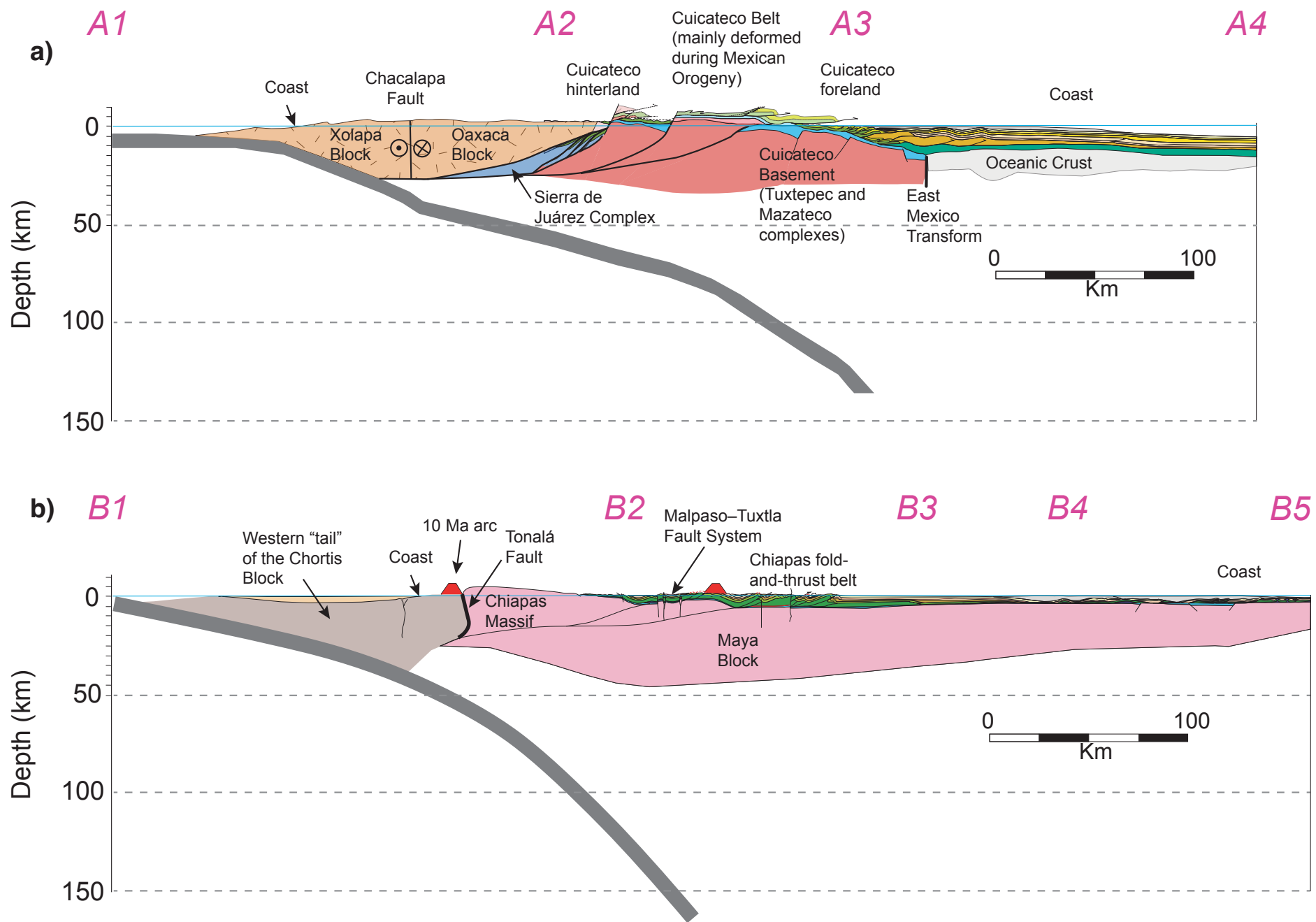
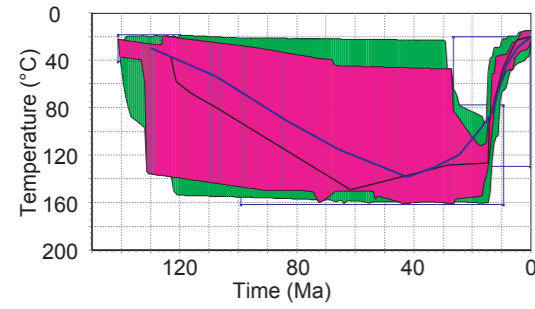
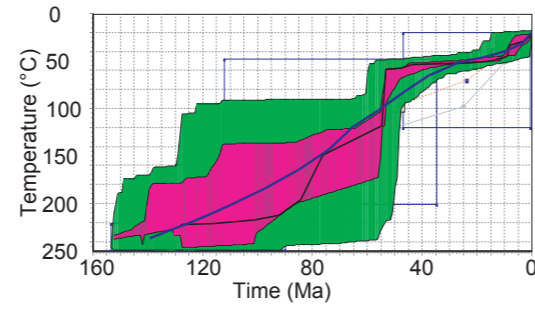
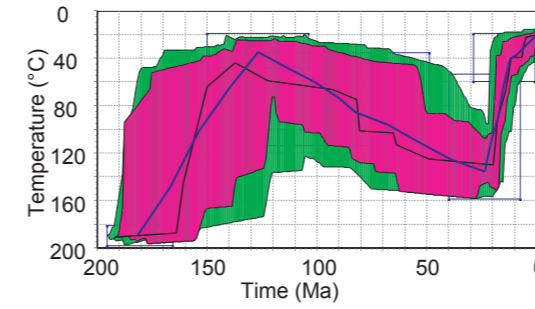
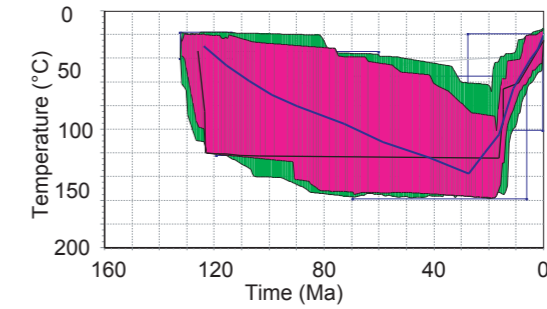
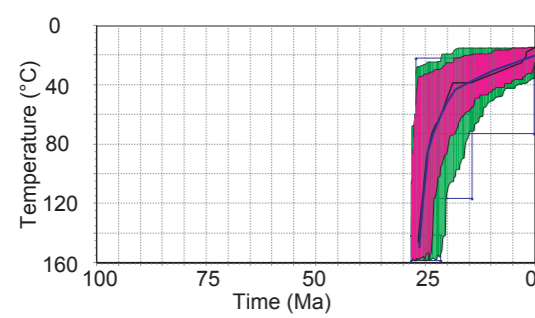
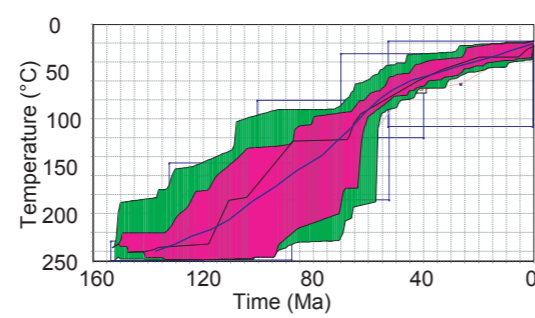
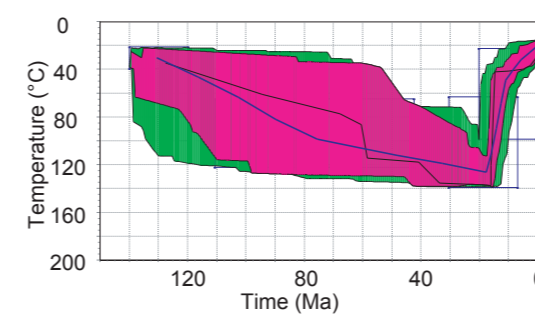
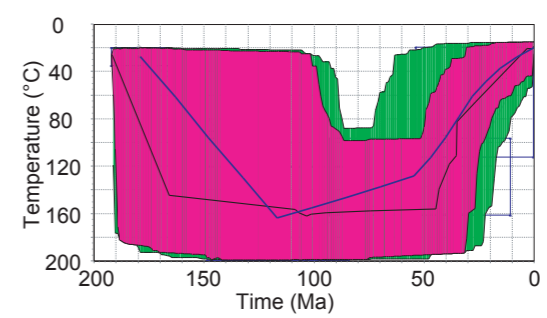
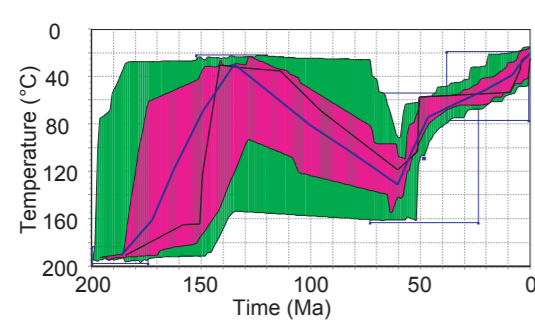
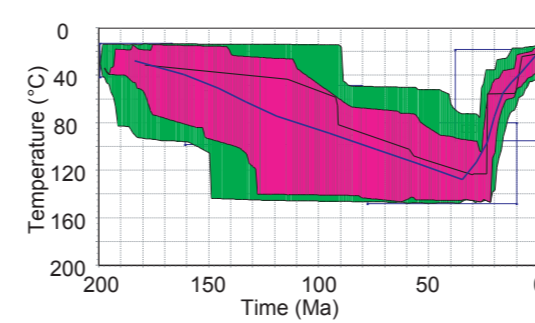
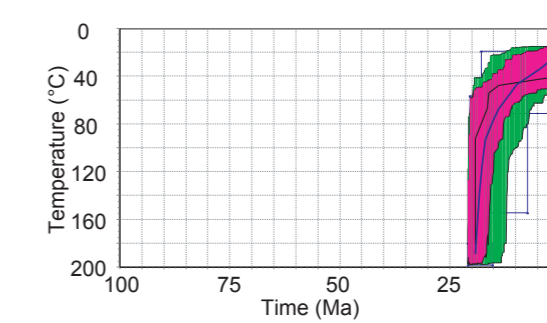
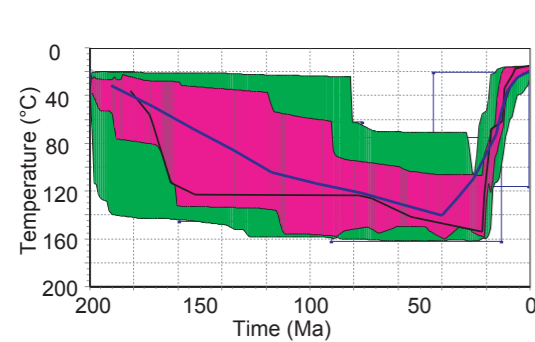
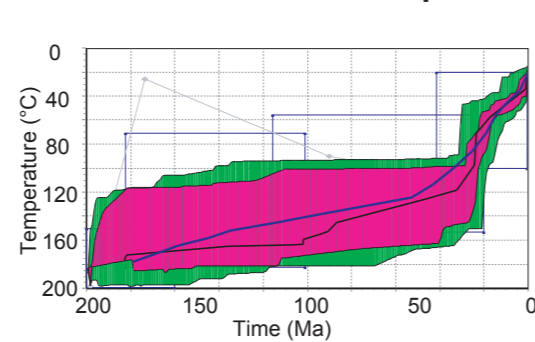
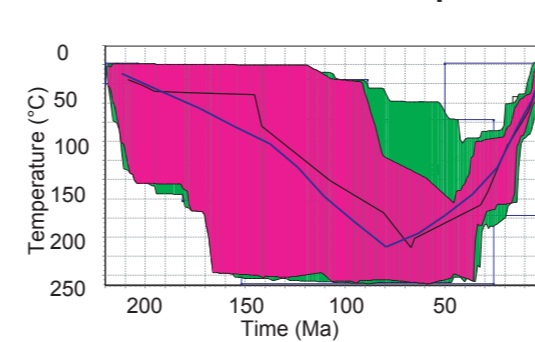
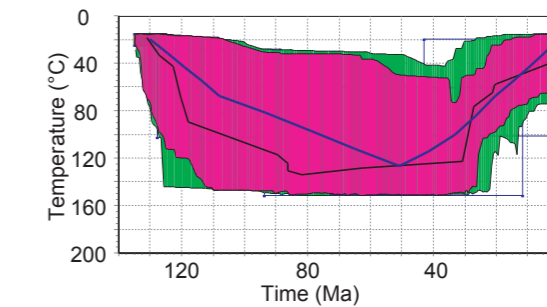
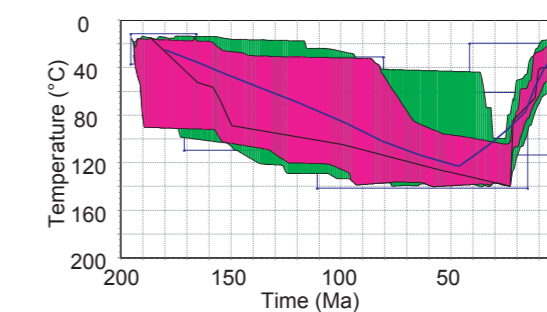


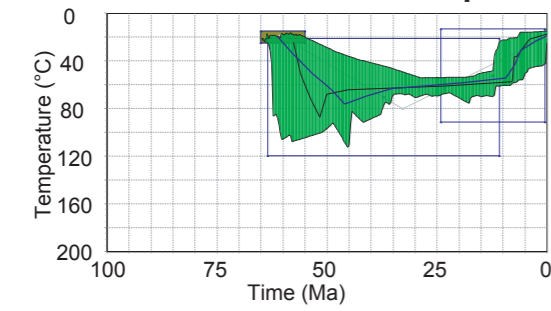
Figure 2



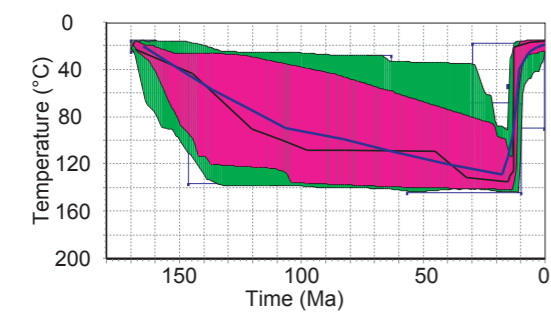
**Mixteca (W) – Oaxaca (E)****Sierra de Juárez Complex****Cuicateco Belt; West of Villa Alta and Aloapán faults,  
East of Siempre Viva Fault****17-01-18-03 Jaltepetongo****5-11-11-02A Teotitlán Migmatitic Complex****18-01-18-03 Quartzitic rock****16-01-18-08A Jaltepetongo Fm.****17-01-18-06 Ejutla batholith****5-11-11-03A Teotitlán Migmatitic Complex****26Feb16-7A Jaltepetongo****16-01-18-09A Muscovite schist****18-01-18-01 Gneiss****16-01-18-05A Todos Santos Fm.****16-01-18-10A San Juan Juquila granitoid****Cuicateco Belt; between Villa Alta/Aloapán and Vista Hermosa faults (Mazateco)****Cuicateco Belt; between Vista Hermosa and Valle Nacional faults****12-9-10-08A Todos Santos Fm.****12-9-10-10A Mazateco Complex****21-01-18-01 Mazateco Complex****19-01-18-06 Xonamanca Fm.****20-01-18-08 Todos Santos Fm.**

## Tampico–Misantla Basin

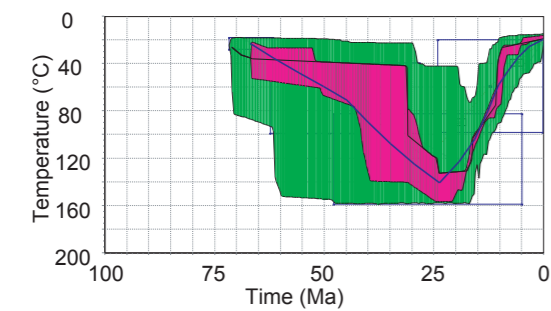
### COAP17-1 Basal? Chicontepec



### ALTO17-2 Cahuasas Jurassic redbeds

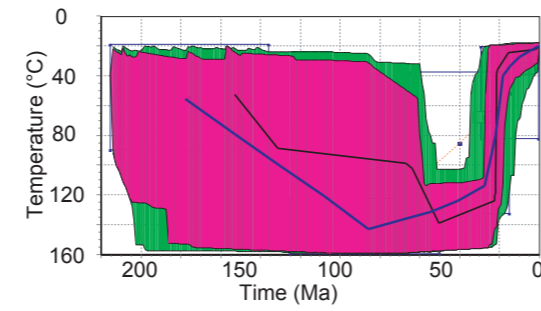


### SANT17-1 K–Pg breccia

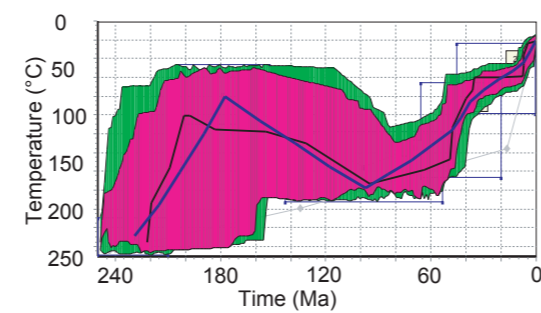


## Mixtequita and Guichicovi blocks

### 19-07-04-1 Guichicovi Complex

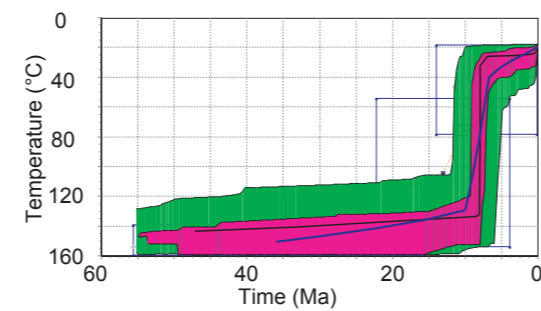


### 27Mar17-3A Mixtequita granite



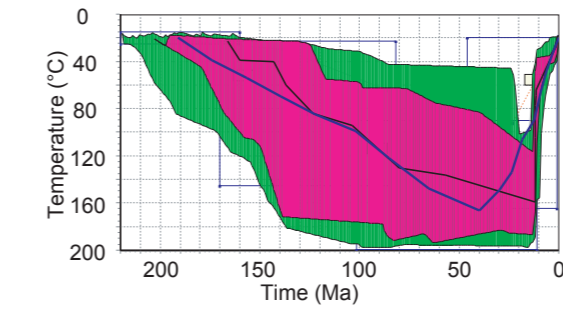
## Chiapas Massif and Basin

### 19-07-05-4 Westernmost Chiapas Massif

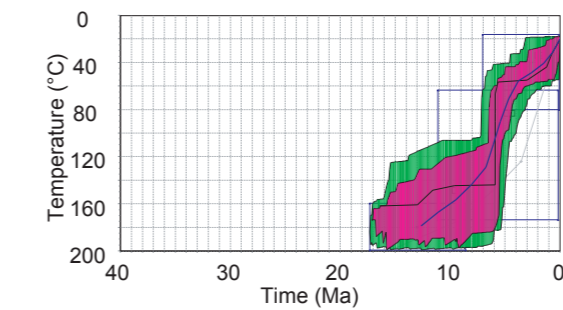


## Chontal

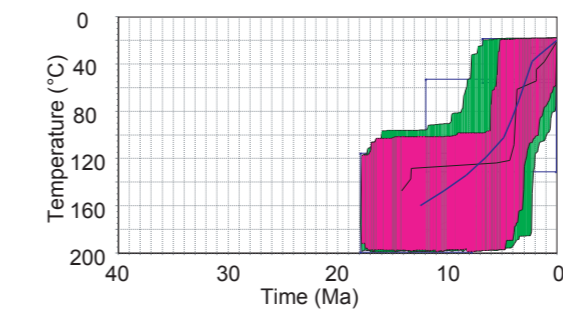
### 19-07-03-2B Chivela lithodeme



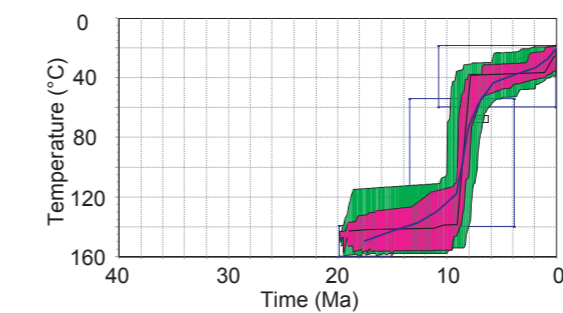
### 9-30-10-09A Juchitán granite



### 9-30-10-11 Western Tehuantepec

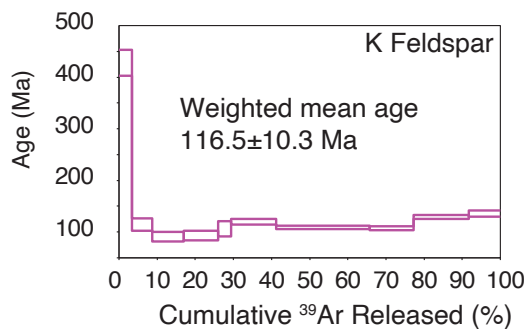


### 19-07-05-1 Migmatite



### Sierra de Juárez Complex

**5-11-11-02A Metagranite**  
(zircon U–Pb:  $158 \pm 13$  Ma; *Pindell et al., 2020a*)



**5-11-11-03A Orthogneiss with mylonitic textures**  
(zircon U–Pb:  $137.2 \pm 2.2$  Ma; *Coombs, 2016*)

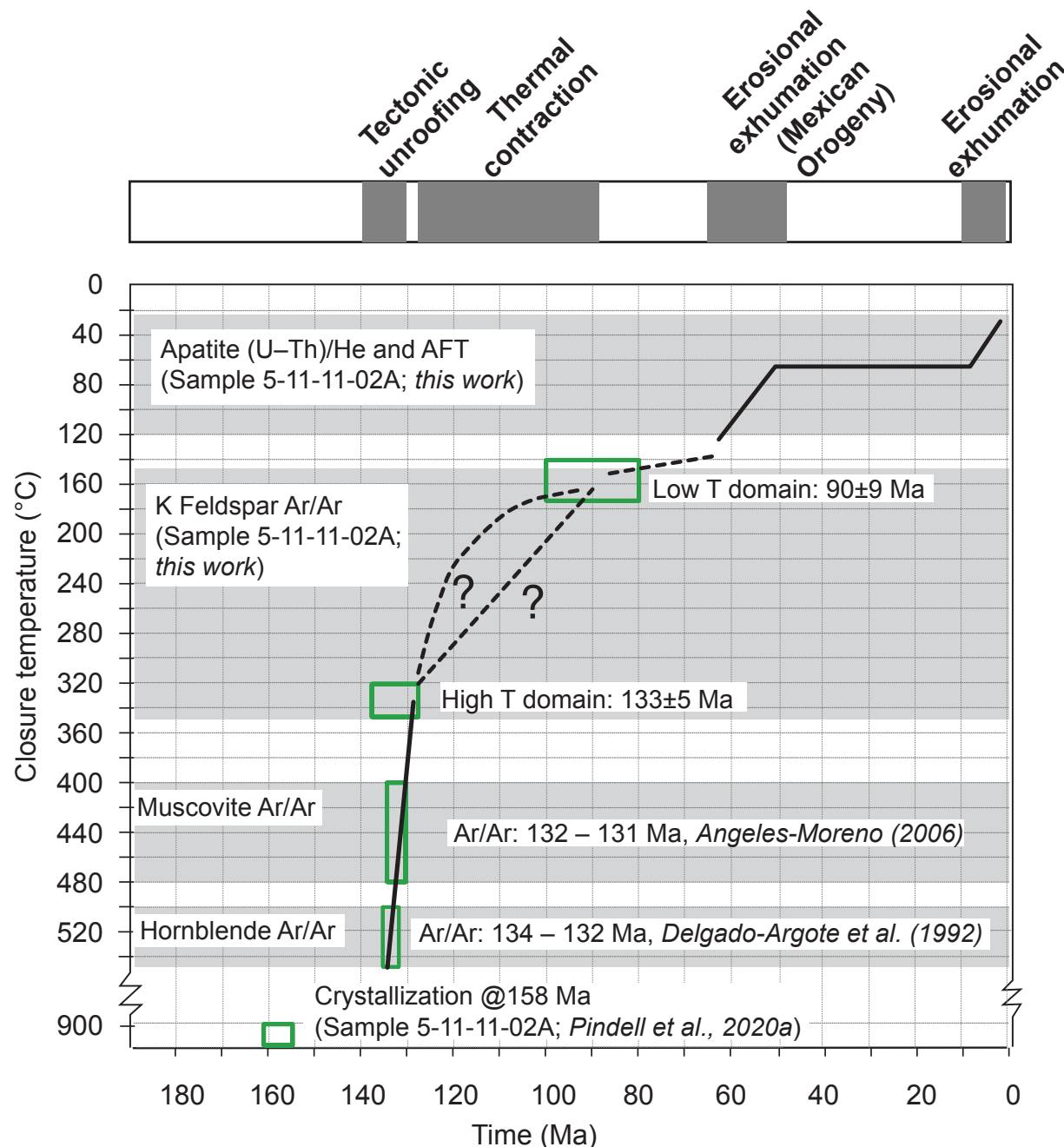
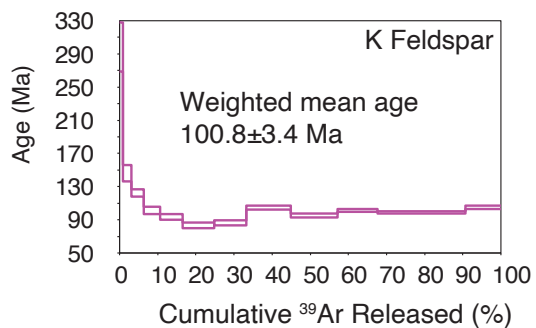


**Figure 5.**

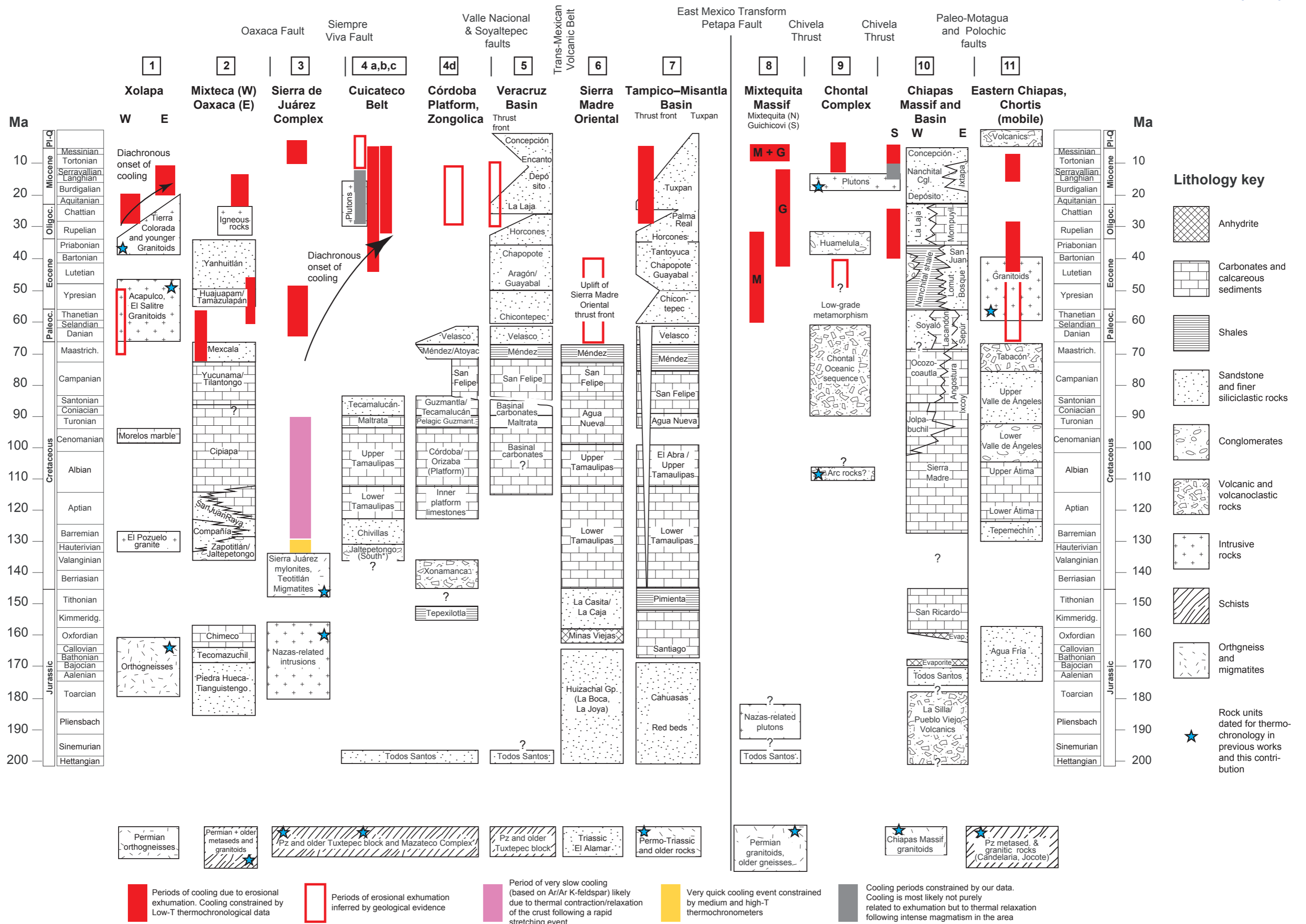


Figure 6.

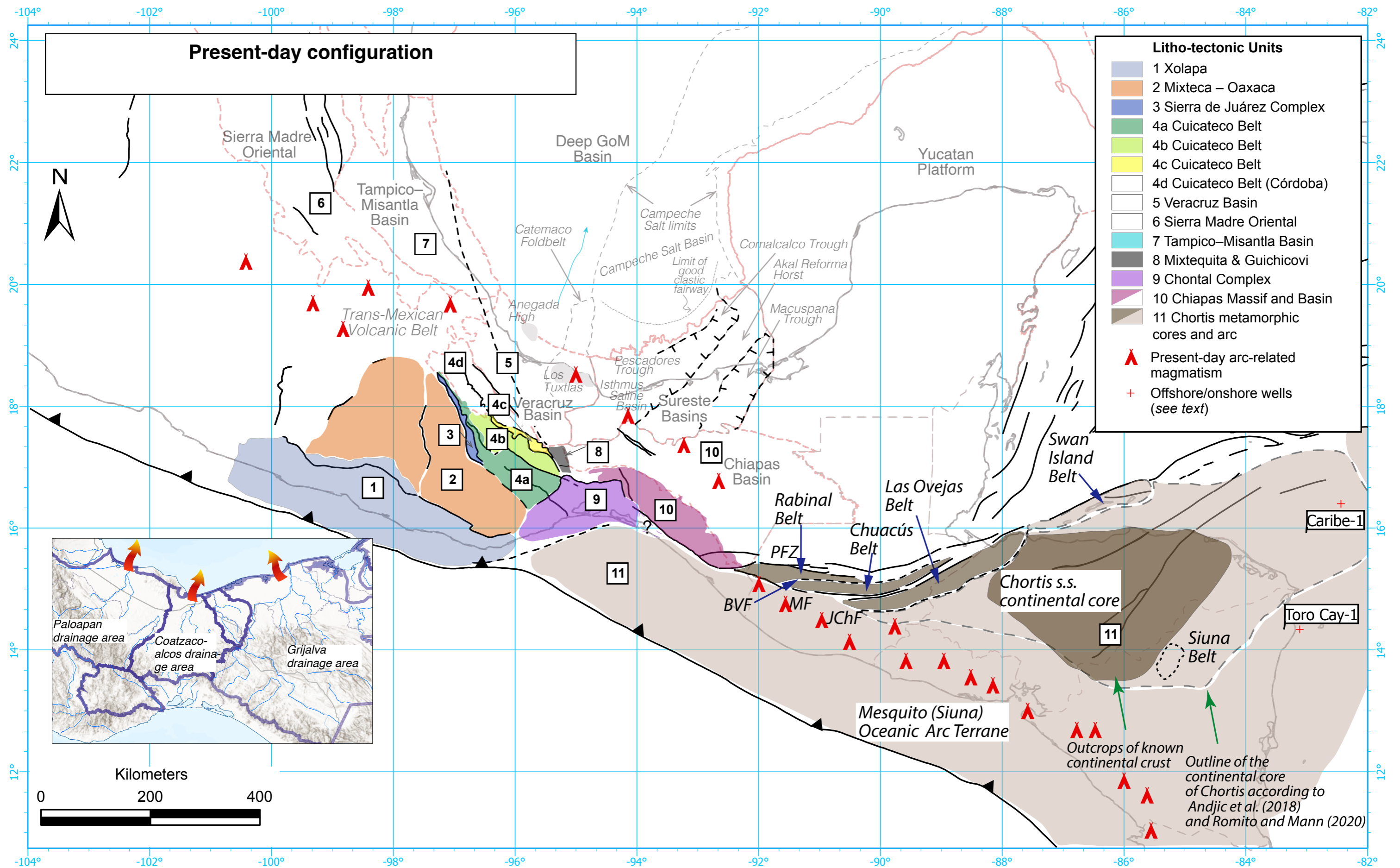


Figure 7a

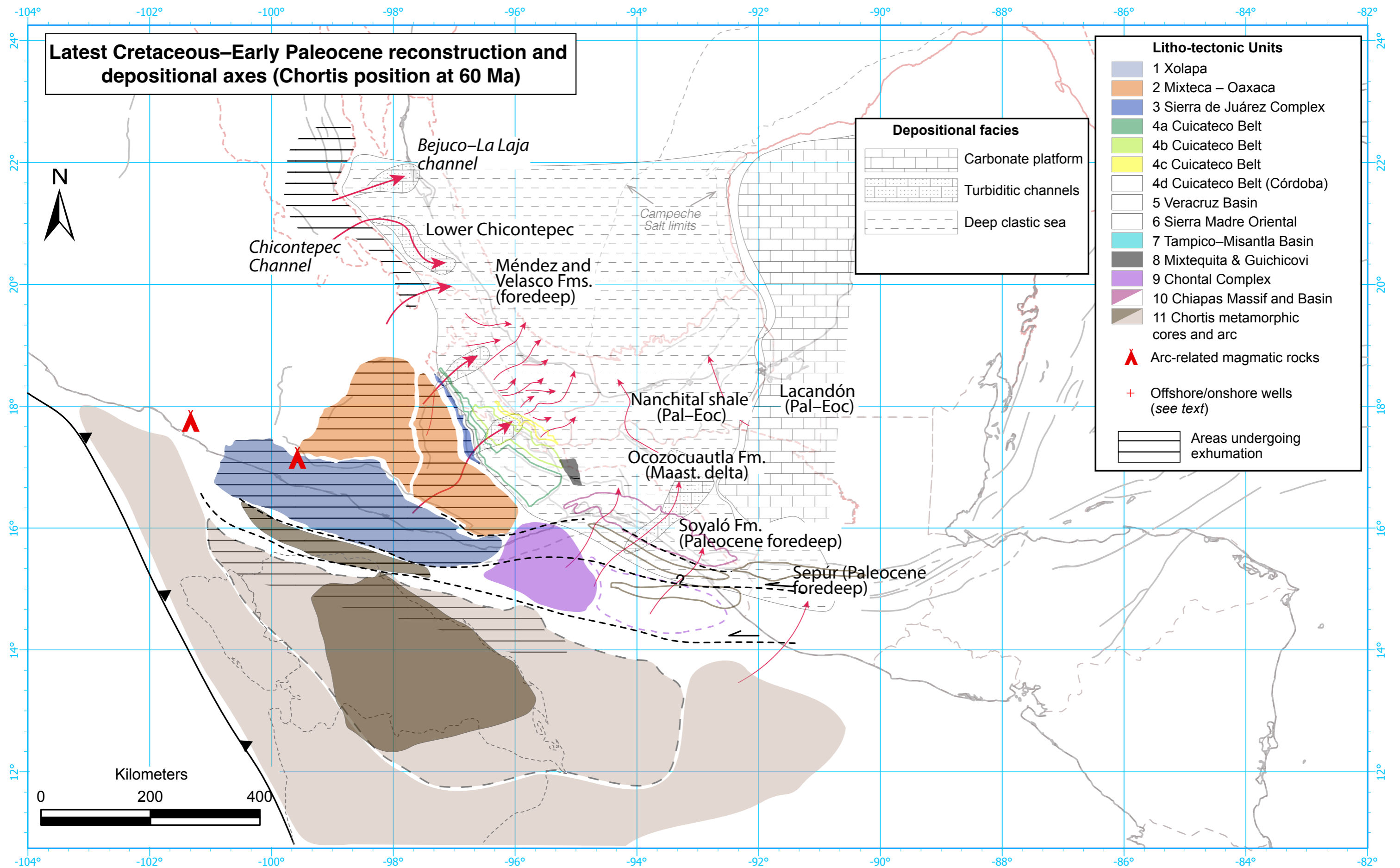


Figure 7b



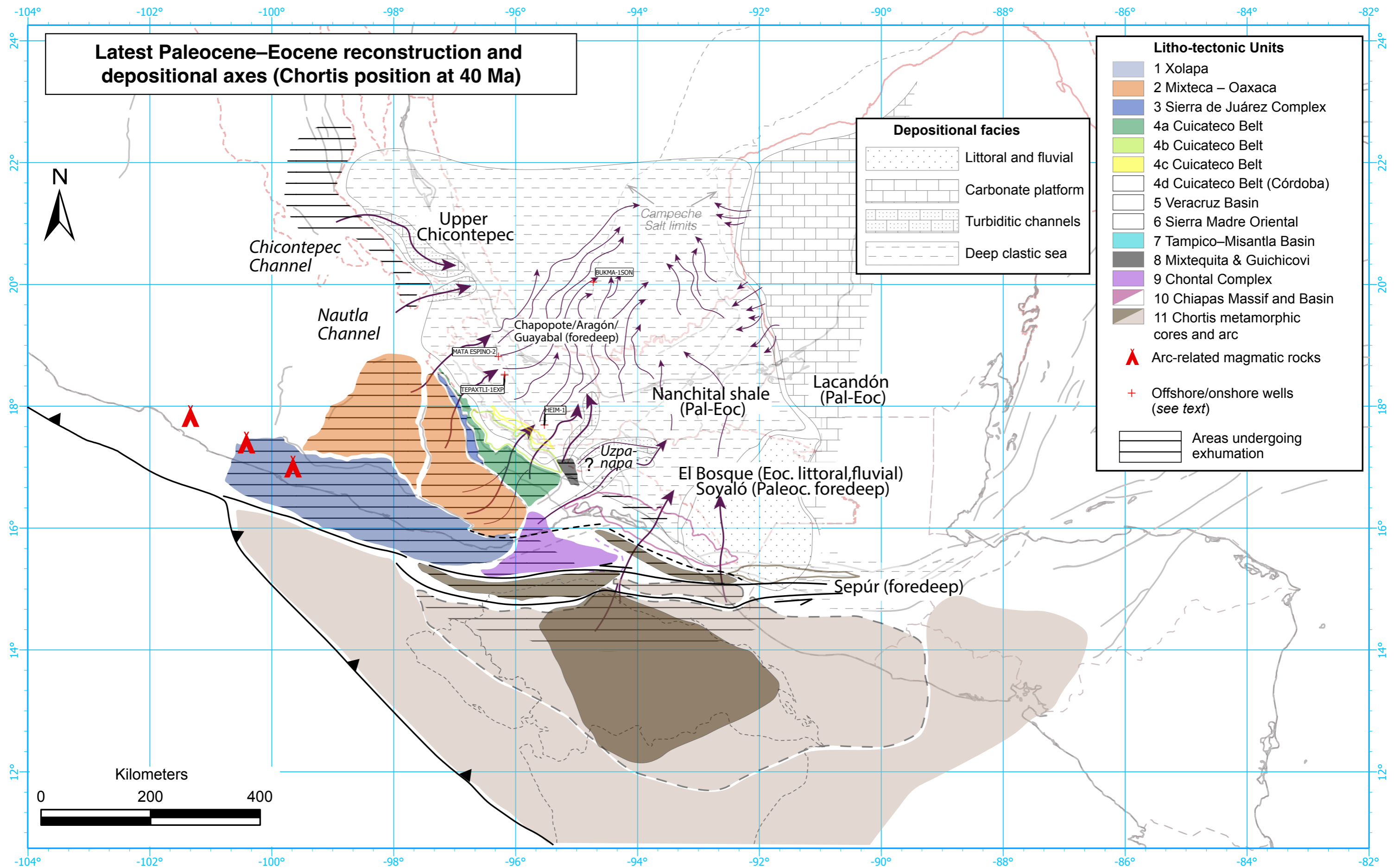


Figure 7c

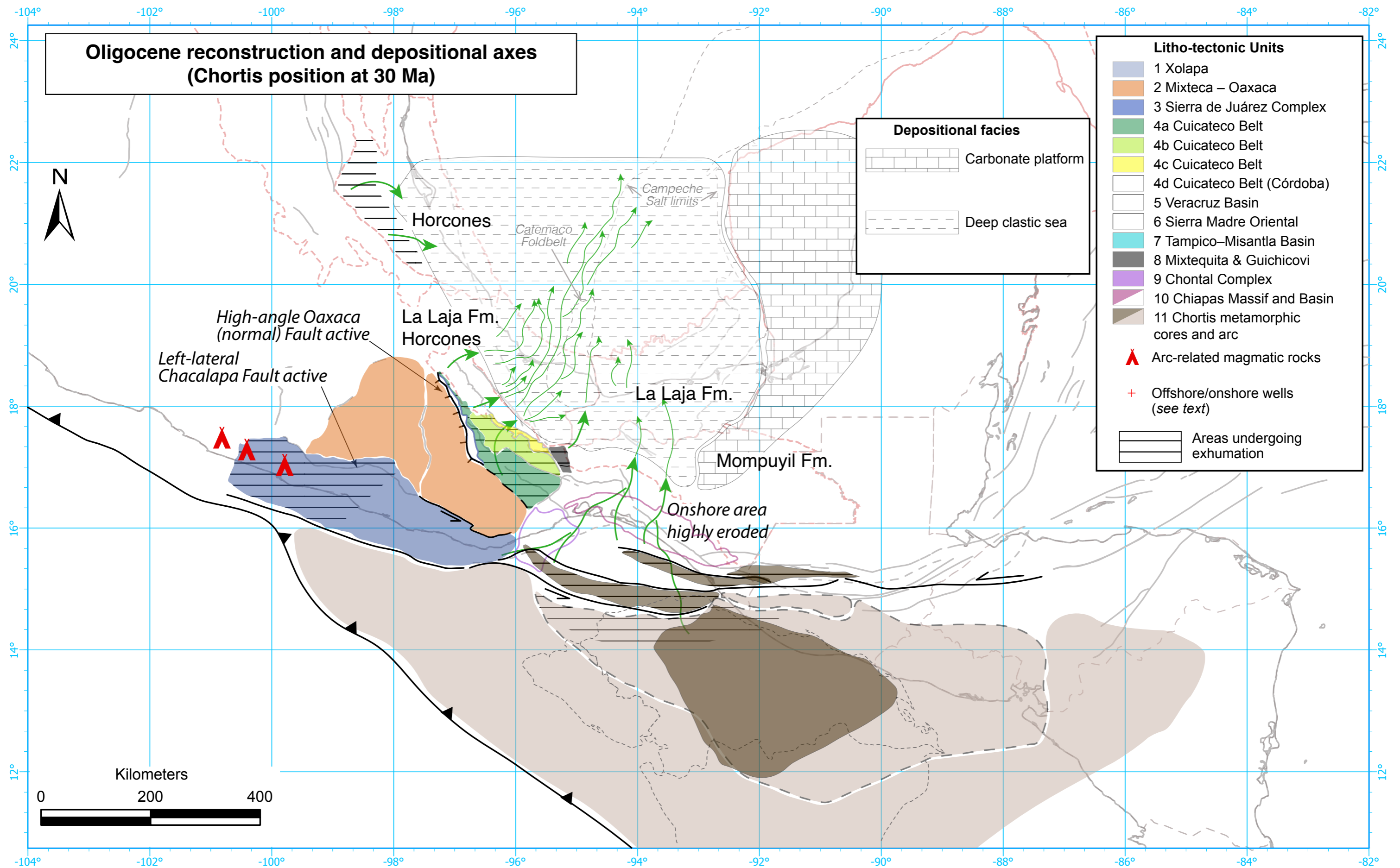


Figure 7d

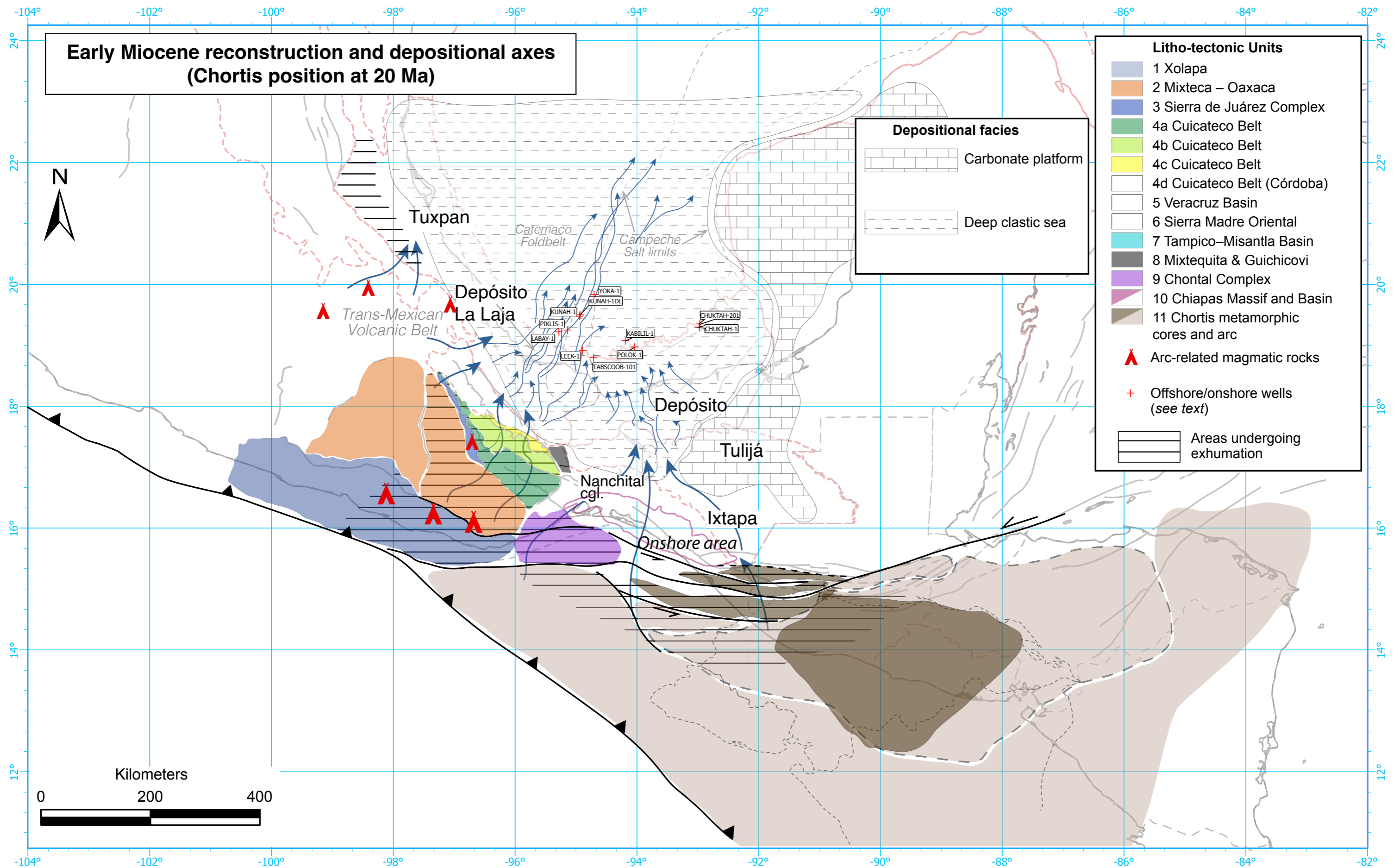


Figure 7e

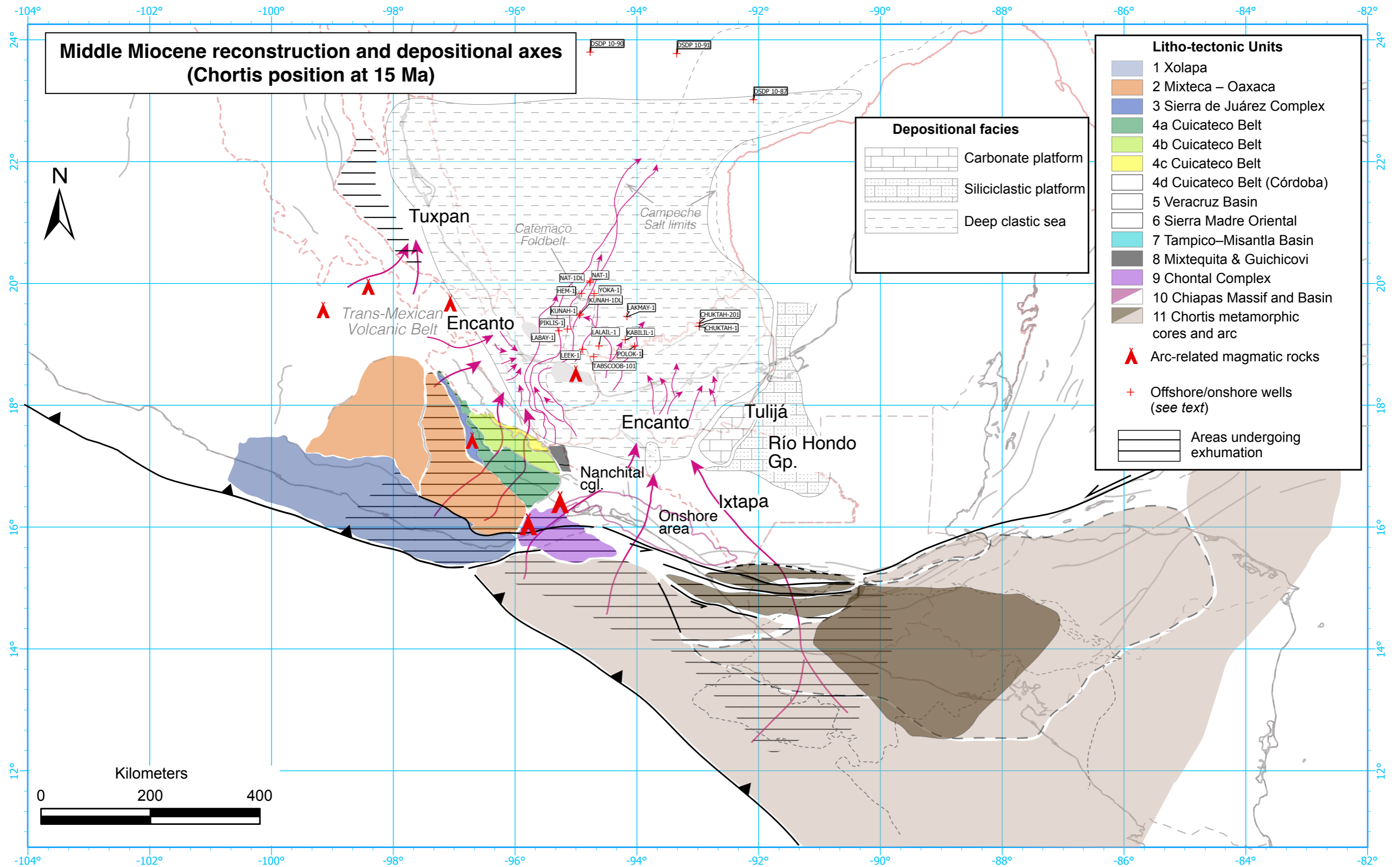


Figure 7f

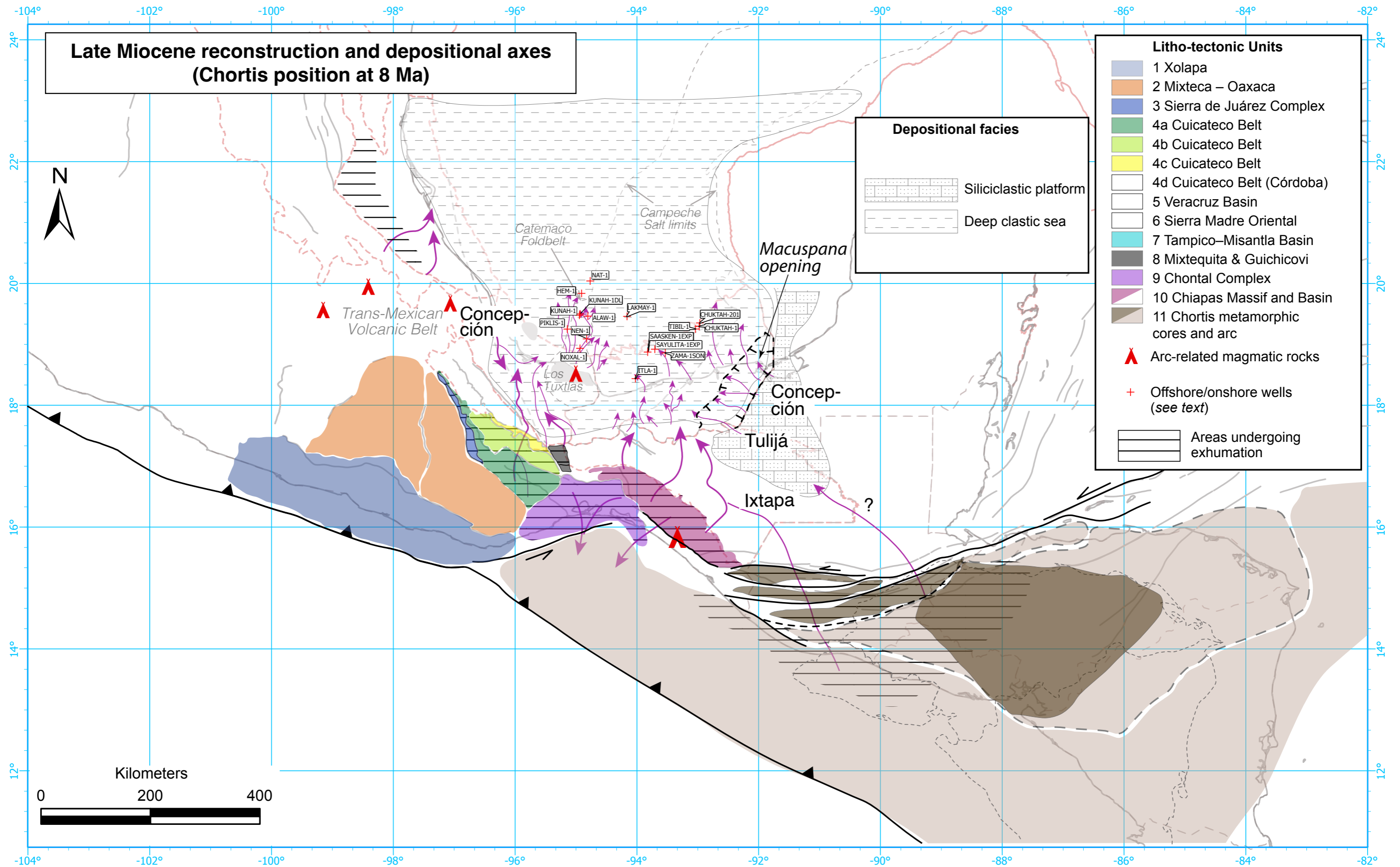


Figure 7g

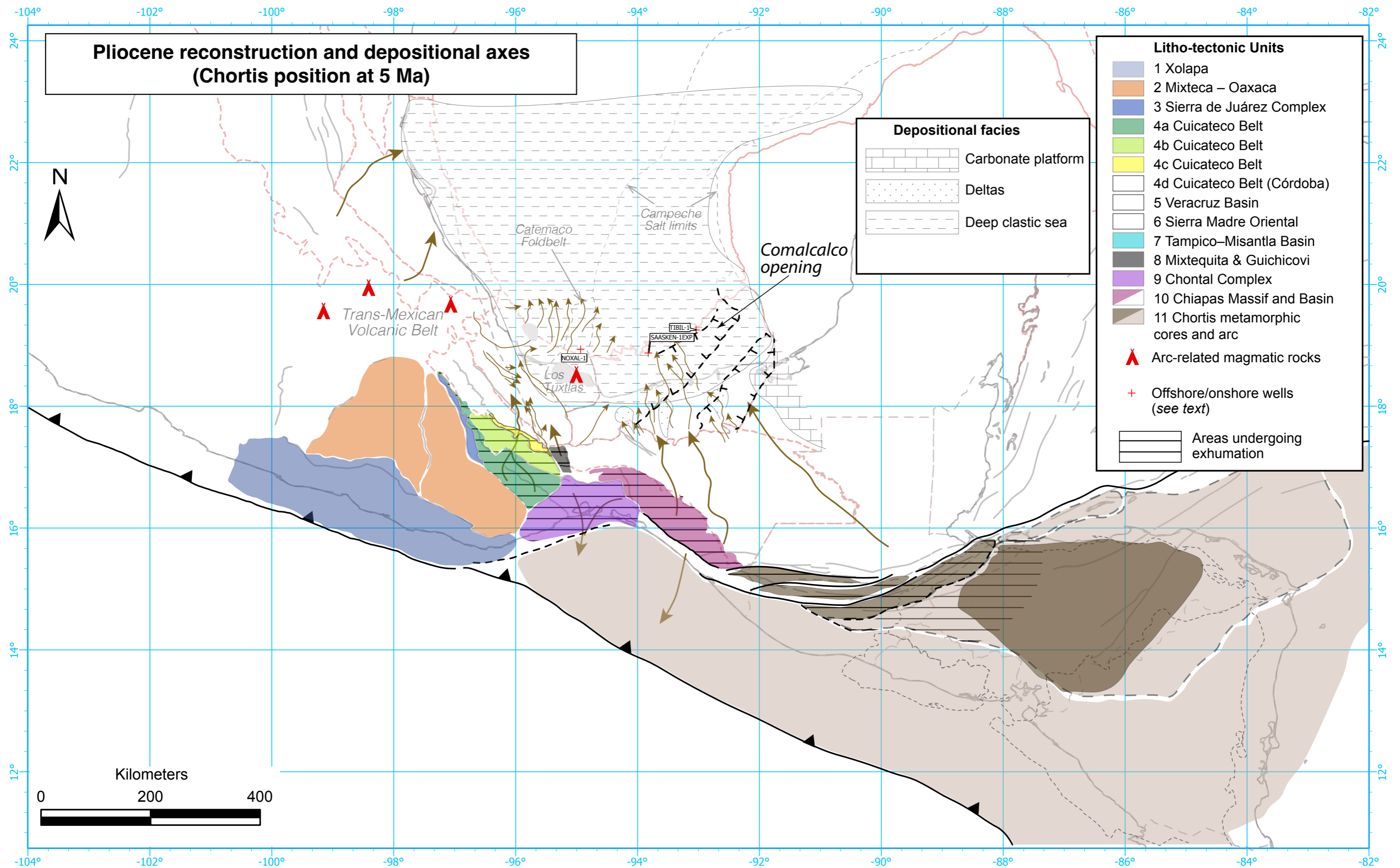


Figure 7h

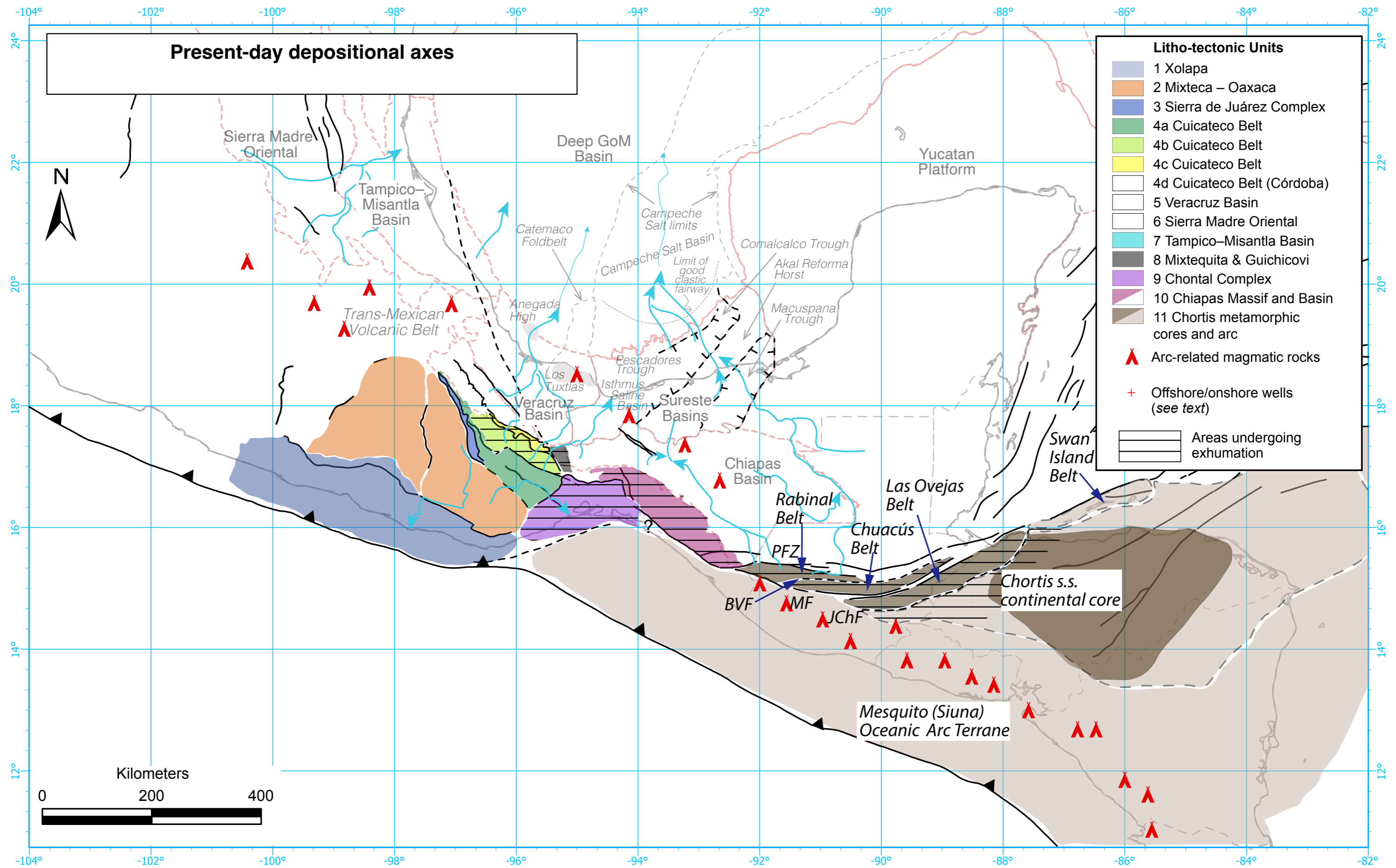


Figure 7i

Table 1. Zircon U–Pb results

Sample	Unit	Lithology	Locality	Elevation (m)	LAT	LON	Grain dated	Main age populations
<b>Mixteca (W) – Oaxaca (E)</b>								
6-15-12-01B	Cobble in detrital Chivillas Fm.	Jurassic granodiorite	Tehuacán–Orizaba,	ND	18.52087	-97.35118	39	The granite cobble mostly contains Mesoproterozoic zircon with a range of inherited ages. One Jurassic age may correspond to the time of magmatism. Youngest population: 820 - 870 Ma. Other populations from 920-970 Ma, 1000-1350 Ma
18-01-18-01	Oaxaqueno, foliated basement sample covered by Lower K Jaltepetongo	Coarse to medium grained metamorphic rock		1466	17.06959	-96.73631	110	
17-01-18-01	San Bartolomé Quialana	Plutonic Rock- Granodiorite- (Qz, Hb, Plg,Bt). Mafic enclaves. 29 Ma	San Bartolomé Quialana, Block west of Tlacolula. East Oaxaca City	1787	16.89447	-96.49601	23	Weighted mean of 29.1±0.19 Ma Youngest population: 33.31 ± 0.16 Ma. Other populations from 400, 1000-1200 Ma
17-01-18-04	Crystal Tuff	Crystal Tuff		1810	16.88886	-96.60350	19	
17-01-18-05	Andesitic tuff	Felsic volcanic rock- subhedral crystal (Hb, Kfs,Plg)	S of Oaxaca City	1743	16.87530	-96.62229	12	Weighted mean age of 23.1±0.1 Ma Weighted mean age of 25.32±0.32 Ma
17-01-18-06	Ejutla batholith	Qtz monzodiorite,(Qz,Plg, Bt,Hbl)	S of Oaxaca City	1561	16.60958	-96.70852	30	
<b>Sierra de Juárez Complex</b>								
<b>Between Siempre Viva Fault and Oaxaca Fault (Teotitlán migmatitic Belt / Sierra de Juárez mylonite complex)</b>								
20-01-30-13A	KnapArLu, mylonite with metasedimentary protolith		road to Teococuilco (Oaxaca myl Road to Teocuilco)	ND	17.31000	-96.67482	95.0	Meso and Neoproterozoic zircons mostly, a single zircon is ca 415 Ma
<b>Cuicateco Belt</b>								
<b>West of Villa Alta and Aloapán faults, East of Siempre Viva Fault:</b>								
16-01-18-10A	San Juan Juquila	Intrusive contact, Felsic rock (intrusive sample).	East Oaxaca City	2087	16.98304	-96.01800	30	Weighted mean age of 17.57±0.28 Ma
16-01-18-11B	San Juan Juquila	Plutonic Rock- Granite (weathered sample)	East Oaxaca City	1995	16.97187	-96.01236	14	Weighted mean age of 17.30 ± 0.1
<b>Veracruz Basin</b>								
16Apr16-2B	Quaternary		Tetela	ND	18.51636	-96.44598	317	Youngest DZ 0.55 ± 0.04 Ma. Other populations from 2 Ma-18 Ma, 80, 100, 270, >900 Ma
<b>Tampico–Misantla Basin</b>								
COAP17-1	Basal? Chicontepec above thrust over eoc Sandstone			171	20.37653	-97.61215	108	Youngest DZ about 59 Ma, population 60-100 Ma, 110-162 Ma, 215-290 Ma, >350Ma-2.6 Ga
SANT17-2A	Basal Chicontepec above K/T breccia	Sandstone	Santiago	484	19.91593	-97.15263	107	Youngest DZ about 65 Ma, population 65-120 Ma, 140-200 Ma, 235-300 Ma, >325Ma-1.9 Ga
SANT17-2B	Chicontepec (Middle and Upper)	Conglomeratic sandstone		301	19.97935	-97.10584	108	Youngest DZ about 55 Ma, population 55-107 Ma, 253-280 Ma, >335Ma-3.1 Ga
SFRAN17-1	Chicontepec (Middle and Upper)	Carbonate-rich volcanosediment		973	21.01527	-98.50159	109	Youngest DZ about 52 Ma, population 55-86 Ma, 104-183 Ma, 250-277, >470 Ma-2.2 Ga
TENA17-1	Oligocene	Medium- Fine-grained sandstone. Volcanoclastic		204	20.16197	-97.40399	108	Youngest DZ about 38 Ma, population 38-93 Ma, 120-176 Ma, 195-280, >335 Ma-2.6 Ga

A more detailed document with the methodology and raw analytical data are presented in Appendixes 2 and 3



Table 2.  $^{40}\text{Ar}/^{39}\text{Ar}$  results

Sample	Unit	Lithology	Locality	Elevation (m)	LAT	LON	Phase	WM $^{40}\text{Ar}/^{39}\text{Ar}$ age $\pm 2\sigma$ (Ma)	Total Fusion age $\pm 2\sigma$ (Ma)	Inverse Isochron age $\pm 2\sigma$ (Ma)	MSWD <sup>1</sup>	Observations
<b>Sierra de Juárez Complex</b>												
<i>Between Siempre Viva Fault and Oaxaca Fault (Teotitlán migmatitic Belt / Sierra de Juárez mylonite complex)</i>												
5-11-11-02A	Teotitlán Migmatitic Suite, Zr U/Pb 158 Ma	Orthogneiss	E Teotitlán	1604	18.17367	-97.05451	K feldspar	116.50 $\pm$ 10.29	124.70 $\pm$ 2.18	81.00 $\pm$ 42.25	21.41	Age gradient (91 - 135 Ma)
5-11-11-03A	Teotitlán Migmatitic Suite, Zr U/Pb 137 Ma	Migmatitic orthogneiss	E Teotitlán	1804	18.18604	-97.04982	K feldspar	100.74 $\pm$ 3.38	101.23 $\pm$ 0.90	93.70 $\pm$ 22.57	15.56	Flat region (approximately 101 Ma), excess Ar

WM: Weighted mean age over >3 contiguous heating steps that yield distinguishable ages that differ by less than 5%, and span > 50%  $^{39}\text{Ar}$  released

<sup>1</sup> Mean Square of Weighted Deviates of the inverse isochron linear regression

Zircon U-Pb published by Pindell et al. (2020a) and Coombs (2016)

Table 3. Apatite Fission Track results

Sample	Unit	Lithology	Locality	Elevation (m)	LAT	LON	Grains	Ns	Total area cm <sup>2</sup>	U average (ppm)	Pooled AFT age (\$)	95%-CI (Ma)	95%+CI (Ma)	Chi-squared	Primary Zeta	+/- 1 sigma	MTL $\mu\text{m}^{(1)}$	SE	SD	MTL proj. $\mu\text{m}^{(2)}$	N (#)	Dpar average $\mu\text{m}$
<b>Mixteca (W) – Oaxaca (E)</b>																						
17-01-18-03 *	Jaltepetongo, intruded by 28 Ma San Bartolomé Quilalana batholith	Arkosic sandstone		1721	16.89245	-96.60584	40	501	1.0E-03	45.1	14.2	1.3	1.4	63.8	8.3	0.1	14.59	0.10	1.03	15.35	106	1.9
17-01-18-06 *	Ejutla batholith (Zr U/Pb age 25 Ma; this work)	Qtz monzodiorite, (Qz, Plg, Bt, Ho)	S of Oaxaca City	1561	16.60958	-96.70852	40	84	1.4E-03	0.4	25.0	5.0	6.2	59.7	8.3	0.1	14.47	0.13	1.19	15.29	85	2.0
18-01-18-01 *	Oaxaqueño, foliated basement sample covered by Lower K Jaltepetongo	Coarse to medium grained metamorphic rock		1466	17.06959	-96.73631	40	1182	1.0E-03	37.2	50.5	3.9	4.2	73.5	8.3	0.1	13.49	0.13	1.41	14.67	127	2.1
DH-22-12-3-11	Acatlan, Upper Pz (Olnala Fm?)	Fine-grained volcanoclastic sandstones		1415	17.75084	-98.73439	35	562	1.7E-03	104.0	83.2	7.6	8.3	72.9	6.2	0.1	ND	ND	ND	ND	ND	ND
DH-23-12-3-11	Cosolepec Fm, Acatlan (Pz)	Fine-grained sandstones (very deformed, slightly metamorphosed)		1688	17.84033	-98.75138	24	1254	6.6E-04	590.9	70.2	5.3	5.7	71.3	6.2	0.1	ND	ND	ND	ND	ND	ND
DH-24-12-3-11	Cosolepec Fm, Acatlan (Pz)	Graywacke interbedded within phyllites (very deformed, slightly metamorphosed)		1279	18.14525	-98.66060	29	856	7.5E-04	455.7	62.4	5.0	5.4	80.9	6.2	0.1	ND	ND	ND	ND	ND	ND
<b>Sierra de Juárez Complex</b>																						
<i>Between Siempre Viva Fault and Oaxaca Fault (Teotitlán migmatitic Belt / Sierra de Juárez mylonite complex)</i>																						
5-11-11-02A **	Teotitlán Migmatitic Suite, Zr U/Pb 158 Ma (Pindell et al., 2020a)	Orthogneiss	E Teotitlán	1604	18.17367	-97.05451	26	527	1.6E-03	9.2	51.9	5.6	6.3	42.5	9.1	0.2	12.97	0.24	1.15	14.37	92	1.2
5-11-11-03A **	Teotitlán Migmatitic Suite, Zr U/Pb 137 Ma (Coombs 2016)	Migmatitic orthogneiss	E Teotitlán	1804	18.18604	-97.04982	31	572	2.7E-03	5.6	57.2	6.0	6.7	51.1	9.1	0.2	12.84	0.22	1.34	14.26	151	1.3
<b>Cuicatenco Belt</b>																						
<i>West of Villa Alta and Aloxapán faults, East of Siempre Viva Fault:</i>																						
16-01-18-10A *	San Juan Juquila (Zr U/Pb age 17.6 Ma; this work)	Intrusive contact- felsic rock (intrusive sample).	East Oaxaca City	2087	16.98304	-96.01800	22	21	2.4E-04	10.5	17.9	6.4	10.0	14.8	8.3	0.1	14.39	0.21	0.88	14.93	19	2.0
16-01-18-09A *	Metamorphic Complex, Zr U/Pb 180 Ma (Pindell et al. 2020)	Muscovite-rich schist	East Oaxaca City	2021	17.01785	-96.08020	29	17	3.5E-04	1.2	33.9	16.8	33.2	101.1	8.3	0.1	14.03	0.38	1.53	14.89	17	1.8
16-01-18-08A *	Jaltepetongo Fm.	Tabular Sandstone (fine size)		1877	16.96214	-96.11690	39	99	4.6E-04	19.4	14.9	2.8	3.4	87.7	8.3	0.1	13.98	0.20	1.31	14.96	46	1.8
16-01-18-05A *	Todos Santos	Tabular red fine-grained sandstone		1653	16.96250	-96.19340	38	91	5.0E-04	15.1	22.2	4.3	5.3	56.4	8.3	0.1	14.18	0.15	1.12	15.03	56	1.8
26Feb16-7A *	Jaltepetongo	Quarry by the road from Oaxaca to Tuxtepec, 3 km before distal facies of turbidites.	Guelatao	1525	17.30611	-96.52531	40	77	5.3E-04	14.0	15.4	3.2	4.1	45.4	8.3	0.1	14.25	0.20	1.27	15.15	40	2.3
18-01-18-03 *	Complejo Oaxaqueño	Quartzitic rock		2482	17.15195	-96.60720	25	81	3.2E-04	19.1	17.6	3.6	4.5	69.4	8.3	0.1	14.26	0.31	1.27	15.14	18	1.9
<b>Between Villa Alta/Aloxapán and Vista Hermosa faults (Mazateco Complex)</b>																						
12-9-10-08A *	Todos Santos Fm. (West of VH Fault)	Red very fine sandstone. Shows thermal effect, cooked		1316	17.65928	-96.33430	45	135	5.7E-04	25.8	20.4	3.3	4.0	72.5	8.3	0.1	14.65	0.21	1.47	15.32	52	2.1
12-9-10-10A *	Mazateco Complex. (West of VH Fault)	Quartzite		1423	17.63692	-96.33977	40	55	6.6E-04	5.6	23.0	5.5	5.5	26.1	8.3	0.1	13.75	0.19	1.40	14.71	54	2.0
21-01-18-01 *	Mazateco (SW of VH Fault)	Low grade metasediment		377	17.14588	-95.40940	15	57	2.2E-04	26.9	15.6	3.7	4.8	20.2	8.3	0.1	13.17	0.81	3.35	14.28	18	1.8
<b>Between Vista Hermosa and Valle Nacional faults</b>																						
20-01-18-08 *	Todos Santos (East of VH Fault)	Sandstone and mudstone with tectonic foliation.	Contact zones between basement and Todos Santos Fm, along the Vista Hermosa Fault	158	17.44420	-95.76623	39	296	9.4E-04	27.5	20.9	2.4	2.8	75.5	8.3	0.1	13.47	0.27	1.85	14.67	49	1.8
19-01-18-06 *	Fm. Xonamanca?, (East of VH Fault)	Sublitharenite		370	17.70332	-96.22829	12	67	9.0E-05	44.3	27.6	7.1	9.5	54.2	8.3	0.1	13.12	0.58	1.42	14.43	7	2.0
19-01-18-10 *	Todos Santos (East of VH Fault)	Sandstone		358	17.64434	-96.15566	40	161	5.6E-04	26.9	19.7	3.0	3.6	90.9	8.3	0.1	13.86	13.86	1.47	14.84	53	1.8

Table 3 (continued). Apatite Fission Track results

Sample	Unit	Lithology	Locality	Elevation (m)	LAT	LON	Grains	Ns	Total area cm <sup>2</sup>	U average (ppm)	Pooled AFT age (\$)	95%-CI (Ma)	95%+CI (Ma)	Chi-squared	Primary Zeta	+/- 1 sigma	MTL $\mu$ m (1)	SE	SD	MTL proj. $\mu$ m (2)	N (#)	Dpar average $\mu$ m
<b>Tampico-Misantla Basin</b>																						
ACAT17-1 *	Chicotepec. MDA 55 Ma (Cossey et al., 2019)	Carbonate-rich volcanosediment	Chicotepec channel at Acatapec	465	20.96020	-98.27656	40	223	1.8E-03	3.6	57.0	7.4	8.4	32.0	8.3	0.1	14.16	0.17	2.08	15.11	152	3.5
ALTO17-2 *	Cahuasas redbeds,	Red tuff (Nazas?), coarse-medium grained		1059	19.86862	-97.22115	40	48	1.2E-03	12.9	11.8	3.0	4.0	58.6	8.3	0.1	14.28	0.37	1.44	15.03	16	2.2
SANT17-1	K/T, K-Pg breccia	Breccia	Santiago	484	19.91593	-97.15263	40	500	1.6E-03	56.4	16.2	1.5	1.7	323.7	8.3	0.1	13.98	0.15	1.82	14.95	140	2.4
COAP17-1 *	Basal? Chicotepec above thrust over eocene	Sandstone		171	20.37653	-97.61215	40	313	9.9E-04	19.5	56.6	6.3	7.1	63.0	8.3	0.1	13.38	0.16	1.64	14.54	112	2.8
<b>Mixtequita (N) &amp; Guichicovi (S) blocks</b>																						
27Mar17-3A	Mixtequita granite, Permo-Triassic	Granite		153	17.14763	-95.14480	25	41	3.8E-03	4.4	42.0	3.5	3.5	ND	12.0	0.2	12.93	0.20	1.56	ND	58	ND
19-07-04-1	Guichicovi Complex, Precambrian	Granulitic gneiss	Sarabia River		17.04996	-95.19520	36	22	8.8E-04	1.8	23.1	8.0	12.3	5.9	8.3	0.1	14.48	0.16	0.86	15.20	29	1.8
<b>Chontal</b>																						
19-07-03-2B	Chivela lithodeme, Cretaceous	Coarse grained phyllite	Ajal town	188	16.76736	-95.02154	36	98	5.3E-04	19.4	11.4	2.1	2.6	37.6	8.3	0.1	14.18	0.14	0.84	14.95	35	1.8
9-30-10-09A	Juchitan, Western Tehuantepec Tertiary magmatic rocks	Biotite tonalite or granodiorite		ND	16.50632	-95.42106	40	122	1.5E-03	20.6	5.7	1.0	1.2	61.0	8.3	0.1	14.17	0.17	1.16	15.01	50	1.6
9-30-10-11	Western Tehuantepec Tertiary magmatic rocks	Biotite Granodiorite/Tonalite		ND	16.54434	-95.45190	6	9	1.8E-04	13.4	4.1	2.1	4.2	4.4	8.3	0.1	14.21	0.44	0.98	15.06	6	1.5
3-8-11-08	Western Tehuantepec Tertiary magmatic rocks	Biotite tonalite Zoned plagioclase	New highway to Oaxaca	220	16.49542	-95.40132	29	284	1.7E-03	14.2	7.1	0.9	1.0	278.4	6.2	0.1	ND	ND	ND	ND	ND	ND
19-07-05-1	Migmatite, Appears to intrude K phyllites	Migmatite	Tehuantepec town	ND	16.35775	-95.22333	40	378	1.4E-03	100.3	8.7	1.0	1.1	229.5	8.3	0.1	14.13	0.09	0.95	14.98	115	1.8
<b>Chiapas Massif and Basin</b>																						
19-07-05-4	Westernmost Chiapas Massif	Porphyritic granite	Road to Sta. Maria Chimalapa	300	16.82889	-94.76931	37	37	5.8E-04	20.6	8.3	2.5	3.5	34.4	8.3	0.1	14.45	0.14	0.69	15.14	25	1.8

<sup>(8)</sup> Pooled age calculated by pooling the spontaneous fission tracks and U content obtained from the individual grains.

MTL—mean track length <sup>(1)</sup> measured, <sup>(2)</sup> c-axis corrected; Dpar — mean etch pit diameter; SE — Standard deviation; SD — Standard deviation

Ns: Number of spontaneous fission tracks counted over the total area.

Nf: Number of fission track lengths measured.

Laser spot size: 16  $\mu$ m. LA-ICP-MS. Zeta method

\* AFT ages published by Gray et al. (2021) integrated into the new thermal models \*\* AFT ages published by Villagomez (2014)

Table 4. Apatite (U–Th)/He data

Sample	Unit	Lithology	Locality	Elevation (m)	LAT	LON	Age (Ma)	$\pm 2\sigma$ (Ma)	U (ppm)	Th (ppm)	$^{147}\text{Sm}$ (ppm)	[U]e	Th/U	He (nmol/g)	Mass ( $\mu\text{g}$ )	Alpha correction (Fr)	Effective radius ( $\mu\text{m}$ )	
<b>Sierra de Juárez Complex</b>																		
<i>Between Siempre Viva Fault and Oaxaca Fault (Teotitlán migmatitic Belt / Sierra de Juárez mylonite complex)</i>																		
5-11-11-02A	158 Ma (Pindell et al., 2020a)	Orthogneiss	E Teotitlán	1604	18.17367	-97.05451	17.4	1.0	21.9	14.2	22.3		0.7	1.5		0.6	39.4	
							<b>16.0</b>	<b>1.0</b>	7.8	2.5	21.1		0.3	0.6		0.8	60.6	
							<b>14.8</b>	<b>0.9</b>	7.6	2.2	25.2		0.3	0.5		0.8	63.4	
							20.5	1.2	8.4	1.8	15.9		0.2	0.7		0.7	52.7	
							21.5	1.3	10.2	3.1	25.1		0.3	0.9		0.7	45.3	
							<b>18.2</b>	<b>1.1</b>	5.2	1.5	13.7		0.3	0.4		0.8	65.1	
							<b>Weighted mean</b>	<b>16.4</b>	<b>0.5</b>	<b>10.6</b>	<b>5.1</b>	<b>20.6</b>		<b>0.4</b>	<b>0.7</b>		<b>0.7</b>	<b>57.1</b>
<b>Cuicateco Belt</b>																		
<i>Between Villa Alta/Aloapán and Vista Hermosa faults (Mazateco Complex)</i>																		
21-01-18-01	Mazateco (SW of VH Fault)	Low grade Metasediment (Paleozoic?)		377	17.14588	-95.40940	7.5	0.4	7.8	19.9	100.6	12.9	2.5	0.3	1.2	0.6	38.5	
							82.0	4.9	32.7	77.7	161.7	51.4	2.4	13.2	0.9	0.6	34.3	
							<b>7.2</b>	<b>0.4</b>	1.7	2.0	26.7	2.2	1.2	0.1	5.8	0.8	62.7	
							<b>4.9</b>	<b>0.3</b>	54.7	96.2	55.9	77.1	1.8	1.5	6.2	0.8	63.5	
							<b>Weighted mean</b>	<b>6.0</b>	<b>0.2</b>	<b>21.4</b>	<b>39.4</b>	<b>61.0</b>	<b>30.8</b>	<b>1.8</b>	<b>0.6</b>	<b>4.4</b>	<b>0.7</b>	<b>54.9</b>
<b>Tampico–Misantla Basin</b>																		
ACAT17-1 *	Chicontepec. MDA 55 Ma (Cossey et al., 2019)		Chicontepec channel at Acataptec	465	20.96020	-98.27656	15.9	1.0	12.6	39.9	156.8	22.6	3.2	1.4	3.5	0.7	50.3	
							15.4	0.9	4.3	32.3	146.2	12.5	7.4	0.8	6.0	0.7	60.7	
							<b>13.3</b>	<b>0.8</b>	3.8	19.4	152.4	9.0	5.1	0.5	6.1	0.7	60.6	
							<b>15.2</b>	<b>6.1</b>	3.7	21.7	130.5	9.4	5.9	0.6	5.8	0.7	63.9	
							<b>Weighted mean</b>	<b>14.8</b>	<b>0.2</b>	<b>6.1</b>	<b>28.3</b>	<b>146.4</b>	<b>13.4</b>	<b>5.4</b>	<b>0.8</b>	<b>5.3</b>	<b>0.7</b>	<b>58.9</b>
COAP17-1 *	Basal? Chicontepec above thrust over Eocene	Sandstone		171	20.37653	-97.61215	16.4	1.0	3.3	17.4	223.6	8.4	5.3	0.6	2.6	0.7	48.9	
							<b>10.3</b>	<b>0.6</b>	10.1	26.2	127.4	16.8	2.6	0.6	2.3	0.7	44.5	
							<b>9.6</b>	<b>0.6</b>	3.5	43.6	147.0	14.3	12.3	0.4	1.0	0.6	34.4	
							<b>9.9</b>	<b>0.4</b>	11.4	44.4	109.2	22.2	3.9	0.7	1.1	0.6	36.5	
							<b>Weighted mean</b>	<b>9.9</b>	<b>0.3</b>	<b>8.4</b>	<b>38.0</b>	<b>127.9</b>	<b>17.8</b>	<b>6.3</b>	<b>0.6</b>	<b>1.5</b>	<b>0.6</b>	<b>38.4</b>
ALTO17-2 *	Cahuasas redbeds, Mid-Jurassic (Max. dep. age: 167 Ma)	Red tuff (Nazas?)		1059	19.86862	-97.22115	12.2	0.7	6.0	12.8	115.9	9.5	2.1	0.5	4.0	0.7	50.9	
							13.4	0.8	2.9	56.5	121.5	16.5	19.7	0.8	1.4	0.6	39.7	
							<b>11.7</b>	<b>0.7</b>	3.0	5.7	198.3	5.3	1.9	0.2	1.3	0.6	38.7	
							<b>Weighted mean</b>	<b>12.3</b>	<b>0.4</b>	<b>3.9</b>	<b>25.0</b>	<b>145.2</b>	<b>10.4</b>	<b>7.9</b>	<b>0.5</b>	<b>2.2</b>	<b>0.6</b>	<b>43.1</b>
							<b>Mixtequita (N) &amp; Guichicovi (S) blocks</b>											
27Mar17-3A	Mixtequita granite, Permo-Triassic	Granite		153	17.14763	-95.14480	7.2	0.4	4.7	4.4	90.8	6.2	0.9	0.2	3.5	0.7	49.8	
							<b>10.9</b>	<b>0.7</b>	6.0	2.8	103.4	7.1	0.5	0.3	1.5	0.6	39.4	
							<b>12.5</b>	<b>0.8</b>	5.7	4.3	84.1	7.1	0.8	0.4	3.6	0.7	51.4	
							<b>6.8</b>	<b>0.4</b>	4.0	3.2	97.5	5.2	0.8	0.1	2.0	0.6	39.4	
							<b>8.8</b>	<b>0.5</b>	4.5	3.2	70.1	5.6	0.7	0.2	1.5	0.6	39.5	
							<b>Weighted mean</b>	<b>8.2</b>	<b>0.2</b>	<b>5.0</b>	<b>3.6</b>	<b>89.2</b>	<b>6.2</b>	<b>0.7</b>	<b>0.2</b>	<b>2.4</b>	<b>0.7</b>	<b>43.9</b>
<b>Chiapas Massif and Basin</b>																		
27Mar17-2A	Chiapas (Mixtequita) granite	Granite		86	17.03590	-94.94886	10.9	0.7	9.2	4.5	247.4	11.5	0.5	0.5	3.9	0.7	54.9	
							<b>15.7</b>	<b>0.9</b>	22.0	3.9	314.2	24.5	0.2	1.7	8.0	0.8	70.0	
							<b>16.3</b>	<b>1.0</b>	15.5	6.7	311.5	18.6	0.4	1.2	2.6	0.7	49.2	
							<b>Weighted mean</b>	<b>13.3</b>	<b>0.5</b>	<b>15.6</b>	<b>5.0</b>	<b>291.0</b>	<b>18.2</b>	<b>0.4</b>	<b>1.1</b>	<b>4.8</b>	<b>0.7</b>	<b>58.0</b>

[U]e = effective Uranium concentration. (U–Th)/He data, numbers in bold indicate the aliquots (one grain per aliquot) used to calculate the weighted mean (see text)

\* Apatite (U–Th)/He ages published by Gray et al. (2021), integrated into the new thermal models

Table 5. Zircon (U–Th)He data

Sample	Unit	Lithology	Locality	Elevation (m)	LAT	LON	Zircon (U–Th)/He Age (Ma)	$\pm 2\sigma$ (Ma)	U (ppm)	Th (ppm)	$^{147}\text{Sm}$ (ppm)	[U]e	Th/U	He (nmol/g)	Mass ( $\mu\text{g}$ )	Alpha correction (Fr)	Effective radius ( $\mu\text{m}$ )
<b>Mixteca (W) – Oaxaca (E)</b>																	
25Feb16-2B	Jaltepetongo Fm.	Laminated metasandstones and filites, rich on quartz and feldspar.	Oaxaca City	ND	17.11408	-96.71640	18.0	1.4	33.4	31.8	1.1	40.7	1.0	3.7	138.6	0.9	154.9
							16.9	1.4	22.0	4.9	0.5	23.1	0.2	1.9	52.1	0.9	110.8
							39.6	3.2	117.0	27.8	2.1	123.4	0.2	22.8	26.5	0.9	88.2
							<b>Weighted mean</b>										
							<b>Discordant single grain ages. Samples was probably only partially reset</b>										
<b>Sierra de Juárez Complex</b>																	
<i>Between Siempre Viva Fault and Oaxaca Fault (Teotitlán migmatitic Belt / Sierra de Juárez mylonite complex)</i>																	
26Feb16-3C	Sierra de Juárez Complex	Amphibolite		3100	17.17224	-96.65426	23.4	1.9	34.2	7.0	0.4	35.9	0.2	3.9	21.2	0.9	81.1
							31.4	2.5	36.7	6.2	0.7	38.2	0.2	5.6	28.5	0.9	90.7
							88.6	7.1	67.4	19.4	5.4	71.9	0.3	29.3	20.9	0.8	78.3
							<b>Weighted mean</b>										
							<b>Discordant single grain ages. Samples was probably only partially reset</b>										
24Feb16-1B	Southernmost Sierra de Juárez Complex	Filonite, banded with white mica. Low metamorphic grade	Road from San Juan Bautista Guelache to Teocuilco	2150	17.22260	-96.75324	16.7	1.3	67.1	20.5	1.0	71.8	0.3	5.5	19.0	0.8	76.8
							20.5	1.6	204.3	25.6	1.8	210.2	0.1	19.6	18.0	0.8	75.4
							19.0	1.5	51.6	21.3	1.5	56.5	0.4	4.8	12.3	0.8	66.6
							<b>Weighted mean</b>										
							18.5	0.4	107.7	22.4	1.4	112.8	0.3	10.0	16.1	0.8	73.0
<b>Cuicatenco Belt</b>																	
<i>West of Villa Alta and Aloapán faults, East of Siempre Viva Fault:</i>																	
26Feb16-6B	Miocene dacite	Dacitic porphyry	Las Animas-ktepeji		17.23741	-96.56561	16.0	1.3	240.2	49.4	6.7	251.6	0.2	19.2	45.5	0.9	100.2
							14.0	1.1	93.0	20.3	9.4	97.8	0.2	6.4	30.3	0.9	86.6
							18.4	1.5	131.4	22.7	3.6	136.6	0.2	11.0	10.7	0.8	60.7
							<b>Weighted mean</b>										
							15.7	0.4	154.9	30.8	6.6	162.0	0.2	12.2	28.8	0.9	82.5
<i>Between Villa Alta/Aloapán and Vista Hermosa faults (Mazateco Complex)</i>																	
27Feb16-3B	Todos Santos (SW of Vista Hermosa Fault)	Red sandstone, massive with quartz, feldspar and lithics.	Mazateco Complex, Guelatao to Tuxtpec	ND	17.66895	-96.32819	56.2	4.5	23.4	13.1	1.3	26.4	0.6	6.6	14.3	0.8	67.0
							35.5	2.8	178.3	36.9	2.5	186.8	0.2	29.4	11.4	0.8	65.7
							32.6	2.6	194.1	31.3	1.4	201.3	0.2	29.6	13.6	0.8	70.0
							26.3	2.1	421.7	156.8	7.4	457.9	0.4	55.6	23.2	0.9	82.5
							<b>Weighted mean</b>										
							30.5	1.4	204.4	59.5	3.1	218.1	0.3	30.3	15.7	0.8	71.3
21-01-18-01	Mazateco (SW of Vista Hermosa Fault)	Low grade Metased		377	17.14588	-95.40940	37.2	3.0	379.3	16.7	0.0	383.1	0.0	54.7	2.6	0.7	38.3
							39.6	3.2	448.1	121.9	1.0	476.1	0.3	82.1	9.7	0.8	60.4
							39.6	3.2	54.1	12.9	1.3	57.0	0.2	9.6	7.4	0.8	54.8
							<b>Weighted mean</b>										
							38.7	1.8	293.8	50.5	0.8	305.4	0.2	48.8	6.6	0.8	51.2
<i>Between Vista Hermosa and Valle Nacional faults</i>																	
27Feb16-4B	Todos Santos (NE of Vista Hermosa Fault)	Very fine to medium-grained sandstone	Mazateco Complex, Guelatao to Tuxtpec		17.73676	-96.32892	49.3	3.9	56.7	15.5	0.0	60.2	0.3	13.1	10.7	0.8	63.4
							66.6	5.3	47.8	26.6	1.3	54.0	0.6	16.1	14.2	0.8	69.7
							25.8	2.1	520.5	116.4	13.3	547.4	0.2	65.0	21.4	0.9	80.3
							<b>Weighted mean</b>										
							<b>Discordant single grain ages. Samples was probably only partially reset</b>										
27Feb16-5B	Todos Santos? Xonamanca? (NE of Vista Hermosa Fault)	Coarse-grained sandstone	Mazateco Complex, Guelatao to Tuxtpec		17.76214	-96.31636	76.9	6.2	105.1	39.1	1.2	114.2	0.4	39.5	15.3	0.8	69.7
							138.7	11.1	48.7	18.3	2.1	52.9	0.4	35.9	59.7	0.9	116.2
							71.5	5.7	133.2	59.4	3.0	148.8	0.4	48.3	21.9	0.8	79.2
							<b>Weighted mean</b>										
							<b>Discordant single grain ages. Samples was probably only partially reset</b>										
<b>Tampico–Misantla Basin</b>																	
SANT17-1 *	K/T, K-Pg breccia	Breccia	Santiago	484	19.91593	-97.15263	238.8	19.1	28.5	14.6	1.7	31.9	0.5	36.4	32.3	0.9	92.7
							77.9	6.2	127.5	41.1	1.0	137.0	0.3	46.9	9.6	0.8	62.7
							228.9	18.3	110.0	26.6	1.5	116.1	0.2	120.7	12.5	0.8	66.6
							<b>Weighted mean</b>										
							<b>Discordant single grain ages. Samples was probably only partially reset</b>										
<b>Mixtequita (N) &amp; Guichicovi (S) blocks</b>																	
27Mar17-3A	Mixtequita granite, Permo-Triassic	Granite		153	17.14763	-95.14480	117.3	9.4	41.1	12.7	0.4	44.1	0.3	23.7	21.1	0.8	76.2
							104.0	8.3	41.1	15.6	0.0	44.7	0.4	21.1	18.0	0.8	73.2
							106.1	8.5	21.9	7.2	0.0	23.5	0.3	11.4	18.1	0.8	72.9
							<b>Weighted mean</b>										
							108.6	5.0	34.7	11.8	0.1	37.4	0.3	18.7	19.1	0.8	74.1
26Mar17-3A	Petapa (South Guichicovi, East of Vista Hermosa Fault), Precambrian	Precambrian metasediment	La Maceta-Loma Santa Cruz	ND	16.95053	-95.24303	30.6	2.4	109.2	26.8	1.5	115.3	0.2	15.5	12.7	0.8	63.1
							32.3	2.6	156.1	48.1	0.9	169.2	0.3	25.4	32.2	0.9	65.1
							31.4	1.8	133.6	37.5	1.2	142.3	0.3	20.4	22.4	0.8	74.1
							<b>Weighted mean</b>										
26Mar17-5A	Petapa (South Guichicovi), Precambrian	Precambrian metaconglomerate	Santo Domingo Petapa	ND	16.82660	-95.14648	41.8	3.3	160.6	31.4	0.0	167.9	0.2	28.3	4.0	0.7	45.3
							42.9	3.4	145.4	62.2	0.0	159.7	0.4	26.8	2.9	0.7	41.6
							42.0	3.4	331.2	156.6	33.4	367.4	0.5	60.4	2.8	0.7	41.6
							44.1	3.5	144.7	76.1	1.4	162.3	0.5	30.6	6.7	0.8	56.1
							<b>Weighted mean</b>										
							42.7	1.7	195.5	81.6	8.7	214.3	0.4	36.6	4.1	0.7	46.2
<b>Chontal</b>																	
25Mar17-5A	Chivela sedimentary	Coarse sandstone	General Pascual	ND	16.47059	-94.22151	36.0	2.9	0.5	-1.8	2.9	0.1	-3.3	0.0	6.4	0.8	68.4
							13.9	1.1	16.8	7.3	0.8	18.5	0.4	1.2	12.0		
							<b>Weighted mean</b>										
							<b>Discordant single grain ages. Samples was probably only partially reset</b>										
<b>Chiapas Massif and Basin</b>																	
25Mar17-1A	Chiapas Massif, Triassic	Migmatite	Tapachula-Juchitán	ND	16.13137	-93.79774	7.1	0.6	115.1	25.3	0.0	120.9	0.2	3.4	3.3	0.7	41.0
							7.2	0.6	120.8	22.4	0.0	126.0	0.2	3.9	7.8	0.8	57.5
							7.7	0.6	135.2	20.3	-0.6	139.8	0.2	4.9	15.1	0.8	72.2
							9.4	0.8	215.1	31.3	0.0	222.3	0.1	8.2	3.5	0.7	42.3
							<b>Weighted mean</b>										
							7.7	0.3	146.5	24.8	-0.2	152.2	0.2	5.1	7.5	0.8	53.3
27Mar17-2A	Chiapas (Mixtequita) granite	Granite		86	17.03590	-94.94886	59.3	4.7	39.1	7.5	0.0	40.8	0.2	9.3	2.4	0.7	38.8
							80.7	6.5	31.0	5.7	-3.1	32.3	0.2	10.1	3.0	0.7	39.5
							94.4	7.6	70.0	121.6	-5.1	98.0	1.7	33.5	1.8	0.7	34.7
							<b>Weighted mean</b>										
							<b>Discordant single grain ages. Samples was probably only partially reset</b>										

[U]e = effective Uranium concentration. (U–Th)/He data, numbers in bold indicate the aliquots (one grain per aliquot) used to calculate the weighted mean (see text)  
 \* Zircon (U–Th)/He age published by Gray et al. (2021), integrated into the new thermal models

Table 6. Zircon Fission Track results

Sample	Unit	Lithology	Locality	Elevation (m)	LAT	LON	Grains	Ns	Total area cm <sup>2</sup>	U average (ppm)	Pooled AFT age ( $\delta$ )	95%-CI (Ma)	95%+CI (Ma)	Chi- squared	Primary Zeta	+/- 1 sigma
<b>Cuicateco Belt</b>																
<i>Between Villa Alta/Aloapán and Vista Hermosa faults (Mazateco Complex)</i>																
21-01-18-04	Mazateco (SW of Vista Hermosa Fault)	Metamorphic rock- schistose texture	Mazateco	543	17.13892	-95.41451	25	1435	1.6E-04	316.2	40.6	2.3	2.4	22.5	0.0401	0.0005

<sup>(6)</sup> Pooled age calculated by pooling the spontaneous fission tracks and U content obtained from the individual grains.

Table 7. Key wells drilled by the state-owned petroleum company (Pemex) and other international operators in onshore and offshore areas

WELL NAME	LOCATION*	WELL TYPE	FIELD	STATUS	HYDROCARBON TYPE	MEASURED DEPTH (m)	TRUE VERTICAL DEPTH (m)	DRILLING COMPLETION		LITHOLOGY	FACIES
								YEAR	PLAY		
ALAW-1	Ultradeep waters	Exploration	N/A	Dry gas producer	Dry gas	5279	5279	2015	Upper Miocene		
AMATL-1 EXP	Shallow waters	New-field wildcat	N/A	Oil and gas producer		3800	3090	2020	Lower Pliocene		
BUKMA-1 SON	Ultradeep waters	Stratigraphic test well	N/A	Non-commercial gas and condensate	Gas condensate	7377	7373	2018	Middle Eocene		
CAHUA-1 EXP	Shallow waters	New-field wildcat	CAHUA	Gas and condensate discovery	Gas condensate	2984	2973	2017	Upper Pliocene		
CHELEM-1	Deep waters	Exploration	N/A	Dry gas producer		3125	3125	2008	Pliocene		
CHINWOL-1 EXP	Deep waters	New-field wildcat	N/A	Oil discovery (P&A)	Oil	1850	1813	2020	Lower Pliocene (3 zones)		
CHUKTAH-1	Shallow waters	Exploration		P&A, dry		4968	4968	1999	Lower, Middle, Upper Miocene		
CHUKTAH-201	Deep waters	Exploration		P&A, dry		4901	4901	2004	Lower, Middle, Upper Miocene		
HEIM-1	Onshore	Exploration	N/A	P&A		5004	5004	1983	Middle Eocene		
HEM-1	Ultradeep waters	Exploration	HEM	Suspended, wet gas	Wet gas	4429	4429	2015	Middle, Upper Miocene		
ITLA-1	Shallow waters	Exploration	ITLA	Oil discovery	Oil	3235	3235	2015	Upper Miocene		
KABILIL-1	Deep waters	Exploration	N/A	P&A, dry		5350	5196	2004	Lower Miocene		
KUNAH-1	Ultradeep waters	Exploration	KUNAH	Wet gas producer (5 zones)	Wet gas	4550	4550	2009	Lower, Middle, Upper Miocene	Litharenite	Turbidite channel, basin floor fan
KUNAH-1DL	Ultradeep waters	Appraisal well	KUNAH	Wet gas producer	Wet gas	4515	4471.5	2012	Lower, Middle, Upper Miocene	Litharenite	Turbidite channel, basin floor fan
LABAY-1	Ultradeep waters	Exploration	LABAY	Dry gas discovery, P&A	Dry gas	3362	3362	2009	Lower Miocene		
LAKACH-1	Deep waters	Exploration	LAKACH	Dry gas discovery, P&A	Dry gas	3813	3813	2006	Middle Pliocene	Litharenite	
LAKMAY-1	Deep waters	Exploration	N/A	Dry, P&A		2600	2417	2014	Middle, Upper Miocene		
LALAIL-1	Deep waters	Exploration	LALAIL	Gas and condensate producer	Dry gas	3815	3787.1	2007	Middle Miocene	Calc./volc. Litharenite	Submarine fan
LEEK-1	Deep waters	Exploration	LEEK	Wet gas producer	Wet gas	3700	3642.1	2009	Lower Miocene	Volcanic-rich litharenite	Base of slope channel
MATA ESPINO-2	Onshore	Exploration	MATA ESPINO	Condensate	Gas condensate	3804.5	3804.5	1956	Upper Eocene		
NAT-1	Ultradeep waters	Exploration	NAT	Wet gas producer		5531	5531	2014	Middle, Upper Miocene	Feldspathic litharenite	Basin floor turbidite channel, channel levee
NAT-1DL	Ultradeep waters	Appraisal well	NAT	Wet gas producer	Wet gas	4569	4349	2015	Middle Miocene		
NEN-1	Ultradeep waters	Exploration	NEN	Dry gas producer	Dry gas	4350	4350	2011	Upper Miocene		
NOXAL-1	Deep waters	Exploration	NOXAL	Dry gas producer	Dry gas	3640	3640	2006	Upper Miocene, Lower Pliocene	Calcareous litharenite	
OCTLI-1 EXP	Shallow waters	New-field wildcat	OCTLI	Oil and gas discovery	Oil and gas	2580	2190	2017	Upper Pliocene		
PIKLIS-1	Ultradeep waters	Exploration	PIKLIS	Gas and condensate discovery	Wet gas	5431	5431	2011	Lower, Upper Miocene		
POLOK-1 EXP	Deep waters	New-field wildcat	N/A	Oil discovery	Oil	2620	2529.6	2020	Lower Miocene (2 zones)		
SAASKEN-1 EXP	Shallow waters	New-field wildcat	N/A	P&A	Oil	3830	3688	2020	Upper Miocene, Pliocene		
SAYULITA-1 EXP	Shallow waters	New-field wildcat	SAYULITA	P&A, oil discovery	Oil	1758	1931	2021	Upper Miocene		
TABSCOOB-1	Shallow waters	Exploration	TABSCOOB	Gas and condensate discovery	Oil	6900	6900	1997	Middle Pliocene		
TABSCOOB-101	Shallow waters	Exploration	TABSCOOB	Dry gas producer	Gas	3150	3150	2006	Lower Miocene		
TECOALLI-1	Shallow waters	Exploration	TECOALLI	Oil and gas discovery	Oil and gas	3930	3930	2008	Lower Pliocene		Fluvial-deltaic mouth bars
TEPAXTLI-1 EXP	Onshore	New-field wildcat	PERDIZ	P&A	Non disclosed	7283	7859	2021	Eocene		
TIBIL-1	Shallow waters	Exploration	N/A	Oil discovery (P&A)	Oil	4334	4334	2005	Upper Miocene, Pliocene		
XAXAMANI-1	Shallow waters	Exploration	XAXAMANI	Gas and oil discovery	Oil	1990	1990	2003	Lower, Middle Pliocene		
YOKA-1	Ultradeep waters	Exploration	N/A	P&A; non-commercial wet gas	Wet gas	4573	4573	2014	Lower Miocene	Feldspathic litharenite	
ZAMA-1 SON	Shallow waters	Stratigraphic test well	ZAMA	Oil discovery	Oil	4109	4109	2017	Upper Miocene	Feldspathic litharenite	Slope channel turbidites
<b>Other wells from DSDP</b>											
DSDP 10-87	Ultradeep waters	Stratigraphic test well					700	1970	Middle Miocene	Sandy silt	
DSDP 10-90	Ultradeep waters	Stratigraphic test well					768	1970	Middle Miocene	Quartz rich clay mineral rich sand	
DSDP 10-91	Ultradeep waters	Stratigraphic test well					900	1970	Middle Miocene	Pebbly coarse sand	

\* Location definition according to the database <https://mapa.hidrocarburos.gob.mx> (Comisión Nacional de Hidrocarburos )

Shallow waters: 0 – 500m; Deep waters: 500 – 1000m; Ultradeep waters: >1000m (meters below sea level)

P&A: Plugged and abandoned